NEW VISIONS IN NATURAL SCIENCE AND MATHEMATICS:

CONCEPTS - THEORIES - APPLICATIONS

Editor
Prof. Dr. N.Gülşah Deniz

DUVAR

NEW VISIONS IN NATURAL SCIENCE AND MATHEMATICS:

CONCEPTS - THEORIES - APPLICATIONS

Editör

Prof. Dr. N.Gülşah Deniz

New Visions In Natural Science And Mathematics: :Concepts - Theories - Applications
Editor: Prof.Dr. N.Gülşah Deniz

Editor in chief: Berkan Balpetek
Cover and Page Design: Duvar Design
Printing : October -2024
Publisher Certificate No: 49837
ISBN: 978-625-6183-32-2

© Duvar Yayınları
853 Sokak No:13 P.10 Kemeraltı-Konak/İzmir
Tel: 0 232 484 88 68

www.duvaryayinlari.com
duvarkitabevi@gmail.com

TABLE OF CONTENTS

Chapter 1

Curvatures Of Tube Surfaces with Frenet Frame In 4-Dimensional Space

Başak YAĞBASAN[1]
Aybüke EKİCİ COŞKUN[2]

[1] Eskişehir Osmangazi University, Department of Mathematics and Computer Science, Eskişehir. bskyagbasan@gmail.com, 05315724143, ORCID NO: 0000-0003- 4067-3034
[2] Eskişehir Osmangazi University, Department of Mathematics and Computer Science, Eskişehir. aybkekici@gmail.com, 05383501819, ORCID NO: 0000-0002-5630-2900

ÖZET

Bu çalışmada öncelikle Öklidyen 4-uzaydaki bir uzay eğrisi için Frenet çatısı ile ilgili tanımlar ile teoremler verilmiştir. Burada Frenet çatılı bir eğri için Frenet vektörleri, Frenet türev denklemleri ve eğrinin κ, τ ve η eğriliklerinden bahsedilmiştir. 4-boyutlu Öklidyen uzayda yüzeyler ile ilgili kavramlar ve onların bir çeşidi olan kanal yüzeyleri için verilmiş incelemeler üzerinde durulmuştur. Bu uzayda kanal yüzeyinin özel hali olan merkezi düzgün bir eğri üzerindeki noktalar ve bu eğrinin bu noktalardaki normal düzleminde bulunan sabit yarıçaplı bir çemberin oluşturduğu dairesel yüzey olan tüp (tubular) yüzey incelenmiştir. Öklid 4-uzayında tüp yüzeyinin Frenet çatılı genel denklemi verilmiştir. Genel denklem kullanılarak birinci ve ikinci kısmi türevler, yüzeyin $\boldsymbol{U_1}$ birim normal vektör alanı ve $\boldsymbol{U_1}$ birim normal vektör alanına Gram-Schmidt yöntemi uygulanarak $\boldsymbol{U_2}$ birim normal vektör alanı bulunup ardından yüzeyin birinci ve ikinci temel form katsayıları elde edilmiştir. Ek olarak yüzeyin $\boldsymbol{U_1}$ ve $\boldsymbol{U_2}$ birim normal vektör alanları için Gauss eğrilikleri ve ortalama eğrilikler hesaplanmıştır. Elde edilen hesaplar için bir örnek verilmiş ve yüzeyin izdüşüm uzaylarındaki şekilleri çizdirilmiştir.

Anahtar Kelimeler: Öklid 4-uzayı, Frenet çatısı, Tüp yüzeyi

ABSTRACT

In this research, the definitions and theorems of a space curve with respect to the Frenet frame are initially presented in Euclidean 4-space. These are Frenet vectors, Frenet derivative equations and curvatures κ, τ and η of a curve with Frenet frame. The concepts related to surfaces in 4-dimensional Euclidean space and their variants, such as canal surfaces, are analyzed. In this space, a special case of the canal surface, the tube surface, a circular surface formed by points on a central smooth curve and a circle of constant radius in the normal plane of this curve at these points, is studied. The general equation of the tube surface in Euclidean 4-space with Frenet frame is given. Using the general equation, the first and second partial derivatives, the $\boldsymbol{U}_1$ unit normal vector field of the surface and the $\boldsymbol{U}_2$ unit normal vector field by applying the Gram-Schmidt method to the $\boldsymbol{U}_1$ unit normal vector field are found and then the first and second fundamental form coefficients of the surface are obtained. In addition, Gaussian curvatures and mean curvatures are calculated for $\boldsymbol{U}_1$ and $\boldsymbol{U}_2$ unit normal vector fields of the surface. An example is given for the obtained calculations and the surface shapes in projection spaces are plotted.

Keywords: Euclid 4-space, Frenet frame, Tube surface

INTRODUCTION

Frenet equations were independently discovered by Frenet in 1847 and Serret in 1851. In 1760, Euler was the first to study curves and surfaces formed by the intersection of various planes. The canal surface, a specific type of surface, was defined by Monge in 1850. Canal surfaces are parametrized with distinct frames in $\mathbb{E}^4$. A tube surface, which is a special case of a canal surface, is the envelope of a moving sphere with a constant radius function $r(t)$, and is simpler to describe both analytically and kinematically (Doğan and Yaylı, 2017). Blaga (2005) introduced a technique for parameterizing tubular surfaces by utilizing the parameter along the generating curve and expressing the position vector of a point on the surface as ψ. Numerous studies in the literature have explored these surfaces in similar spaces (Bayram et al., 2009; Alessio, 2009; Bulca et al., 2017). Otsuki demonstrated the existence of a graphical representation of a surface in $\mathbb{E}^4$ and investigated the isometric immersions of two-dimensional connected oriented manifolds in $\mathbb{E}^4$. Furthermore, Otsuki (1966) provided a characterization of surfaces within hyperplanes, compact surfaces with constant mean curvature and non-negative Gaussian curvature, as well as surfaces in the three-dimensional sphere in $\mathbb{E}^4$. In 2008, Ganchev and Milousheva classified several important classes of surfaces in four-dimensional Euclidean space, distinguished by their invariants. Óláh-Gál and Pál (2009) studied the global isometry of two surfaces in $\mathbb{E}^4$, demonstrating that, while these surfaces are not globally isomorphic, they remain globally isometric. Mello (2009) analyzed the properties of surfaces immersed in $\mathbb{E}^4$ and provided conditions under which such surfaces exhibit hypersphericity. Kişi et al. (2019) examined the conditions under which canal surfaces with parallel transport frame vectors in $\mathbb{E}^4$are flat, minimal, or linear Weingarten, and also determined the normal vectors of canal surfaces. Finally, Bulca et al. (2017) characterized surfaces in $\mathbb{E}^4$ using the coefficients of the first and second fundamental forms. Tube surfaces have been studied using different spaces and different frames (Maekawa et. al., 1998; Abdel-Aziz and Saad, 2011; Dede, 2013; Dede et. al., 2015; Ekici et. al., 2017; Kızıltuğ et.al., 2019; Tozak et. al., 2019; Yağbasan and Ekici, 2023; Yağbasan et. al., 2023; Yağbasan et. al., 2023a). Similarly, different studies are given for the canal surface, which is the general form of the tube surface (Xu et. al., 2006; Kim et. al., 2016; Uçum and İlarslan, 2016; Doğan and Yaylı, 2017; Bulca et. al., 2017; Kaymanlı et. al., 2018; Şekerci and Çimdiker, 2019). In addition, there have been studies on surfaces created using different frame vectors in 3 and 4-space (Kaymanlı et. al., 2022; Ekici et. al., 2023; Ekici Coşkun and Akça, 2023; Dede et. al., 2024). In this research, investigations into tube surfaces are discussed in

$\mathbb{E}^4$. We offer the parametrization of the tube surface using the Frenet frame in $\mathbb{E}^4$. Furthermore, we are given the first and second unit normal vector fields, principal curvatures, Gaussian curvature, and mean curvature of tube surfaces in 4-dimensional space. Finally, an example of a tube surface is provided, with corresponding figures of the surface plotted in projection spaces.

PRELIMINARIES

Let $\boldsymbol{X} = (x_1, x_2, x_3, x_4)$, $\boldsymbol{Y} = (y_1, y_2, y_3, y_4)$ and $\boldsymbol{Z} = (z_1, z_2, z_3, z_4)$ be three vectors in $\mathbb{E}^4$. Here the inner product is expressed as $< \boldsymbol{X}, \boldsymbol{Y} >= x_1y_1 + x_2y_2 + x_3y_3 + x_4y_4$, the norm of a vector as $\|\boldsymbol{X}\| = \sqrt{< \boldsymbol{X}, \boldsymbol{X} >}$ and the vector product as

$$\begin{aligned} \boldsymbol{X} \wedge \boldsymbol{Y} \wedge \boldsymbol{Z} = \; & (x_2y_3z_4 - x_2y_4z_3 - x_3y_2z_4 + x_3y_4z_2 + x_4y_2z_3 - x_4y_3z_2)\boldsymbol{e}_1 \\ & -(x_1y_3z_4 - x_1y_4z_3 - x_3y_1z_4 + x_3y_4z_1 + x_4y_1z_3 - x_4y_3z_1)\boldsymbol{e}_2 \\ & +(x_1y_2z_4 - x_1y_4z_2 - x_2y_1z_4 + x_2y_4z_1 + x_4y_1z_2 - x_4y_2z_1)\boldsymbol{e}_3 \\ & -(x_1y_2z_3 - x_1y_3z_2 - x_2y_1z_3 + x_2y_3z_1 + x_3y_1z_2 - x_3y_2z_1)\boldsymbol{e}_4 \end{aligned} \tag{1}$$

where $\boldsymbol{e}_1 \wedge \boldsymbol{e}_2 \wedge \boldsymbol{e}_3 = \boldsymbol{e}_4$, $\boldsymbol{e}_2 \wedge \boldsymbol{e}_3 \wedge \boldsymbol{e}_4 = \boldsymbol{e}_1$, $\boldsymbol{e}_3 \wedge \boldsymbol{e}_4 \wedge \boldsymbol{e}_1 = \boldsymbol{e}_2$ and $\boldsymbol{e}_4 \wedge \boldsymbol{e}_1 \wedge \boldsymbol{e}_2 = -\boldsymbol{e}_3$ (Allesio, 2009; Elsayied et. al., 2021).If $< \alpha', \alpha' >= 1$, $a(t) = a : I \subset \mathbb{R} \to \mathbb{E}^4$ is the unit speed curve. The Frenet equations of variation for the $a(t)$ curve given by the spring parameter are

$$\begin{bmatrix} \boldsymbol{T}' \\ \boldsymbol{N}' \\ \boldsymbol{B}_1' \\ \boldsymbol{B}_2' \end{bmatrix} = \begin{bmatrix} 0 & \kappa & 0 & 0 \\ -\kappa & 0 & \tau & 0 \\ 0 & -\tau & 0 & \eta \\ 0 & 0 & -\eta & 0 \end{bmatrix} \begin{bmatrix} \boldsymbol{T} \\ \boldsymbol{N} \\ \boldsymbol{B}_1 \\ \boldsymbol{B}_2 \end{bmatrix} \tag{2}$$

where the functions

$$\kappa = \langle \boldsymbol{T}', \boldsymbol{N} \rangle, \qquad \tau = \langle \boldsymbol{N}', \boldsymbol{B}_1 \rangle, \qquad \eta = \langle \boldsymbol{B}_1', \boldsymbol{B}_2 \rangle \tag{3}$$

respectively (Gray, 1993; Gluck, 1966). A canal surface, centered at a spine curve $a(t)$ with radius $r(t)$, is parametrized by

$$\psi(t, v) = a(t) + r(t)(cosv\boldsymbol{e}_1(t) + sinv\boldsymbol{e}_2(t)) \tag{4}$$

where $r(t)$ is a real differentiable function (Kişi et. al., 2019; Bulca et. al., 2017). Let M be a smooth surface in $\mathbb{R}^4$ given with the patch $\psi: U \subset \mathbb{R}^2 \to \mathbb{R}^4$, $\psi(t, v)$. The tangent space to M at an arbitrary point $p = \psi(t, v)$ of M span

$\{\psi_t, \psi_v\}$. In the chart (t, v) the coefficients of the first fundamental form of M are given by

$$E = \langle \psi_t, \psi_t \rangle, F = \langle \psi_t, \psi_v \rangle, G = \langle \psi_v, \psi_v \rangle \text{ and } \mathrm{W} = EG - F^2 \qquad (5)$$

where $<,>$ is the Euclidean inner product (Mello, 2009; Bayram et. al., 2009). Consider $\psi_{tt}, \psi_{tv}, \psi_{vv}$ as the second-order partial derivatives, and let $\boldsymbol{U}_1, \boldsymbol{U}_2, \dots, \boldsymbol{U}_{n-2}$ represent the normal vector fields of the manifold M with the coefficients of its second fundamental form given by, $1 \leq k \leq n-2$,

$$L_k = \langle \psi_{tt}, \boldsymbol{U}_k \rangle, \qquad M_k = \langle \psi_{tv}, \boldsymbol{U}_k \rangle \ \ and \ \ N_k = \langle \psi_{vv}, \boldsymbol{U}_k \rangle. \qquad (6)$$

The Gaussian and mean curvatures of the surface are typically expressed as

$$K = \frac{LN - M^2}{EG - F^2} \ and \ H = \frac{LG - 2MF + NE}{EG - F^2}. \qquad (7)$$

respectively (Chen and Piccini, 1973; Mello, 2009; Bulca et. al., 2017).

TUBE SURFACES CREATED WİTH $\boldsymbol{T}$ AND $\boldsymbol{B}_1$ FRENET VECTORS IN 4-DIMENSIONAL SPACE

In order to form the equation of the 2-dimensional Frenet frame tube surface in 4-dimensional space, a circle that accepts each point on $\alpha(t)$ as the centre in the plane stretched by $\boldsymbol{T}$ and $\boldsymbol{B}_1$ vectors must be moved.

Thus, the formed tube surface

$$\psi(t, v) = a(t) + r(cosv\boldsymbol{T}(t) + sinv\boldsymbol{B}_1(t)) \qquad (8)$$

The necessary theorems and proofs for the parametric equation are given. Here r ∈ R is taken. Frenet curvatures are taken constant throughout this study.

Theorem Let $M \subset \mathbb{E}^4$ be a tube surface at a distance r from the spine curve $\alpha(t)$ according to Frenet frame $\{\boldsymbol{T}, \boldsymbol{N}, \boldsymbol{B}_1, \boldsymbol{B}_2\}$ with parametrization $\psi(t, v)$, given by $\psi: U \subset \mathbb{E}^2 \to \mathbb{E}^4$, $(t, v) \in U$ and let tangent space to M at a point $p \in \psi(t, v)$ be spanned by $\{\psi_t, \psi_v\}$. As a result, the following assertions are true:

1. The unit normal vector fields $\boldsymbol{U}_1$ and $\boldsymbol{U}_2$ of tube surface in $\mathbb{E}^4$ are found to be

$$\boldsymbol{U}_1 = \frac{-r\eta sinv\boldsymbol{N} + r(\kappa cosv - \tau sinv)\boldsymbol{B}_2}{r\sqrt{cos^2v(\kappa^2 - \tau^2 - \eta^2) - \kappa\tau sin2v + \eta^2 + \tau^2}}$$

and

$$\boldsymbol{U}_2 = \frac{r\tau cosvsinv\boldsymbol{T} + (r\tau - r\tau cos^2v)\boldsymbol{N} - cosv\boldsymbol{B}_1}{r\sqrt{cos^2v(\kappa^2 - \tau^2 - \eta^2) - \kappa\tau sin2v + \eta^2 + \tau^2}}$$

respectively.

2. Gaussian curvature K_1 and Mean curvature H_1 of tube surface with unit normal vector fields $\boldsymbol{U}_1$ in $\mathbb{E}^4$ are obtained as

$$K_1 = \frac{-r^2\kappa^2\eta^2[cos^2v(\kappa^2 - \tau^2 - \eta^2) - \kappa\tau sin2v + \eta^2 + \tau^2]^{-1}}{r^2[1 + r^2cos^2v(\kappa^2 - \tau^2 - \eta^2) - r^2\kappa\tau sin2v + r^2(\eta^2 + \tau^2)] - r^2sin^2v}$$

and

$$H_1 = \frac{r^2sinv[\kappa\eta + r\eta(\tau' sinv - \kappa' cosv) + r\eta'(\kappa cosv - \tau sinv)](cos^2v(\kappa^2 - \tau^2 - \eta^2) - \kappa\tau sin2v + \eta^2 + \tau^2)^{-1/2}}{r^2(1 + r^2[cos^2v(\kappa^2 - \tau^2 - \eta^2) + (\eta^2 + \tau^2) - \kappa\tau sin2v]) - r^2sin^2v}$$

respectively.

3. Gaussian curvature K_2 and Mean curvature H_2 of tube surface with unit normal vector fields $\boldsymbol{U}_2$ in $\mathbb{E}^4$ are obtained as

$$K_2 = \frac{-r^2\eta[2r^2\kappa\tau\eta cosvsinv(cos^2v - 1) + r^2cos^2v(\kappa^2\eta - 2\tau^2\eta - 2r^2\tau^3)]}{[cos^2v(r^2\eta^2 - 1) - r^2\eta^2][r^2(1 + r^2cos^2v(\kappa^2 - \tau^2 - \eta^2) - r^2\kappa\tau sin2v + r^2(\eta^2 + \tau^2)) - r^2sin^2v]} - \frac{r^2\eta[r^2\eta cos^4v(\tau^2 - \kappa^2 + \eta^2) + r\eta' cosv(1 - cos^2v) + r^2\eta(\tau^2 + \eta^2) + \eta cos^4v]}{[cos^2v(r^2\eta^2 - 1) - r^2\eta^2][r^2(1 + r^2cos^2v(\kappa^2 - \tau^2 - \eta^2) - r^2\kappa\tau sin2v + r^2(\eta^2 + \tau^2)) - r^2sin^2v]}$$

and

$$H_2 = \frac{2\eta cos^2vsinv(1 + r^2\eta^2 - r^2\kappa^2) + 4r^2\kappa\tau\eta cosv(1 - cos^2v)}{\sqrt{r^2\eta^2sin^2v + cos^2v}[cos^2v(\kappa^2 - \tau^2 - \eta^2) + r^2(\eta^2 + \tau^2) - 2r^2\kappa\tau cosvsinv + cos^2v]} + \frac{2r^2\eta sinv(\tau^2cos^2v - \eta^2 - \tau^2) + \eta sinv + r\eta' cosvsinv}{\sqrt{r^2\eta^2sin^2v + cos^2v}[cos^2v(\kappa^2 - \tau^2 - \eta^2) + r^2(\eta^2 + \tau^2) - 2r^2\kappa\tau cosvsinv + cos^2v]}$$

respectively.

Proof Tube surface, at a distance r from the spine curve $\alpha(t)$ with Frenet frame $\{\boldsymbol{T}, \boldsymbol{N}, \boldsymbol{B}_1, \boldsymbol{B}_2\}$ are parametrized by

$$\psi(t,v) = a(t) + r(cosv\boldsymbol{T} + sinv\boldsymbol{B}_1)$$

The partial derivatives of $\psi(t,v)$, with respect to t and v, are determined by

$$\psi_t = 1 + (r\kappa cosv - r\tau sinv)\boldsymbol{N} + r\eta sinv\boldsymbol{B}_2 \tag{9}$$

and

$$\psi_v = r(-sinv\boldsymbol{T} + cosv\boldsymbol{B}_1). \tag{10}$$

Then, second order partial derivatives of $\psi(t,v)$, with respect to t and v, are given as

$$\psi_{tt} = (r\kappa\tau sinv - r\kappa^2 cosv)\boldsymbol{T} + \kappa\boldsymbol{N} + (r\kappa\tau cosv - r\tau^2 sinv - r\eta^3 sinv)\boldsymbol{B}_1 \tag{11}$$

$$\psi_{tv} = (-r\kappa sinv - r\tau cosv)\boldsymbol{N} + r\eta cosv\boldsymbol{B}_2 \tag{12}$$

and

$$\psi_{vv} = -rcosv\boldsymbol{T} - rsinv\boldsymbol{B}_1. \tag{13}$$

The unit normal vector fields $\boldsymbol{U}_1$ and $\boldsymbol{U}_2$ of the surface should be provided with the following conditions

$$\begin{array}{lll} <\psi_t, \boldsymbol{U}_1> = 0 & <\psi_t, \boldsymbol{U}_2> = 0 & \\ <\psi_v, \boldsymbol{U}_1> = 0 & <\psi_v, \boldsymbol{U}_2> = 0 & and\ <\boldsymbol{U}_1, \boldsymbol{U}_2> = 0 \\ <\boldsymbol{U}_1, \boldsymbol{U}_1> = 1 & <\boldsymbol{U}_2, \boldsymbol{U}_2> = 1 & \end{array} \tag{14}$$

where ψ_t and ψ_v are the partial derivatives of $\psi(t,v)$, with respect to t and v. The unit normal vector field $\boldsymbol{U}_1$ of tube surface is obtained as

$$\boldsymbol{U}_1 = \frac{-r\eta sinv\boldsymbol{N} + r(\kappa cosv - \tau sinv)\boldsymbol{B}_2}{r\sqrt{cos^2 v(\kappa^2 - \tau^2 - \eta^2) - \kappa\tau sin2v + \eta^2 + \tau^2}} \tag{15}$$

using equation

$$\boldsymbol{U}_1 = \frac{a_1\boldsymbol{T} + a_2\boldsymbol{N} + a_3\boldsymbol{B}_1 + a_4\boldsymbol{B}_2}{\sqrt{a_1^2 + a_2^2 + a_3^2 + a_4^2}}$$

where $a_3 = 0$ and $a_1 = 0$ then $a_4 = r\kappa cosv - r\tau sinv$ and $a_2 = -r\eta sinv$.

Since $< \boldsymbol{U}_1, \boldsymbol{U}_1 >= 1$, $\boldsymbol{U}_1$ is the unit normal vector field of the tube surface. Then using methods of Gram Schmidt with $\boldsymbol{U}_1$, the unit vector field $\boldsymbol{U}_2$ is given as

$$\boldsymbol{U}_2 = \frac{r\tau cosvsinv\boldsymbol{T} + (r\tau - r\tau cos^2 v)\boldsymbol{N} - cosv\boldsymbol{B}_1}{r\sqrt{cos^2 v(\kappa^2 - \tau^2 - \eta^2) - \kappa\tau sin2v + \eta^2 + \tau^2}} \tag{16}$$

Using equation (14), the vector fields $\boldsymbol{U}_1$ and $\boldsymbol{U}_2$ are identified as unit normal vector fields for the tube surfaces. By substituting equations (9) and (10) into equation (5), the coefficients of the first fundamental form for the tube surfaces

$$\begin{aligned} E &= 1 + r^2[cos^2 v(\kappa^2 - \tau^2 - \eta^2) + \eta^2 + \tau^2 - \kappa\tau sin2v] \\ F &= -rsinv \\ G &= r^2 \end{aligned} \tag{17}$$

and

$$W = r^2(1 + r^2[cos^2 v(\kappa^2 - \tau^2 - \eta^2) + \eta^2 + \tau^2 - \kappa\tau sin2v]) - r^2 sin^2 v$$

are subsequently derived. Equations (6), (11), (12), (13), and (15) lead to the coefficients of the second fundamental form of the tube surface with the unit vector field $\boldsymbol{U}_1$ in $\mathbb{E}^4$ obtained as,

$$\begin{aligned} L_1 &= \frac{r\kappa\eta sinv}{r\sqrt{cos^2 v(\kappa^2 - \tau^2 - \eta^2) - \kappa\tau sin2v + \eta^2 + \tau^2}} \\ M_1 &= \frac{r\kappa\eta}{\sqrt{cos^2 v(\kappa^2 - \tau^2 - \eta^2) - \kappa\tau sin2v + \eta^2 + \tau^2}} \\ N_1 &= 0 \end{aligned} \tag{18}$$

Substituting equations (17) and (18) into equation (7) implies that Gaussian and mean curvatures with respect to $\boldsymbol{U}_1$ following as

$$K_1 = \frac{-r^2\kappa^2\eta^2[cos^2 v(\kappa^2 - \tau^2 - \eta^2) - \kappa\tau sin2v + \eta^2 + \tau^2]^{-1}}{r^2[1 + r^2 cos^2 v(\kappa^2 - \tau^2 - \eta^2) - r^2\kappa\tau sin2v + r^2(\eta^2 + \tau^2)] - r^2 sin^2 v}$$

and

$$H_1 = \frac{sinv[\kappa\eta + r\eta(\tau' sinv - \kappa' cosv) + r\eta'(\kappa cosv - \tau sinv)](cos^2 v(\kappa^2 - \tau^2 - \eta^2) - \kappa\tau sin2v + \eta^2 + \tau^2)^{-1/2}}{(1 + r^2[cos^2 v(\kappa^2 - \tau^2 - \eta^2) + \eta^2 + \tau^2 - \kappa\tau sin2v]) - sin^2 v}$$

equations (6), (11), (12), (13), and (16) lead to the coefficients of the second fundamental form of the tube surface with the unit vector field $\boldsymbol{U}_2$ in $\mathbb{E}^4$ obtained as,

$$L_2 = \frac{-r^2\eta sinv[cos^2v(\kappa^2-\tau^2-\eta^2)+\eta^2+\tau^2-\kappa\tau sin2v]}{\sqrt{cos^2v+r\eta^2(1+cos^2v)}}$$
$$M_2 = \frac{-r\eta cos^2v}{\sqrt{cos^2v+r\eta^2(1+cos^2v)}} \quad (19)$$
$$N_2 = \frac{-r^2\eta sinv}{\sqrt{cos^2v+r\eta^2(1+cos^2v)}}$$

Substituting equations (17) and (19) into equation (7) implies that Gaussian and mean curvatures with respect to $\boldsymbol{U}_2$ following as

$$K_2 = \frac{-r^2\eta[-2r^2\kappa\tau\eta cosvsin^3v+r^2cos^2v(\kappa^2\eta-2\tau^2\eta-2r^2\tau^3)]}{[cos^2v(r^2\eta^2-1)-r^2\eta^2][r^2(1+r^2cos^2v(\kappa^2-\tau^2-\eta^2)-r^2\kappa\tau sin2v+r^2(\eta^2+\tau^2))-r^2sin^2v]}$$
$$-\frac{r^2\eta[r^2\eta cos^4v(\tau^2-\kappa^2+\eta^2)+r\eta' cosvsin^2v+r^2\eta(\tau^2+\eta^2)+\eta cos^4v]}{[cos^2v(r^2\eta^2-1)-r^2\eta^2][r^2(1+r^2cos^2v(\kappa^2-\tau^2-\eta^2)-r^2\kappa\tau sin2v+r^2(\eta^2+\tau^2))-r^2sin^2v]}$$

and

$$H_2 = \frac{2\eta cos^2vsinv(1+r^2\eta^2-r^2\kappa^2)+4r^2\kappa\tau\eta cosvsin^2v}{[cos^2v(\kappa^2-\tau^2-\eta^2)+r^2(\eta^2+\tau^2)-2r^2\kappa\tau cosvsinv+cos^2v]\sqrt{r^2\eta^2sin^2v+cos^2v}}$$
$$+\frac{2r^2\eta sinv(\tau^2cos^2v-\eta^2-\tau^2)+\eta sinv+r\eta' cosvsinv}{[cos^2v(\kappa^2-\tau^2-\eta^2)+r^2(\eta^2+\tau^2)-2r^2\kappa\tau cosvsinv+cos^2v]\sqrt{r^2\eta^2sin^2v+cos^2v}}.$$

Corollary If the Gaussian and mean curvatures corresponding to the unit normal vector fields obtained for the Frenet vectors $\boldsymbol{T}$ and $\boldsymbol{B}_1$ are similarly calculated using the shape operators corresponding to the unit normal vector fields, the same result is obtained.

TUBE SURFACES CREATED WİTH $\boldsymbol{T}$ AND $\boldsymbol{B}_2$ FRENET VECTORS IN 4-DIMENSIONAL SPACE

In order to form the equation of the 2-dimensional Frenet frame tube surface in 4-dimensional space, a circle that accepts each point on $\alpha(t)$ as the centre in the plane stretched by $\boldsymbol{T}$ and $\boldsymbol{B}_2$ vectors must be moved. Thus, the formed tube surface

$$\psi(t,v) = a(t) + r(cosv\boldsymbol{T}(t) + sinv\boldsymbol{B}_2(t)) \quad (20)$$

The necessary theorems and proofs for the parametric equation are given. Here r ∈ R is taken.

Theorem Let $M \subset \mathbb{E}^4$ be a tube surface at a distance r from the spine curve $\alpha(t)$ according to Frenet frame $\{\boldsymbol{T},\boldsymbol{N},\boldsymbol{B}_1,\boldsymbol{B}_2\}$ with parametrization $\psi(t,v)$, given by $\psi: U \subset \mathbb{E}^2 \to \mathbb{E}^4$, $(t,v) \in U$ and let tangent space to M at a point $p \in \psi(t,v)$ be spanned by $\{\psi_t,\psi_v\}$. Then, the following statements hold:

1. Unit normal vector fields $\boldsymbol{U}_1$ and $\boldsymbol{U}_2$ of tube surface in $\mathbb{E}^4$ are obtained as

$$\boldsymbol{U}_1 = \frac{r cosv\boldsymbol{T} + (\eta sinv - 1)\boldsymbol{N} + \kappa cosv\boldsymbol{B}_1 - r\kappa sinv\boldsymbol{B}_2}{\sqrt{1 + \kappa^2(r^2 + cos^2v) + \eta^2 sin^2v - 2\eta sinv}}$$

and

$$\boldsymbol{U}_2 = \frac{-r\kappa cosv(\kappa^2 cos^2v + \eta^2 sin^2v - \eta sinv)\boldsymbol{T} + \kappa^2(r^2\eta sinv + cos^2v)\boldsymbol{N}}{\kappa[1 + \eta^2 - 2\eta sinv + r^2\kappa^2 + cos^2v(\kappa^2 - \eta^2)]^{3/2}[\kappa^2 cos^2v + \eta^2 sin^2v]\sqrt{cos^2v(1 + r^2\kappa^2) + r^2\eta^2 sin^2v}}$$
$$- \frac{\kappa cosv(\eta sinv - 1 - r^2\kappa^2)\boldsymbol{B}_1 + \kappa(rcos^2vsinv(\kappa^2 - \eta^2) + r\eta^2 sinv - r\eta sin^2v)\boldsymbol{B}_2}{\kappa[1 + \eta^2 - 2\eta sinv + r^2\kappa^2 + cos^2v(\kappa^2 - \eta^2)]^{3/2}[\kappa^2 cos^2v + \eta^2 sin^2v]\sqrt{cos^2v(1 + r^2\kappa^2) + r^2\eta^2 sin^2v}}$$

respectively.

2. Gaussian curvature K_1 and Mean curvature H_1 of tube surface with unit normal vector fields $\boldsymbol{U}_1$ in $\mathbb{E}^4$ are obtained as

$$K_1 = \frac{r^2\kappa[\eta sinv(\kappa + r\tau) + cos^2v(r^2\kappa^3 - r\kappa^2\tau - r^2\tau\eta^2 + \kappa) + \eta^2(r^2\kappa - \kappa - r\tau)]}{[r^2 + r^4(\kappa^2 cos^2v + \eta^2 sin^2v) - r^2 sin^2v][1 + cos^2v(\kappa^2 - \eta^2) + r^2\kappa^2 + \eta^2 - 2\eta sinv]}$$

and

$$H_1 = \frac{-r^2[\eta sinv(\kappa + r\tau) + cos^2v(2r^2\kappa^3 - r\kappa^2\tau - 2r^2\kappa\eta^2 + r\tau\eta^2 + 2\kappa) + r\eta^2(2r\kappa - \tau)]}{[r^2 + r^4(\kappa^2 cos^2v + \eta^2 sin^2v) - r^2 sin^2v][1 + \eta^2 sin^2v + \kappa^2(cos^2v + r^2)]}$$

respectively.

3. Gaussian curvature K_2 and Mean curvature H_2 of tube surface with unit normal vector fields $\boldsymbol{U}_2$ in $\mathbb{E}^4$ are obtained as

$$K_2 = \frac{-\kappa^2\eta^2}{[\kappa^2 cos^2v + \eta^2 sin^2v][r^2\eta^2 sin^2v + r^2\kappa^2 cos^2v + cos^2v]}$$

and

$$H_2 = \frac{[-\kappa\eta sinv + r\tau cos^2v(\kappa^2 - \eta^2) + r\tau\eta^2]}{[r^2\eta^2 sin^2v + r^2\kappa^2 cos^2v + cos^2v]\sqrt{\kappa^2 cos^2v + \eta^2 sin^2v}}$$

respectively.

Proof Tube surface, at a distance r from the spine curve $\alpha(t)$ with Frenet frame $\{\boldsymbol{T}, \boldsymbol{N}, \boldsymbol{B}_1, \boldsymbol{B}_2\}$ are parametrized by

$$\psi(t, v) = a(t) + r(cosv\boldsymbol{B}_1 + sinv\boldsymbol{B}_2)$$

The partial derivatives of $\psi(t,v)$, with respect to t and v, are determined by

$$\psi_t = \boldsymbol{T} + r\kappa cosv\boldsymbol{N} - r\eta sinv\boldsymbol{B}_1 \tag{21}$$

and

$$\psi_v = r(-sinv\boldsymbol{T} + cosv\boldsymbol{B}_2). \tag{22}$$

Then, second order partial derivatives of $\psi(t,v)$, with respect to t and v, are given as

$$\psi_{tt} = \quad -r\kappa^2 cosv\boldsymbol{T} + (\kappa + r\tau\eta sinv)\boldsymbol{N} + r\kappa\tau cosv\boldsymbol{B}_1 - r\eta^2 sinv\boldsymbol{B}_2 \tag{23}$$

$$\psi_{tv} = \quad -r\kappa sinv\boldsymbol{N} - r\eta cosv\boldsymbol{B}_1 \tag{24}$$

and

$$\psi_{vv} = -rcosv\boldsymbol{T} - rsinv\boldsymbol{B}_2. \tag{25}$$

The unit normal vector fields $\boldsymbol{U}_1$ and $\boldsymbol{U}_2$ of the surface should be provided with the following conditions

$$\begin{array}{llll} < \psi_t, \boldsymbol{U}_1 >= 0 & < \psi_t, \boldsymbol{U}_2 >= 0 & & \\ < \psi_v, \boldsymbol{U}_1 >= 0 & < \psi_v, \boldsymbol{U}_2 >= 0 & and & < \boldsymbol{U}_1, \boldsymbol{U}_2 >= 0 \\ < \boldsymbol{U}_1, \boldsymbol{U}_1 >= 1 & < \boldsymbol{U}_2, \boldsymbol{U}_2 >= 1 & & \end{array} \tag{26}$$

where ψ_t and ψ_v are the partial derivatives of $\psi(t,v)$, with respect to t and v.

The unit normal vector field $\boldsymbol{U}_1$ of tube surface is obtained as

$$\boldsymbol{U}_1 = \frac{rcosv\boldsymbol{T} + (\eta sinv - 1)\boldsymbol{N} + \kappa cosv\boldsymbol{B}_1 - r\kappa sinv\boldsymbol{B}_2}{\sqrt{1 + \kappa^2(r^2 + cos^2 v) + \eta^2 sin^2 v - 2\eta sinv}} \tag{27}$$

using equation

$$\boldsymbol{U}_1 = \frac{a_1\boldsymbol{T} + a_2\boldsymbol{N} + a_3\boldsymbol{B}_1 + a_4\boldsymbol{B}_2}{\sqrt{a_1^2 + a_2^2 + a_3^2 + a_4^2}}$$

where $a_3 = cosv$ and $a_1 = r\tau cosv$ then $a_4 = sinv$ and $a_2 = 1$. Since $< \boldsymbol{U}_1, \boldsymbol{U}_1 >= 1$, $\boldsymbol{U}_1$ is the unit normal vector field of the tube surface. Then using methods of Gram Schmidt with $\boldsymbol{U}_1$, the unit vector field $\boldsymbol{U}_2$ is given as

$$\begin{aligned} \boldsymbol{U}_2 = & \frac{-r\kappa cosv(\kappa^2 cos^2 v + \eta^2 sin^2 v - \eta sinv)\boldsymbol{T} + \kappa^2(r^2\eta sinv + cos^2 v)\boldsymbol{N}}{\kappa[1 + \eta^2 - 2\eta sinv + r^2\kappa^2 + cos^2 v(\kappa^2 - \eta^2)]^{3/2}[\kappa^2 cos^2 v + \eta^2 sin^2 v]\sqrt{cos^2 v(1 + r^2\kappa^2) + r^2\eta^2 sin^2 v}} \\ & - \frac{\kappa cosv(\eta sinv - 1 - r^2\kappa^2)\boldsymbol{B}_1 + \kappa(rcos^2 vsinv(\kappa^2 - \eta^2) + r\eta^2 sinv - r\eta sin^2 v)\boldsymbol{B}_2}{\kappa[1 + \eta^2 - 2\eta sinv + r^2\kappa^2 + cos^2 v(\kappa^2 - \eta^2)]^{3/2}[\kappa^2 cos^2 v + \eta^2 sin^2 v]\sqrt{cos^2 v(1 + r^2\kappa^2) + r^2\eta^2 sin^2 v}} \end{aligned} \tag{28}$$

Using equation (26), the vector fields $\boldsymbol{U_1}$ and $\boldsymbol{U_2}$ are identified as unit normal vector fields for the tube surfaces. By substituting equations (21) and (22) into equation (5), the coefficients of the first fundamental form for the tube surfaces

$$\begin{aligned} E &= 1 + r^2\kappa^2 cos^2 v + r^2\eta^2 cos^2 v \\ F &= -r sin v \\ G &= r^2 \end{aligned} \tag{29}$$

and

$$W = r^2 + r^4(\kappa^2 cos^2 v + \eta^2 sin^2 v) - r^2 sin^2 v$$

are subsequently derived.

Equations (6), (23), (24), (25), and (27) lead to the coefficients of the second fundamental form of the tube surface with the unit vector field $\boldsymbol{U_1}$ in $\mathbb{E}^4$ obtained as,

$$\begin{aligned} L_1 &= \frac{\eta sin v(r\tau - \kappa) + \kappa + r\tau cos^2 v(\eta^2 - \kappa^2) + r^2\kappa cos^2 v(\kappa^2 - \eta^2) + r\eta^2(r\kappa - \tau)}{(1 + \kappa^2(r^2 + cos^2 v) + \eta^2 sin^2 v - 2\eta sin v)^{1/2}} \\ M_1 &= \frac{r\kappa(sin v - \eta)}{(1 + \kappa^2(r^2 + cos^2 v) + \eta^2 sin^2 v - 2\eta sin v)^{1/2}} \\ N_1 &= \frac{-r^2\kappa}{(1 + \kappa^2(r^2 + cos^2 v) + \eta^2 sin^2 v - 2\eta sin v)^{1/2}}. \end{aligned} \tag{30}$$

Substituting equations (29) and (30) into equation (7) implies that Gaussian and mean curvatures with respect to $\boldsymbol{U_1}$ following as

$$K_1 = \frac{r^2\kappa[\eta sin v(\kappa + r\tau) + cos^2 v(r^2\kappa^3 - r\kappa^2\tau - r^2\tau\eta^2 + \kappa) + \eta^2(r^2\kappa - \kappa - r\tau)]}{[r^2 + r^4(\kappa^2 cos^2 v + \eta^2 sin^2 v) - r^2 sin^2 v][1 + cos^2 v(\kappa^2 - \eta^2) + r^2\kappa^2 + \eta^2 - 2\eta sin v]}$$

and

$$H_1 = \frac{-r^2[\eta sin v(\kappa + r\tau) + cos^2 v(2r^2\kappa^3 - r\kappa^2\tau - 2r^2\kappa\eta^2 + r\tau\eta^2 + 2\kappa) + r\eta^2(2r\kappa - \tau)]}{[r^2 + r^4(\kappa^2 cos^2 v + \eta^2 sin^2 v) - r^2 sin^2 v][1 + \eta^2 sin^2 v + \kappa^2(cos^2 v + r^2)]}$$

equations (6), (23), (24), (3), and (28) lead to the coefficients of the second fundamental form of the tube surface with the unit vector field $\boldsymbol{U_2}$ in $\mathbb{E}^4$ obtained as,

$$\begin{aligned} L_2 &= \frac{\kappa\eta sin v + r\tau\eta^2 + r\tau cos^2 v(\kappa^2 - \eta^2)}{\sqrt{\kappa^2 cos^2 v + \eta^2 sin^2 v}} \\ M_2 &= \frac{-r\kappa\eta}{\sqrt{\kappa^2 cos^2 v + \eta^2 sin^2 v}} \\ N_2 &= 0 \end{aligned} \tag{31}$$

Substituting equations (29) and (31) into equation (7) implies that Gaussian and mean curvatures with respect to $\boldsymbol{U}_2$ following as

$$K_2 = \frac{-\kappa^2\eta^2}{[\kappa^2 cos^2 v + \eta^2 sin^2 v][r^2\eta^2 sin^2 v + r^2\kappa^2 cos^2 v + cos^2 v]}$$

and

$$H_2 = \frac{[-\kappa\eta sinv + r\tau cos^2 v(\kappa^2 - \eta^2) + r\tau\eta^2]}{[r^2\eta^2 sin^2 v + r^2\kappa^2 cos^2 v + cos^2 v]\sqrt{\kappa^2 cos^2 v + \eta^2 sin^2 v}}.$$

Corollary If the Gaussian and mean curvatures corresponding to the unit normal vector fields obtained for the Frenet vectors $\boldsymbol{T}$ and $\boldsymbol{B}_2$ are similarly calculated using the shape operators corresponding to the unit normal vector fields, the same result is obtained.

Example 1 Let $\alpha(s)$ be a centre curve with Frenet frame of tube surface in $\mathbb{E}^4$ such as

$$\alpha(t) = (\sqrt{3}cos\frac{s}{\sqrt{7}} - \frac{\sqrt{5}}{2}, -2 + \sqrt{3}sin\frac{s}{\sqrt{7}}, 5 + cos\frac{2s}{\sqrt{7}}, sin\frac{2s}{\sqrt{7}}) \tag{32}$$

From $\left|\left|\alpha(s)\right|\right| = 1$, it is easy to see that Frenet vectors are given as

$$\begin{aligned}
\boldsymbol{T} &= (-\frac{\sqrt{3}}{\sqrt{7}}sin\frac{s}{\sqrt{7}}, \frac{\sqrt{3}}{\sqrt{7}}cos\frac{s}{\sqrt{7}}, -\frac{2}{\sqrt{7}}sin\frac{2s}{\sqrt{7}}, \frac{2}{\sqrt{7}}cos\frac{2s}{\sqrt{7}})\\
\boldsymbol{N} &= (-\frac{\sqrt{3}}{\sqrt{19}}cos\frac{s}{\sqrt{7}}, -\frac{\sqrt{3}}{\sqrt{19}}sin\frac{s}{\sqrt{7}}, -\frac{4}{\sqrt{19}}cos\frac{2s}{\sqrt{7}}, -\frac{4}{\sqrt{19}}sin\frac{2s}{\sqrt{7}})\\
\boldsymbol{B}_1 &= (\frac{2}{\sqrt{7}}sin\frac{s}{\sqrt{7}}, -\frac{2}{\sqrt{7}}cos\frac{s}{\sqrt{7}}, -\frac{\sqrt{3}}{\sqrt{7}}sin\frac{2s}{\sqrt{7}}, \frac{\sqrt{3}}{\sqrt{7}}cos\frac{2s}{\sqrt{7}})\\
\boldsymbol{B}_2 &= (\frac{4\sqrt{3}}{\sqrt{57}}cos\frac{s}{\sqrt{7}}, \frac{4\sqrt{3}}{\sqrt{57}}sin\frac{s}{\sqrt{7}}, -\frac{3}{\sqrt{57}}cos\frac{2s}{\sqrt{7}}, -\frac{3}{\sqrt{57}}sin\frac{2s}{\sqrt{7}})
\end{aligned} \tag{33}$$

and from equation (3), Frenet curvatures are given as

$$\kappa = \frac{19}{7\sqrt{19}}, \quad \tau = -\frac{6\sqrt{3}}{7\sqrt{19}} \; and \; \eta = \frac{2}{\sqrt{19}}.$$

Substituting equations (32) and (33) into equation (5), the tube surface formed by the Frenet vectors $\boldsymbol{T}$ and $\boldsymbol{B}_1$ is parametrized as

$$\psi(s,v) = \left(\sqrt{3}cos\frac{s}{\sqrt{7}} - \frac{\sqrt{5}}{2} + r\left(-\frac{\sqrt{3}}{\sqrt{7}}sin\frac{s}{\sqrt{7}}cosv + \frac{2}{\sqrt{7}}sin\frac{s}{\sqrt{7}}sinv\right),\right.$$
$$-2 + \sqrt{3}sin\frac{s}{\sqrt{7}} + r\left(\frac{\sqrt{3}}{\sqrt{7}}cos\frac{s}{\sqrt{7}}cosv - \frac{2}{\sqrt{7}}cos\frac{s}{\sqrt{7}}sinv\right),$$
$$5 + cos\frac{2s}{\sqrt{7}} + r\left(-\frac{2}{\sqrt{7}}sin\frac{2s}{\sqrt{7}}cosv - \frac{\sqrt{3}}{\sqrt{7}}sin\frac{2s}{\sqrt{7}}sinv\right),$$
$$\left.sin\frac{2s}{\sqrt{7}} + r\left(\frac{2}{\sqrt{7}}cos\frac{2s}{\sqrt{7}}cosv + \frac{\sqrt{3}}{\sqrt{7}}cos\frac{2s}{\sqrt{7}}sinv\right)\right).$$

Hence for $r = 7$, it is easily say that

$$\psi(s,v) = \left(\sqrt{3}cos\frac{s}{\sqrt{7}} - \frac{\sqrt{5}}{2} + -\frac{7\sqrt{3}}{\sqrt{7}}sin\frac{s}{\sqrt{7}}cosv + \frac{14}{\sqrt{7}}sin\frac{s}{\sqrt{7}}sinv,\right.$$
$$-2 + \sqrt{3}sin\frac{s}{\sqrt{7}} + \frac{7\sqrt{3}}{\sqrt{7}}cos\frac{s}{\sqrt{7}}cosv - \frac{14}{\sqrt{7}}cos\frac{s}{\sqrt{7}}sinv,$$
$$5 + cos\frac{2s}{\sqrt{7}} - \frac{14}{\sqrt{7}}sin\frac{2s}{\sqrt{7}}cosv - \frac{7\sqrt{3}}{\sqrt{7}}sin\frac{2s}{\sqrt{7}}sinv, \quad (34)$$
$$\left.sin\frac{2s}{\sqrt{7}} + \frac{14}{\sqrt{7}}cos\frac{2s}{\sqrt{7}}cosv + \frac{7\sqrt{3}}{\sqrt{7}}cos\frac{2s}{\sqrt{7}}sinv\right).$$

Then for $r = 7$, the unit normal vector fields in equation (35) of tube surface are given as

$$\boldsymbol{U}_1 = \frac{1}{\sqrt{16 + 3cos^2v + 6\sqrt{3}sin2v}}(0, -\frac{14}{\sqrt{19}}sinv, 0, \frac{19cosv + 6\sqrt{3}sinv}{\sqrt{19}})$$
$$\boldsymbol{U}_2 = \frac{\sqrt{4 + cos^2v + 3\sqrt{3}cosvsinv}}{\sqrt{16 + 3cos^2v + 6\sqrt{3}sin2v}}(\frac{cosv}{2}, \frac{-cosv\sqrt{19}(19cosv + 6\sqrt{3}sinv)}{38(16 + 3cos^2v + 6\sqrt{3}sin2v)}, \frac{sinv}{2}, \frac{-7cosvsinv}{(16 + 3cos^2v + 6\sqrt{3}sin2v)\sqrt{19}}) \quad (35)$$

Gaussian and mean curvatures in equations (36) and (37) of tube surface are given as

$$K_1 = \frac{-1}{48\sqrt{3}sin2v + 64 + cos^2v(21\sqrt{3}cosvsinv - 105cos^2v + 136)}$$
$$H_1 = \frac{sinv}{2(4 + cos^2v + 3\sqrt{3}cosvsinv)\sqrt{4\sqrt{3}sin2v + 16 + 3cos^2v}} \quad (36)$$

and

$$K_2 = \frac{cos^2v\left(2142cos^4v + 2394\sqrt{3}cos^3vsinv + 8076cos^2v - 4425\sqrt{3}cosvsinv - 11726\right) - 2048 - 2328\sqrt{3}sin2v}{392(-256 + cos^2v(294cos^4v + 294\sqrt{3}cos^3vsinv + 959cos^2v - 294\sqrt{3}sin2v - 1472) + 288\sqrt{3}sin2v)}$$
$$H_2 = -\frac{264 + 3\sqrt{3}cosvsinv(129 + 28cos^2v) + 4cos^2v(134 - 105cos^2v)}{\left[64 + cos^2v(136 - 105cos^2v) + \sqrt{3}cosvsinv(96 + 21cos^2v)\right]\sqrt{3\sqrt{3}cosvsinv + 4 + cos^2v}\sqrt{4\sqrt{3}sin2v + 16 + 3cos^2v}} \quad (37)$$

respectively. Finally for $r = 7$, a tube surface shown in Figure 1 is parametrized as

$$\psi(s,v) = \left(\sqrt{3}cos\frac{s}{\sqrt{7}} - \frac{\sqrt{5}}{2} + -\frac{7\sqrt{3}}{\sqrt{7}}sin\frac{s}{\sqrt{7}}cosv + \frac{14}{\sqrt{7}}sin\frac{s}{\sqrt{7}}sinv,\right.$$
$$-2 + \sqrt{3}sin\frac{s}{\sqrt{7}} + \frac{7\sqrt{3}}{\sqrt{7}}cos\frac{s}{\sqrt{7}}cosv - \frac{14}{\sqrt{7}}cos\frac{s}{\sqrt{7}}sinv,$$
$$\left.5 + cos\frac{2s}{\sqrt{7}} - \frac{14}{\sqrt{7}}sin\frac{2s}{\sqrt{7}}cosv - \frac{7\sqrt{3}}{\sqrt{7}}sin\frac{2s}{\sqrt{7}}sinv\right)$$

in projection space, xyz. Finally for $r = 7$, a tube surface shown in Figure 1 is parametrized as

$$\psi(s,v) = \left(\sqrt{3}cos\frac{s}{\sqrt{7}} - \frac{\sqrt{5}}{2} + -\frac{7\sqrt{3}}{\sqrt{7}}sin\frac{s}{\sqrt{7}}cosv + \frac{14}{\sqrt{7}}sin\frac{s}{\sqrt{7}}sinv,\right.$$
$$-2 + \sqrt{3}sin\frac{s}{\sqrt{7}} + \frac{7\sqrt{3}}{\sqrt{7}}cos\frac{s}{\sqrt{7}}cosv - \frac{14}{\sqrt{7}}cos\frac{s}{\sqrt{7}}sinv,$$
$$\left.sin\frac{2s}{\sqrt{7}} + \frac{14}{\sqrt{7}}cos\frac{2s}{\sqrt{7}}cosv + \frac{7\sqrt{3}}{\sqrt{7}}cos\frac{2s}{\sqrt{7}}sinv\right)$$

in projection space, xyt. Finally for $r = 7$, a tube surface shown in Figure 1 is parametrized as

$$\psi(s,v) = \left(\sqrt{3}cos\frac{s}{\sqrt{7}} - \frac{\sqrt{5}}{2} + -\frac{7\sqrt{3}}{\sqrt{7}}sin\frac{s}{\sqrt{7}}cosv + \frac{14}{\sqrt{7}}sin\frac{s}{\sqrt{7}}sinv,\right.$$
$$5 + cos\frac{2s}{\sqrt{7}} - \frac{14}{\sqrt{7}}sin\frac{2s}{\sqrt{7}}cosv - \frac{7\sqrt{3}}{\sqrt{7}}sin\frac{2s}{\sqrt{7}}sinv,$$
$$\left.sin\frac{2s}{\sqrt{7}} + \frac{14}{\sqrt{7}}cos\frac{2s}{\sqrt{7}}cosv + \frac{7\sqrt{3}}{\sqrt{7}}cos\frac{2s}{\sqrt{7}}sinv\right)$$

in projection space, xzt. Finally for $r = 7$, a tube surface shown in Figure 1 is parametrized as

$$\psi(s,v) = \left(-2 + \sqrt{3}sin\frac{s}{\sqrt{7}} + \frac{7\sqrt{3}}{\sqrt{7}}cos\frac{s}{\sqrt{7}}cosv - \frac{14}{\sqrt{7}}cos\frac{s}{\sqrt{7}}sinv,\right.$$
$$5 + cos\frac{2s}{\sqrt{7}} - \frac{14}{\sqrt{7}}sin\frac{2s}{\sqrt{7}}cosv - \frac{7\sqrt{3}}{\sqrt{7}}sin\frac{2s}{\sqrt{7}}sinv,$$
$$\left.sin\frac{2s}{\sqrt{7}} + \frac{14}{\sqrt{7}}cos\frac{2s}{\sqrt{7}}cosv + \frac{7\sqrt{3}}{\sqrt{7}}cos\frac{2s}{\sqrt{7}}sinv\right)$$

in projection space, yzt.

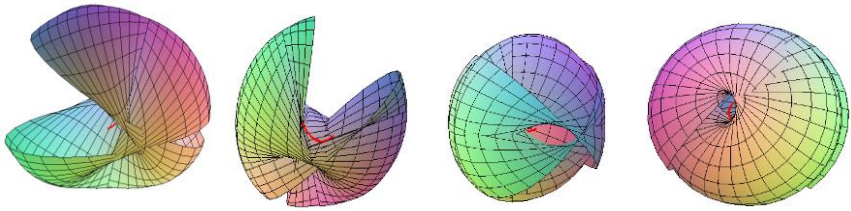

Figure 1 Tube surfaces in xyz, xyt, xzt and yzt projection spaces.

The tube surface formed by the Frenet vectors $\boldsymbol{T}$ and $\boldsymbol{B}_2$ in $\mathbb{E}^4$ is parametrized as

$$\begin{aligned}\psi(s,v) = \Big(&\sqrt{3}cos\frac{s}{\sqrt{7}} - \frac{\sqrt{5}}{2} + r\Big(-\frac{\sqrt{3}}{\sqrt{7}}sin\frac{s}{\sqrt{7}}cosv + \frac{4\sqrt{3}}{\sqrt{57}}cos\frac{s}{\sqrt{7}}sinv\Big),\\ &-2 + \sqrt{3}sin\frac{s}{\sqrt{7}} + r\Big(\frac{\sqrt{3}}{\sqrt{7}}cos\frac{s}{\sqrt{7}}cosv + \frac{4\sqrt{3}}{\sqrt{57}}sin\frac{s}{\sqrt{7}}sinv\Big),\\ &5 + cos\frac{2s}{\sqrt{7}} + r\Big(-\frac{2}{\sqrt{7}}sin\frac{2s}{\sqrt{7}}cosv - \frac{3}{\sqrt{57}}cos\frac{2s}{\sqrt{7}}sinv\Big),\\ &sin\frac{2s}{\sqrt{7}} + r\Big(\frac{2}{\sqrt{7}}cos\frac{2s}{\sqrt{7}}cosv - \frac{3}{\sqrt{57}}sin\frac{2s}{\sqrt{7}}sinv\Big)\Big)\end{aligned}$$

Hence for $r = 7$, it is easily say that

$$\begin{aligned}\psi(s,v) = \Big(&\sqrt{3}cos\frac{s}{\sqrt{7}} - \frac{\sqrt{5}}{2} - \frac{7\sqrt{3}}{\sqrt{7}}sin\frac{s}{\sqrt{7}}cosv + \frac{28\sqrt{3}}{\sqrt{57}}cos\frac{s}{\sqrt{7}}sinv,\\ &-2 + \sqrt{3}sin\frac{s}{\sqrt{7}} + \frac{7\sqrt{3}}{\sqrt{7}}cos\frac{s}{\sqrt{7}}cosv + \frac{28\sqrt{3}}{\sqrt{57}}sin\frac{s}{\sqrt{7}}sinv,\\ &5 + cos\frac{2s}{\sqrt{7}} - \frac{14}{\sqrt{7}}sin\frac{2s}{\sqrt{7}}cosv - \frac{21}{\sqrt{57}}cos\frac{2s}{\sqrt{7}}sinv,\\ &sin\frac{2s}{\sqrt{7}} + \frac{14}{\sqrt{7}}cos\frac{2s}{\sqrt{7}}cosv - \frac{21}{\sqrt{57}}sin\frac{2s}{\sqrt{7}}sinv\Big)\end{aligned} \tag{38}$$

Then for $r = 7$, the unit normal vector fields in equation (39) of tube surface are given as

$$\boldsymbol{U}_1 = \frac{1}{\sqrt{18816 + 165cos^2v - 196\sqrt{19}sinv}}\Big(133cosv, \frac{7(-19 + 2\sqrt{19}sinv)}{\sqrt{19}}, 19cosv, 133sinv\Big) \tag{39}$$

$$\boldsymbol{U}_2 = \frac{\sqrt{49 + 46cos^2v}\sqrt{3724 + 3135cos^2v}}{\Gamma\big[18816 + 165cos^2v - 196\sqrt{19}sinv\big]}\Big(\frac{\sqrt{19}cosv(98\sqrt{19}sinv - 165cos^2v - 196)}{2}, \frac{2(98sinv + \sqrt{19}cos^2v)}{\sqrt{19}},$$
$$7\sqrt{19}cosv\,(190 - \sqrt{19}sinv), \frac{-\sqrt{19}sinv(98\sqrt{19}sinv - 165cos^2v - 196)}{2}\Big).$$

respectively, where

$$\Gamma = \sqrt{15cos^2v(2089132 + 1815cos^2v) - 98\sqrt{19}(165cosvsin2v - 392sinv) + 3687936}.$$

Gaussian and mean curvatures in equations (40) and (41) of tube surface are given as

$$\begin{aligned}
K_1 = \; & \frac{1}{3724\Delta}\big[\sqrt{19}cos^2vsinv(156408\sqrt{3} - 84966 + 689871) + cosvsinv(1038597 + 256956\sqrt{3}) \\
& + cos^4v(9693441 + 312816\sqrt{3} + 44688\sqrt{57}) - \sqrt{19}cosv(500346 + 44688\sqrt{3}) - 406847 \\
& + sinv\sqrt{3}(2013012cos^3v + 70756) + cos^3v(500346\sqrt{19} - 24738\sqrt{3}) - 2665322cos^2v\big] \\
H_1 = \; & \frac{cos^4v(4332\sqrt{3} - 7581) - cosvsinv(16758\sqrt{3} + 11913) - 266\sqrt{19}sinv + cos^2vsinv(532\sqrt{19} - 1083cosv)}{532\big(4 + 3\sqrt{3}cosvsinv + cos^2v\big)\sqrt{18816 - 196\sqrt{19}sinv + 165cos^2v}} \\
& + \frac{\sqrt{19}cosv(3724 + 168\sqrt{3}) - cos^2v(6498\sqrt{3} + 96026 + 30324\sqrt{3}) - \sqrt{19}cos^3v(3724 + 168\sqrt{3}) + 2427}{532\big(4 + 3\sqrt{3}cosvsinv + cos^2v\big)\sqrt{18816 - 196\sqrt{19}sinv + 165cos^2v}}
\end{aligned} \tag{40}$$

and

$$\begin{aligned}
K_2 = \; & \frac{1}{\Theta}\big[2cos^4v(1131735\sqrt{19} + 5943504\sqrt{3}\sqrt{19} - 94125696\sqrt{3} - 139632652cos^2v - 4014243464) \\
& - 47045881 - \sqrt{3}cos^2v(11887008\sqrt{19} + 249627168) + cos^2v(8468249869 + 2688728\sqrt{19}) \\
& + \sqrt{3}cosvsin2v\big(60060672\sqrt{19} + 11887008\big) - cosvsin2v\big(30224768\sqrt{19} + 12771458\big) \\
& + cos^4vsinv(30331392\sqrt{19} + 20013840\sqrt{3} + 1053360\sqrt{3}\sqrt{19}) + \sqrt{19}cos^7v(14747040\sqrt{3} - 6144600) \\
& + \sqrt{19}cos^3v\big(700707840 - 51480576\sqrt{3}\big) + cos^5v(36733536\sqrt{3}\sqrt{19} - 694563240\sqrt{19} + 63377160) \\
& + cos^6vsinv(12414600\sqrt{3}cosv - 72053520\sqrt{19}) + sin2v(14856594\sqrt{3} + 576156\sqrt{19}) \\
& - cos^5vsinv(1098133120 + 554131150\sqrt{3}) + cosv(60657300cos^7v - 71635396 + 8258236cos^2v) \\
& + cos^3vsinv(3328898496\sqrt{3} - 37642192\sqrt{19} - 1456158480)\big] \\
H_2 = \; & \frac{-7(294\sqrt{3}sin2v + 784 + 196cos^2v)^{-1}\sqrt{3135cos^2v + 3724}\sqrt{49 - 46cos^2v}}{4\sqrt{165cos^2v + 196}\sqrt{196\sqrt{19}sinv - 18816 - 165cos^2v}}\big[cos^5v(44688\sqrt{3} + 7644) - 6859 \\
& - cos^4vsinv(11172 + 6384\sqrt{3}) - cos^3v(22344\sqrt{3} + 14224 + 21448\sqrt{19}sinv) + cos^4v\big(13056\sqrt{19} + 63840\sqrt{3}\sqrt{19}\big) \\
& + cos^2vsinv(9576\sqrt{3} - 134064) + \sqrt{57}cos^3vsinv(6684 + 3960cos^2v) + 990\sqrt{19}cos^6v + cosv(6580 - 22344\sqrt{3}) \\
& + cos^2v\big(13419 - 95760\sqrt{3}\sqrt{19} + 14112\sqrt{19}\big) + sin2v(1176\sqrt{19}\sqrt{3} + 2166\sqrt{3} + 85036\sqrt{19})\big]
\end{aligned} \tag{41}$$

respectively, where

$$\begin{aligned}
\Delta = \; & cosvsinv\big(56448\sqrt{3} - 196\sqrt{19}cosv + 495\sqrt{3}cos^2vs\big) + 75264 - 784\sqrt{19}sinv \\
& + cos^2v(19476 + 165cos^2v) + 588\sqrt{57}cosv(cosv - 1).
\end{aligned}$$

and

$$\begin{aligned}
\Theta = \; & \sqrt{3}cos^3v(2620863sinv + 1764\sqrt{19}) + \sqrt{3}cosv(2765952sinv - 28812\sqrt{19}) + cos^4v(903981 - 9016\sqrt{19}sinv) \\
& - 38416\sqrt{19}sinv + 3687936 + \sqrt{57}cos^5v(27048 + 22770sinv) + 7590cos^6v + cos^2v\big(4416468 - 45668\sqrt{19}sinv\big).
\end{aligned}$$

Finally for $r = 7$, a tube surface shown in Figure 2 is parametrized as

$$\begin{aligned}
\psi(s,v) = \; & \Big(\sqrt{3}cos\frac{s}{\sqrt{7}} - \frac{\sqrt{5}}{2} - \frac{7\sqrt{3}}{\sqrt{7}}sin\frac{s}{\sqrt{7}}cosv + \frac{28\sqrt{3}}{\sqrt{57}}cos\frac{s}{\sqrt{7}}sinv, \\
& -2 + \sqrt{3}sin\frac{s}{\sqrt{7}} + \frac{7\sqrt{3}}{\sqrt{7}}cos\frac{s}{\sqrt{7}}cosv + \frac{28\sqrt{3}}{\sqrt{57}}sin\frac{s}{\sqrt{7}}sinv, \\
& 5 + cos\frac{2s}{\sqrt{7}} - \frac{14}{\sqrt{7}}sin\frac{2s}{\sqrt{7}}cosv - \frac{21}{\sqrt{57}}cos\frac{2s}{\sqrt{7}}sinv\Big)
\end{aligned}$$

in projection space, xyz. Finally for $r = 7$, a tube surface shown in Figure 2 is parametrized as

$$\psi(s,v) = \left(\sqrt{3}cos\frac{s}{\sqrt{7}} - \frac{\sqrt{5}}{2} - \frac{7\sqrt{3}}{\sqrt{7}}sin\frac{s}{\sqrt{7}}cosv + \frac{28\sqrt{3}}{\sqrt{57}}cos\frac{s}{\sqrt{7}}sinv,\right.$$
$$-2 + \sqrt{3}sin\frac{s}{\sqrt{7}} + \frac{7\sqrt{3}}{\sqrt{7}}cos\frac{s}{\sqrt{7}}cosv + \frac{28\sqrt{3}}{\sqrt{57}}sin\frac{s}{\sqrt{7}}sinv,$$
$$\left.sin\frac{2s}{\sqrt{7}} + \frac{14}{\sqrt{7}}cos\frac{2s}{\sqrt{7}}cosv - \frac{21}{\sqrt{57}}sin\frac{2s}{\sqrt{7}}sinv\right)$$

in projection space, xyt. Finally for $r = 7$, a tube surface shown in Figure 2 is parametrized as

$$\psi(s,v) = \left(\sqrt{3}cos\frac{s}{\sqrt{7}} - \frac{\sqrt{5}}{2} - \frac{7\sqrt{3}}{\sqrt{7}}sin\frac{s}{\sqrt{7}}cosv + \frac{28\sqrt{3}}{\sqrt{57}}cos\frac{s}{\sqrt{7}}sinv,\right.$$
$$5 + cos\frac{2s}{\sqrt{7}} - \frac{14}{\sqrt{7}}sin\frac{2s}{\sqrt{7}}cosv - \frac{21}{\sqrt{57}}cos\frac{2s}{\sqrt{7}}sinv,$$
$$\left.sin\frac{2s}{\sqrt{7}} + \frac{14}{\sqrt{7}}cos\frac{2s}{\sqrt{7}}cosv - \frac{21}{\sqrt{57}}sin\frac{2s}{\sqrt{7}}sinv\right)$$

in projection space, xzt. Finally for $r = 7$, a tube surface shown in Figure 2 is parametrized as

$$\psi(s,v) = \left(-2 + \sqrt{3}sin\frac{s}{\sqrt{7}} + \frac{7\sqrt{3}}{\sqrt{7}}cos\frac{s}{\sqrt{7}}cosv + \frac{28\sqrt{3}}{\sqrt{57}}sin\frac{s}{\sqrt{7}}sinv,\right.$$
$$5 + cos\frac{2s}{\sqrt{7}} - \frac{14}{\sqrt{7}}sin\frac{2s}{\sqrt{7}}cosv - \frac{21}{\sqrt{57}}cos\frac{2s}{\sqrt{7}}sinv,$$
$$\left.sin\frac{2s}{\sqrt{7}} + \frac{14}{\sqrt{7}}cos\frac{2s}{\sqrt{7}}cosv - \frac{21}{\sqrt{57}}sin\frac{2s}{\sqrt{7}}sinv\right)$$

in projection space, yzt.

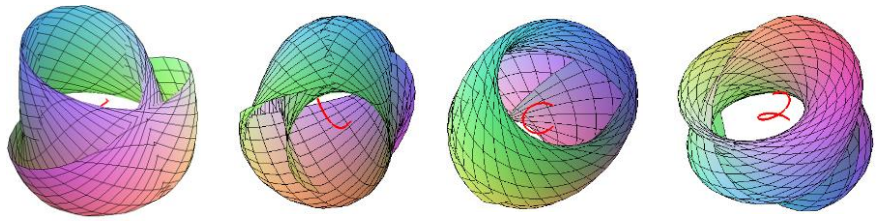

Figure 2 Tube surfaces in xyz, xyt, xzt and yzt projection spaces.

The visualization of all tube surfaces are given with using Maple programme.

CONCLUSION

In this study, using the parametrization of the tube, we investigate the tube surface generated by Frenet vectors $\boldsymbol{T}$, $\boldsymbol{B}_1$ and $\boldsymbol{B}_2$. The unit normal vector fields of this surface are obtained. In addition, Gaussian curvatures, mean curvatures, and first and second fundamental forms of this tube surface are calculated. An example is given and plotted in projection spaces.

REFERENCES

Abdel-Aziz H. S. & Saad M. K. (2011). Weingarten timelike tube surfaces around a spacelike curve, Int. Journal of Math. Analysis, 5, 1225-1236.

Alessio, O. (2009). Differential geometry of intersection curves in R^4 of three implicit surfaces, Comput. Aided Geom. Des., 26, 455-471.

Bayram, B. K., Bulca B., Arslan K. & Öztürk G. (2009). Superconformal ruled surfaces in E^4, Math. Commun., 14(2), 235-244.

Bulca B., Arslan K., Bayram B., & Öztürk G. (2017). Canal surfaces in 4-dimensional Euclidean space, 7(1), 83-89.

Chen B. Y. & Piccini P. (1987). Submanifolds with finite type Gauss map, Bulletin of the Australian Mathematical. Society, 35(2), 161-186.

Dede, M. (2013). Tubular surfaces in Galilean space, Math. Commun., 18(2013), 209-217.

Dede, M., Ekici, C. & Tozak, H. (2015). Directional tubular surfaces, International Journal of Algebra, 9(12), 527-535.

Dede, M., Ekici, C., & Koçak, M. (2024). Reconstruction of a Ruled Surface in 3-dimensional Euclidean Space. Erzincan University Journal of Science and Technology, 17(1), 259-267.

Doğan, F. & Yaylı, Y. (2017). The relation between parameter curves and lines of curvature on canal surfaces, Kuwait Journal of Science, 44(1), 29-35.

Ekici, C., Dede, M & Tozak, H. (2017). Timelike directional tubular surfaces, Int. J. Mathematical Anal., 8(5), 1-11.

Ekici, A., Akça, Z., & Ekici, C. (2023). The ruled surfaces generated by quasi-vectors in E4 space. 7. International Biltek Congress on Current Developments in Science, Technology and Social Sciences (p. 400-418).

Ekici Coşkun, A., & Akça, Z. (2023). The Ruled Surfaces Generated by Quasi-Vectors in E^4 Space. Hagia Sophia Journal of Geometry, 5(2), 6-17.

Ganchev G. & Milousheva V. (2008). On the theory of surfaces in the four-dimensional Euclidean space, Kodai Math. J., 31, 183–198.

Gluck, H. (1966). Higher curvatures of curves in Euclidean space. Amer. Math. Monthly,

73, 699-704.

Gray, A. (1993). Modern differential geometry of curves and surface, CRS Press, Inc.

Kaymanlı, U. G., Ekici, C. & Dede, M. (2018). Directional canal surfaces in E^3, 5th International Symposium on Multidisciplinary Studies (ISMS), 90-107.

Kaymanlı, U. G., Ekici, C. & Ünlütürk, Y. (2022). Constant Angle Ruled Surfaces due to The Bishop Frame in Minkowski 3-space. Journal of Science and Arts, 22(1), 105-114.

Kim, Y.H., Liu, H. & Qian, J. (2016). Some characterizations of canal surfaces, Bulletin of the Korean Mathematical Society, 53(2), 461-477.

Kişi, İ., Öztürk, G., Arslan, K. (2019). A new type of canal surface in Euclidean 4-space IE 4. Sakarya Üniversitesi Fen Bilimleri Enstitüsü Dergisi, 23(5), 801 - 809.

Kızıltuğ, S., Dede, M. & Ekici, C. (2019). Tubular Surfaces with Darboux Frame in Galilean 3-space, Facta Universitatis, Series: Mathematics and Informatics, 34(2), 253-260.

Patrikalakis, N.M., Sakkalis, T. & Yu, G. (1998). Analysis and applications of tube surfaces, Computer Aided Geometric Design, 15, 437-458.

Mello, L. F. (2009). Orthogonal asymptotic lines on surfaces immersed in R^4, Rocky Mountain Journal of Mathematics, 39(5), 1597-1612.

Óláh-Gál, R. & Pál, L. (2009). Some notes on drawing twofolds in 4-dimensional Euclidean Space, Acta Universitatis Sapientiae, Informatica, 1(2), 125-134.

Şekerci, A. G. & Çimdiker, M. (2019). Bonnet canal surfaces, DEU FMD., 21(61), 195-200.

Tozak, H., Ekici, C. & Dede, M., (2019). A Study on Directional Generalized Tubes. 17th International Geometry Symposium, 2(2), 126-128. (Tam Metin Bildiri/Sözlü Sunum).

Uçum, A. & İlarslan, K. (2016). New types of canal surfaces in Minkowski 3-space, Adv. Appl. Clifford Algebras, 29, 449-468.

Xu, Z., Feng, R. & Sun, J.G. (2006). Analytic and algebraic properties of canal surfaces. Journal of Computational and Applied Mathematics, 195, 220-228.

Yağbasan, B. & Ekici, C. (2023). Tube surfaces in 4 dimensional Euclidean space. 4th International Black Sea Modern Scientific Research Congress, (p.1951-1962).

Yağbasan, B., Tozak, H., & Ekici, C. (2023). The curvatures of the tube surface in 4 dimensional Euclidean space . 7.International Biltek Congress On Current Developments In Science, Technology And Social Sciences (p. 419-436).

Yağbasan, B., Ekici, C. & Tozak, H. (2023a). Directional Tube Surface in Euclidean 4-Space. Hagia Sophia Journal of Geometry (HSJG), 5(2), 18-30.

Chapter 2

Relations Between Quasi Frame and Frenet Frame In Euclidean 4-Space

Buket GEZER[1]
Cumali EKİCİ[2]

[1] Eskişehir Osmangazi Üniversitesi, Department of Mathematics and Computer Science, Eskişehir. buketgezer26@windowslive.com, 05535318471, ORCID. 0000-0001-8880-4043
[2] Prof. Dr., Eskişehir Osmangazi Üniversitesi, Department of Mathematics and Computer Science, Eskişehir. cekici@ogu.edu.tr, 05323056666, ORCID. 0000-0002-3247-5727

ÖZET

Bu çalışmada 4-boyutlu Öklid uzayında regüler bir eğri için Frenet çatısı ve quasi çatısı hakkında bilgi verilmiştir. 4-boyutlu Öklid uzayında bir uzay eğrisi, örneğin xy-düzlemindeki $\boldsymbol{k}_x$ ve $\boldsymbol{k}_y$ izdüşüm vektörleri olmak üzere üzere $\boldsymbol{t}$ birim teğet, $\boldsymbol{n}_q$ birim quasi normal, $\boldsymbol{b}_{q1}$ birinci birim quasi binormal ve $\boldsymbol{b}_{q2}$ ise ikinci birim quasi binormal kullanılarak quasi çatısı ve quasi eğrilikleri verilmiştir. Sonra 4-boyutlu Öklid uzayında bir uzay eğrisi için Frenet çatısı ve quasi çatısı arasındaki geçiş matrisleri hesaplanmıştır. Ayrıca bu çatıların eğrilikleri arasındaki bağıntılar da verilmiştir. Bulunan bu hesapların daha anlaşılabilir olması adına 4-boyutlu Öklid uzayında bir uzay eğrisi için quasi çatı ve quasi eğriliklerinin elde edildiği bir örnek yapılmıştır.

Anahtar Kelimeler: Quasi çatı, Frenet çatısı, quasi eğrilikleri

ABSTRACT

In this paper we give information about the Frenet frame and quasi frame for a regular curve in 4-dimensional Euclidean space. For a space curve in 4-dimensional Euclidean space, e.g. $\boldsymbol{k}_x$ and $\boldsymbol{k}_y$ are projection vectors in the xy -plane, $\boldsymbol{t}$ is the unit tangent, $\boldsymbol{n}_q$ is the unit quasi normal, $\boldsymbol{b}_{q1}$ is the first unit quasi binormal and $\boldsymbol{b}_{q2}$ is the second unit quasi binormal, the quasi frame and quasi curvatures are given. Then, for a space curve in 4-dimensional Euclidean space, the transition matrices between the Frenet frame and the quasi frame are calculated. The relations between the curvatures of these frames are also given. In order to make these calculations more understandable, an example is given in which the quasi frame and quasi curvatures are obtained for a space curve in 4-dimensional Euclidean space.

Keywords: Quasi frame, Frenet frame, quasi curvatures

INTRODUCTION

The study of curves with in Euclidean 3-space is a key area in differential geometry, with the Frenet frame being particularly significant in classical geometry. However, the Frenet frame has certain limitations in practical applications, such as its inability to be defined when curvature is zero. Additionally, a major drawback of the Frenet frame is the unwanted rotation around the tangent vector (Bloomenthal, 1990). It's well understood that for a differentiable curve in an open interval, a set of mutually orthogonal unit vectors can be constructed at every point, known as the Frenet frame or moving frame vectors. The changes in these vectors along the curve define the curvatures of the curve. The collection of these vectors and curvatures is known as the Frenet apparatus of the curve. Recently, the theory of degenerate submanifolds has attracted attention, with extensions of classical differential geometry concepts being applied to Minkowski space (Turgut, 2009; Turgut and Yılmaz, 2008; Öztürk et al., 2014) and Galilean space (Magden and Yılmaz, 2014). The Bishop frame (Bishop, 1975), also called the parallel transport frame, provides an alternative framework for describing a moving frame, which remains well-defined even when the curve's second derivative is zero. By parallel transporting each element of an orthonormal frame along the curve in Euclidean 4-space, we achieve this frame. When curvatures vanish at certain points, the Frenet frame cannot be used, and the Bishop frame takes its place (Bishop, 1975). For curves with unit speed α in 4-dimensional Euclidean space E^4, where $\alpha'' \neq 0$, Frenet curvature functions k_1 , k_2 and k_3 are provided by Alessio (Alessio, 2009). This concept was later extended to 4-dimensional space with the introduction of a parallel transport frame (Çelik et al., 2014). In four-dimensional Euclidean space, this parallel transport frame is known as the Bishop frame, and it has been discussed in various studies (Ateş et al., 2019; Körpınar and Turhan, 2013; Özdemir et al., 2015; Hanson and Ma, 1995). Klok (1987) introduced sweep surfaces using rotation-minimizing frames, and a reliable computation of the rotation-minimizing frame for such surfaces was presented by Wang et al. (2008). Coquillart's work (Coquillart, 1987) inspired Mustafa to develop a new adapted frame for space curves, termed the quasi-frame (O'Neil, 1983). Çelik et al. (2014) conducted further investigations into the parallel transport frame within four dimensional space. They introduced the quasi frame as an alternative to the Frenet frame, which offers computational ease without sacrificing precision. This quasi frame can be viewed as an extension of the parallel transport frame. The concept of the quasi frame is based on a constant projection vector and the Euclidean angle between the principal normal and the quasi-normal vector field (Dede et al., 2015). When the second derivative vanishes, the frame rotates by a Euclidean

angle, with the quasi-normal being the unit vector orthogonal to both the tangent and projection vectors. Several studies have been carried out in 4-dimensional space using this frame (Gezer and Ekici, 2023; Ekici Coşkun and Akça, 2023; Yağbasan et. al., 2023). This paper is structured as follows: We provide some basic definitions of Euclidean 4-space (E^4) and the quasi-frame in 4-space. We then introduce both the Frenet and quasi-frames for curves in 4-dimensional Euclidean space. Additionally, we derive the transition matrices between the Frenet and quasi-frames for a space curve in 4-dimensional space and establish the relationships between the curvatures of the two frames in Euclidean 4-space (E^4).

PRELIMINARIES

Let $\alpha(s) = \alpha: I \subset \mathbb{R} \to E^4$ be any space curve in Euclidean 4-space. Let $\mathbf{u} = (u_1, u_2, u_3, u_4)$, $\mathbf{v} = (v_1, v_2, v_3, v_4)$ and $\mathbf{w} = (w_1, w_2, w_3, w_4)$ be three vectors in E^4, with the standard inner product as $< \mathbf{u}, \mathbf{v} >= u_1v_1 + u_2v_2 + u_3v_3 + u_4v_4$. The norm of vector of E^4 is given by $\|\mathbf{u}\| = \sqrt{g(\mathbf{u}, \mathbf{u})}$. The curve α is said to be parametrized by arc length s if $g(\alpha', \alpha') = 1$. The vector product of **u**, **v**, **w** is given by the determinant as follows

$$\mathbf{u} \times \mathbf{v} \times \mathbf{w} = \begin{bmatrix} e_1 & e_2 & e_3 & e_4 \\ u_1 & u_2 & u_3 & u_4 \\ v_1 & v_2 & v_3 & v_4 \\ w_1 & w_2 & w_3 & w_4 \end{bmatrix},$$

where $\boldsymbol{e}_1 \wedge \boldsymbol{e}_2 \wedge \boldsymbol{e}_3 = \boldsymbol{e}_4$, $\boldsymbol{e}_2 \wedge \boldsymbol{e}_3 \wedge \boldsymbol{e}_4 = \boldsymbol{e}_1$, $\boldsymbol{e}_3 \wedge \boldsymbol{e}_4 \wedge \boldsymbol{e}_1 = \boldsymbol{e}_2$ and $\boldsymbol{e}_4 \wedge \boldsymbol{e}_1 \wedge \boldsymbol{e}_2 = -\boldsymbol{e}_3$ (Allesio, 2009; Elsayied et al., 2021).

Let u, v and w vectors in E^4. If these vectors are linearly independent, then the vector $\mathbf{u} \wedge \mathbf{v} \wedge \mathbf{w} \in E^4$ is orthogonal to u, v, and w, and swapping any two vectors reverses the sign. If the vectors are linearly dependent, the cross product results in the zero vector. In four dimensions, $\mathbf{u} \wedge \mathbf{v}$ is undefined, as there is no determinant calculation of the 3 x 4 (Alessio, 2009).

The Frenet vectors for the curve with unit speed $\alpha: I \to E^4$ in Euclidean 4-space E^4 with $\alpha'' \neq 0$ are given by

$$\begin{aligned} \boldsymbol{t}(\boldsymbol{s}) &= \alpha'(s) & \boldsymbol{n}(s) &= \frac{\alpha''(s)}{\|\alpha''(s)\|} \\ \boldsymbol{b}_2(s) &= \frac{\alpha'(s) \wedge \alpha''(s) \wedge \alpha'''(s)}{\|\alpha'(s) \wedge \alpha''(s) \wedge \alpha'''(s)\|} & \boldsymbol{b}_1(s) &= \boldsymbol{b}_2(s) \wedge \boldsymbol{t}(\boldsymbol{s}) \wedge \boldsymbol{n}(s) \end{aligned} \quad (1)$$

(Alessio, 2009).

Given an $\alpha(t) = \alpha: I \subset \mathbb{R} \rightarrow E^4$ curve with arc parameter in 4-dimensional space. Let $\boldsymbol{t}(\boldsymbol{s}) = \alpha'(s)$, representing the unit tangent vector of α\alphaα at the point s. The first Serret-Frenet curvature of α is defined as $k_1(\mathrm{s}) = \|\alpha''\|$. Then we have the Serret-Frenet formulae (Gluck, 1966):

$$\begin{aligned} \boldsymbol{t}'(s) &= k_1(s)\boldsymbol{n}(s) \\ \boldsymbol{n}'(s) &= -k_1(s)\boldsymbol{t}(s) + k_2(s)\boldsymbol{b}_1(s) \\ \boldsymbol{b}_1'(s) &= -k_2(s)\boldsymbol{n}(s) + k_3(s)\boldsymbol{b}_2(s) \\ \boldsymbol{b}_2'(s) &= -k_3(s)\boldsymbol{b}_1(s) \end{aligned} \tag{2}$$

Here Frenet curvatures $\kappa = k_1$, $\tau = k_2$ and $\eta = k_3$ are the first, second and third curvature functions of the α curve, respectively (Öztürt et al., 2017).

The transformation matrix should be chosen to keep the tangent vector **t** unchanged. Then, we consider three possible planes of rotations for the Frenet vectors, $\{\boldsymbol{t}, \boldsymbol{n}, \boldsymbol{b}_1, \boldsymbol{b}_2\}$**.** The first rotation is in the space spanned by $\boldsymbol{b}_1$ and $\boldsymbol{b}_2$ with an angle ϕ. The second rotation in the space plane spanned by $\boldsymbol{n}$ and $\boldsymbol{b}_2$ with an angle θ. The third rotation in the space plane spanned by $\boldsymbol{n}$ and $\boldsymbol{b}_1$ with an angle ψ (Elsayied et. al. 2021). The transformation matrix M is of the form

$$M = \begin{bmatrix} 1 & 0 & 0 & 0 \\ 0 & cos\theta cos\psi & cos\theta sin\psi & -sin\theta \\ 0 & cos\psi sin\theta sin\phi - cos\phi sin\psi & cos\phi cos\psi + sin\theta sin\phi sin\psi & cos\theta sin\phi \\ 0 & cos\phi cos\psi sin\theta + sin\phi sin\psi & -cos\psi sin\phi + cos\phi sin\theta sin\psi & cos\theta cos\phi \end{bmatrix}.$$

The quasi frame is an alternative to the Frenet frame, and involves a fixed unit vector $\boldsymbol{k}$. For a curve $\alpha(t)$ in E^3, the quasi-frame consist of three orthogonal vectors called the unit tangent $\boldsymbol{t}$, the quasi-normal $\boldsymbol{n}_q$ and the quasi-binormal $\boldsymbol{b}_q$ with a Euclidean angle θ between the principal normal and quasi-normal. The quasi frame $\{\boldsymbol{t}, \boldsymbol{n}_q, \boldsymbol{b}_q, \boldsymbol{k}\}$ is defined by

$$\boldsymbol{t} = \frac{\alpha'}{||\alpha'||}, \qquad \boldsymbol{n}_q = \frac{\boldsymbol{t} \wedge \boldsymbol{k}}{||\boldsymbol{t} \wedge \boldsymbol{k}||}, \quad \boldsymbol{b}_q = \boldsymbol{t} \wedge \boldsymbol{n}_q \tag{3}$$

where **k** is the projection vector. The quasi frame becomes singular in all cases where **t** and **k** are parallel and in these cases we change the projection i.e. near a point where **t=**(0,0,1) we could choose **k**=(0,1,0) or (1,0,0) but not (0,0,1). Let θ be the angle between the vectors $\boldsymbol{n}$ and $\boldsymbol{n}_q$ given as in Figure 3.3 in Euclidean 3-space. The connection between the Frenet frame and the quasi-frame, as described by equation (3), is represented by

$$\begin{bmatrix} \boldsymbol{t} \\ \boldsymbol{n}_q \\ \boldsymbol{b}_q \end{bmatrix} = \begin{bmatrix} 1 & 0 & 0 \\ 0 & cos\theta & sin\theta \\ 0 & -sin\theta & cos\theta \end{bmatrix} \begin{bmatrix} \boldsymbol{t} \\ \boldsymbol{n} \\ \boldsymbol{b} \end{bmatrix}$$

(Dede et al., 2015). For the unit speed $\alpha(s)$ curve, the angle θ between $\boldsymbol{n}$ normal and $\boldsymbol{n}_q$ quasi-normal vectors is expressed in the form of a relationship between Frenet curvatures and quasi curvatures as

$$\begin{aligned} k_{q1} &= k_1 cos\theta \\ k_{q2} &= -k_1 \sin\theta \\ k_{q3} &= d\theta + k_2 \end{aligned} \tag{4}$$

and angle θ as

$$cos\theta = \frac{\det(\alpha'', \alpha', \kappa)}{\|\alpha' \wedge k\| \|\alpha''\|}$$

(Dede et al., 2015). Let $\alpha = \alpha(s)$ be a space curve, the quasi frame in E^4 consists of four orthonormal vectors $\{\boldsymbol{t}, \boldsymbol{n}_q, \boldsymbol{b}_{q1}, \boldsymbol{b}_{q2}\}$, where **t** is the unit tangent vector, $\boldsymbol{n}_q$ is the quasi-normal vector field, $\boldsymbol{b}_{q1}$ and $\boldsymbol{b}_{q2}$ are the first and second quasi-binormals, respectively. The frame is given by

$$\begin{aligned} \boldsymbol{t} &= \frac{\alpha'(s)}{||\alpha'(s)||} & \boldsymbol{n}_q &= \frac{\boldsymbol{t} \wedge \boldsymbol{k}_x \wedge \boldsymbol{k}_y}{||\boldsymbol{t} \wedge \boldsymbol{k}_x \wedge \boldsymbol{k}_y||} \\ \boldsymbol{b}_{q2} &= \frac{\alpha'(s) \wedge \boldsymbol{n}_q \wedge \alpha'''(s)}{\left|\left|\alpha'(s) \wedge \boldsymbol{n}_q \wedge \alpha'''(s)\right|\right|} & \boldsymbol{b}_{q1} &= \boldsymbol{b}_{q2} \wedge \boldsymbol{t} \wedge \boldsymbol{n}_q \end{aligned} \tag{5}$$

where $\mathbf{k}_x$ and $\mathbf{k}_y$ are the projection vectors.

To simplify the calculations, we select $\mathbf{k}_x = (1,0,0,0)$ and $\mathbf{k}_y = (0,1,0,0)$. The expression becomes singular when ttt is contained within the plane defined by $\mathbf{k}_x$ and $\mathbf{k}_y$. In such instances, we can modify our projection vectors accordingly. Thus, we classified the quasi frame into six types; *xy*-plane, *xz*-plane, *xt*-plane, *yz*-plane, *yt*-plane and *zt*-plane directional quasi frames denoted by

$$\begin{aligned} &\{\boldsymbol{t}, \boldsymbol{n}_q, \boldsymbol{b}_{q1}, \boldsymbol{b}_{q2}, \boldsymbol{k}_x, \boldsymbol{k}_y\}, \{\boldsymbol{t}, \boldsymbol{n}_q, \boldsymbol{b}_{q1}, \boldsymbol{b}_{q2}, \boldsymbol{k}_y, \boldsymbol{k}_z\}, \{\boldsymbol{t}, \boldsymbol{n}_q, \boldsymbol{b}_{q1}, \boldsymbol{b}_{q2}, \boldsymbol{k}_x, \boldsymbol{k}_z\}, \\ &\{\boldsymbol{t}, \boldsymbol{n}_q, \boldsymbol{b}_{q1}, \boldsymbol{b}_{q2}, \boldsymbol{k}_y, \boldsymbol{k}_t\}, \{\boldsymbol{t}, \boldsymbol{n}_q, \boldsymbol{b}_{q1}, \boldsymbol{b}_{q2}, \boldsymbol{k}_x, \boldsymbol{k}_t\}, \{\boldsymbol{t}, \boldsymbol{n}_q, \boldsymbol{b}_{q1}, \boldsymbol{b}_{q2}, \boldsymbol{k}_z, \boldsymbol{k}_t\} \end{aligned} \tag{6}$$

with the projection vectors $\mathbf{k}_t = (0,0,0,1), \mathbf{k}_z = (0,0,1,1), \mathbf{k}_y = (0,1,0,0)$ and $\mathbf{k}_x = (1,0,0,0)$. Let $\alpha(s)$ be a curve without unit speed that is parameterized by s (Gezer and Ekici, 2023). By differentiating equation (5) with respect to s, we obtain the variation equations of the quasi-frame in the form

$$\begin{bmatrix} \boldsymbol{t}' \\ \boldsymbol{n}_q' \\ \boldsymbol{b}_{q1}' \\ \boldsymbol{b}_{q2}' \end{bmatrix} = ||\alpha'|| \begin{bmatrix} 0 & k_{q1} & k_{q2} & 0 \\ -k_{q1} & 0 & k_{q3} & 0 \\ -k_{q2} & -k_{q3} & 0 & k_{q4} \\ 0 & 0 & -k_{q4} & 0 \end{bmatrix} \begin{bmatrix} \boldsymbol{t} \\ \mathbf{n}_q \\ \mathbf{b}_{q1} \\ \mathbf{b}_{q2} \end{bmatrix}. \tag{7}$$

The q-curvatures (quasi-curvatures) are also

$$\begin{aligned} k_{q1} &= \frac{< \boldsymbol{t}', \boldsymbol{n}_q >}{||\alpha'||} \qquad k_{q2} = \frac{< \boldsymbol{t}', \boldsymbol{b}_{q1} >}{||\alpha'||} \\ k_{q3} &= \frac{< \boldsymbol{n}_q{}', \boldsymbol{b}_{q1} >}{||\alpha'||} \quad k_{q4} = \frac{< \boldsymbol{b}_{q1}{}', \boldsymbol{b}_{q2} >}{||\alpha'||} \end{aligned} \tag{8}$$

In this here, when the fourth curvature k_{q4} calculated with respect to the quasi frame, is taken to be zero, the derivative formulas of the quasi frame fort he space curve in 3-dimensional Euclidean space are obtained (Dede et al., 2015; Gezer and Ekici, 2023).

RELATIONS BETWEEN QUASI FRAME AND FRENET FRAME IN EUCLIDEAN 4-SPACE

In this section, we first have obtained the matrix forms in 4-dimensional Euclidean space in which we will express the relations that will make possible the transitions between the Frenet frame and the quasi frame.

Theorem 1 In 4-dimensional Euclidean space, let

$$M = \begin{bmatrix} 1 & 0 & 0 & 0 \\ 0 & cos\theta\cos\psi & cos\theta\sin\psi & sin\theta \\ 0 & -sin\psi cos\phi - sin\phi sin\theta cos\psi & cos\psi cos\phi - sin\phi sin\theta sin\psi & cos\theta\sin\phi \\ 0 & sin\psi sin\phi - cos\psi sin\theta cos\phi & -cos\phi sin\theta sin\psi - cos\psi sin\phi & cos\theta\cos\phi \end{bmatrix}$$

be the transformation matrix, and the quasi frame vectors are $\{\boldsymbol{t}, \boldsymbol{n}_q, \boldsymbol{b}_{q1}, \boldsymbol{b}_{q2}\}$ and the Frenet frame vectors are $\{\boldsymbol{t}, \boldsymbol{n}, \boldsymbol{b}_1, \boldsymbol{b}_2\}$ the equality

$$\begin{bmatrix} \boldsymbol{t} \\ \boldsymbol{n}_q \\ \boldsymbol{b}_{q1} \\ \boldsymbol{b}_{q2} \end{bmatrix} = M \begin{bmatrix} \boldsymbol{t} \\ \boldsymbol{n} \\ \boldsymbol{b}_1 \\ \boldsymbol{b}_2 \end{bmatrix}$$

is satisfied.

Proof Let the tangent vector of the transformation matrix be chosen to remain unchanged. Consider three possible rotation planes where $\{\boldsymbol{t}, \boldsymbol{n}_q, \boldsymbol{b}_{q1}, \boldsymbol{b}_{q2}\}$ are quasi frame vectors and $\{\boldsymbol{t}, \boldsymbol{n}, \boldsymbol{b}_1, \boldsymbol{b}_2\}$ are Frenet frame vectors. The first return is taken such that the angle between the vectors $\boldsymbol{b}_1$ and $\boldsymbol{b}_{q1}$ in the space covered by the first binormal $\boldsymbol{b}_1$ and the second binormal $\boldsymbol{b}_2$ is ϕ, as shown in Figure 1, then the inner product is $< \boldsymbol{b}_1, \boldsymbol{b}_{q1} >= cos\ \phi$.

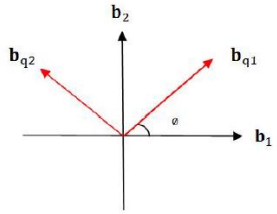

Figure 1 The first rotation plane, the plane Span$\{\boldsymbol{b}_1, \boldsymbol{b}_2\}$ at angle ϕ

Here are

$$\boldsymbol{b}_{q1} = cos\phi \boldsymbol{b}_1 + cos\ (\frac{\pi}{2} - \phi)\boldsymbol{b}_2$$

and

$$\boldsymbol{b}_{q2} = cos(\frac{\pi}{2} + \phi)\boldsymbol{b}_1 + sin\ (\frac{\pi}{2} - \phi)\boldsymbol{b}_2$$

and from here

$$\boldsymbol{b}_{q1} = cos\phi \boldsymbol{b}_1 + sin\phi \boldsymbol{b}_2$$

is written with

$$\boldsymbol{b}_{q2} = -sin\phi \boldsymbol{b}_1 + cos\phi \boldsymbol{b}_2$$

In that case,

$$\begin{bmatrix} \boldsymbol{t} \\ \boldsymbol{n}_q \\ \boldsymbol{b}_{q1} \\ \boldsymbol{b}_{q2} \end{bmatrix} = \begin{bmatrix} 1 & 0 & 0 & 0 \\ 0 & 1 & 0 & 0 \\ 0 & 0 & cos\phi & \sin\phi \\ 0 & 0 & -sin\phi & \cos\phi \end{bmatrix} \begin{bmatrix} \boldsymbol{t} \\ \boldsymbol{n} \\ \boldsymbol{b}_1 \\ \boldsymbol{b}_2 \end{bmatrix} \tag{9}$$

will be. If the angle between the normal vector $\boldsymbol{n}$ and the second binormal vector $\boldsymbol{b}_2$ in the space they encompass is taken to be θ, as shown in Figure 2, then $< \boldsymbol{n}, \boldsymbol{n}_q >= cos\ \theta$.

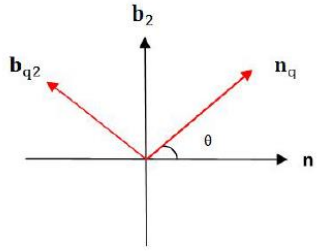

Figure 2 The second rotation plane, angle θ in the Span$\{\boldsymbol{n}, \boldsymbol{b}_2\}$

Since there will be

$$\boldsymbol{n}_q = cos\theta\boldsymbol{n} + sin\,(\frac{\pi}{2} - \theta)\boldsymbol{b}_2$$

and

$$\boldsymbol{b}_{q2} = cos(\frac{\pi}{2} + \theta)\boldsymbol{n} + sin\,(\frac{\pi}{2} - \theta)\boldsymbol{b}_2$$

here,

$$\boldsymbol{n}_q = cos\theta\boldsymbol{n} + sin\ \theta\boldsymbol{b}_2$$

and

$$\boldsymbol{b}_{q2} = cos\theta\boldsymbol{b}_2 - sin\ \theta\boldsymbol{n}$$

are written. Then it becomes

$$\begin{bmatrix} \boldsymbol{t} \\ \boldsymbol{n}_q \\ \boldsymbol{b}_{q1} \\ \boldsymbol{b}_{q2} \end{bmatrix} = \begin{bmatrix} 1 & 0 & 0 & 0 \\ 0 & cos\theta & 0 & \sin\theta \\ 0 & 0 & 1 & 0 \\ 0 & -sin\theta & 0 & \cos\theta \end{bmatrix} \begin{bmatrix} \boldsymbol{t} \\ \boldsymbol{n} \\ \boldsymbol{b}_1 \\ \boldsymbol{b}_2 \end{bmatrix} \tag{10}$$

The third rotation is taken such that the angle between the vector $\boldsymbol{n}$ and the vector $\boldsymbol{n}_q$ in the space formed by the normal vector **t** and the first binormal vector $\boldsymbol{b}_1$is ψ, as shown in Figure 3 which means $< \boldsymbol{n}, \boldsymbol{n}_q >= cos\ \psi$.

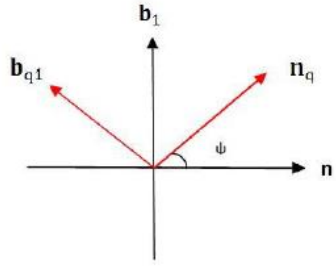

Figure 3 Third rotation plane, angle ψ in the Span$\{\boldsymbol{t}, \boldsymbol{b}_1\}$plane

Since there are

$$\boldsymbol{n}_q = cos\psi\boldsymbol{n} + cos\,(\frac{\pi}{2}+\psi)\boldsymbol{b}_1$$

and

$$\boldsymbol{b}_{q1} = cos\,(\frac{\pi}{2}+\left(\frac{\pi}{2}+\psi\right))\boldsymbol{n} + cos\,(\frac{\pi}{2}-(\frac{\pi}{2}-\psi))\boldsymbol{b}_1$$

here

$$\boldsymbol{n}_q = cos\psi\boldsymbol{n} + sin\psi\boldsymbol{b}_1$$

and

$$\boldsymbol{b}_{q1} = -sin\psi\boldsymbol{n} + cos\psi\boldsymbol{b}_1$$

are written then it becomes,

$$\begin{bmatrix}\boldsymbol{t}\\ \boldsymbol{n}_q\\ \boldsymbol{b}_{q1}\\ \boldsymbol{b}_{q2}\end{bmatrix} = \begin{bmatrix}1 & 0 & 0 & 0\\ 0 & cos\psi & \sin\psi & 0\\ 0 & -\sin\psi & cos\psi & 0\\ 0 & 0 & 0 & 1\end{bmatrix}\begin{bmatrix}\boldsymbol{t}\\ \boldsymbol{n}\\ \boldsymbol{b}_1\\ \boldsymbol{b}_2\end{bmatrix} \tag{11}$$

Accordingly, the transformation matrix M is written as

$$M = \left(\begin{bmatrix}1 & 0 & 0 & 0\\ 0 & 1 & 0 & 0\\ 0 & 0 & cos\phi & \sin\phi\\ 0 & 0 & -sin\phi & \cos\phi\end{bmatrix}\begin{bmatrix}1 & 0 & 0 & 0\\ 0 & cos\theta & 0 & \sin\theta\\ 0 & 0 & 1 & 0\\ 0 & -sin\theta & 0 & \cos\theta\end{bmatrix}\right)\begin{bmatrix}1 & 0 & 0 & 0\\ 0 & cos\psi & \sin\psi & 0\\ 0 & -\sin\psi & cos\psi & 0\\ 0 & 0 & 0 & 1\end{bmatrix}$$

It is also found as

$$M = \begin{bmatrix}1 & 0 & 0 & 0\\ 0 & cos\theta\cos\psi & cos\theta\sin\psi & sin\theta\\ 0 & -sin\psi cos\phi - sin\phi sin\theta cos\psi & cos\psi cos\phi - sin\phi sin\theta sin\psi & cos\theta\sin\phi\\ 0 & sin\psi sin\phi - cos\psi sin\theta cos\phi & -cos\phi sin\theta sin\psi - cos\psi sin\phi & cos\theta\cos\phi\end{bmatrix}$$

from here. As a result, using M as the transformation matrix, the relationship between the Frenet frame and the quasi frame is derived as

$$\begin{bmatrix}\boldsymbol{t}\\ \boldsymbol{n}_q\\ \boldsymbol{b}_{q1}\\ \boldsymbol{b}_{q2}\end{bmatrix} = M\begin{bmatrix}\boldsymbol{t}\\ \boldsymbol{n}\\ \boldsymbol{b}_1\\ \boldsymbol{b}_2\end{bmatrix}.$$

Theorem 2 In 4-dimensional Euclidean space, let the inverse transformation matrix be

$$M^{-1}=\begin{bmatrix}1 & 0 & 0 & 0\\ 0 & cos\theta\cos\psi & -sin\theta\sin\phi cos\psi-sin\psi cos\phi & -sin\theta\cos\phi cos\psi+sin\psi sin\phi\\ 0 & sin\psi cos\theta & -sin\theta sin\phi sin\psi+cos\psi cos\phi & -sin\theta\cos\phi sin\psi-sin\phi cos\psi\\ 0 & sin\theta & sin\phi cos\theta & cos\theta\cos\phi\end{bmatrix}$$

and the quasi frame vectors be $\{\boldsymbol{t},\boldsymbol{n}_q,\boldsymbol{b}_{q1},\boldsymbol{b}_{q2}\}$ and the Frenet frame vectors be $\{\boldsymbol{t},\boldsymbol{n},\boldsymbol{b}_1,\boldsymbol{b}_2\}$ the equality

$$\begin{bmatrix}\boldsymbol{t}\\ \boldsymbol{n}\\ \boldsymbol{b}_1\\ \boldsymbol{b}_2\end{bmatrix}=M^{-1}\begin{bmatrix}\boldsymbol{t}\\ \boldsymbol{n}_q\\ \boldsymbol{b}_{q1}\\ \boldsymbol{b}_{q2}\end{bmatrix}$$

is satisfied.

Proof In the equalities (9), the expression $\boldsymbol{b}_{q1}$ is expanded with $cos\phi$ and the expression $\boldsymbol{b}_{q2}$ is expanded with $(-sin\phi)$. If these expressions are added side by side, we obtain the quality

$$\boldsymbol{b}_1=cos\phi\boldsymbol{b}_{q1}-sin\phi\boldsymbol{b}_{q2}$$

Similarly, if the expression $\boldsymbol{b}_{q1}$ is expanded with $sin\phi$ and the expression $\boldsymbol{b}_{q2}$ is expanded with $(cos\phi)$, and if these expressions are added side by side, we arrive at the equation

$$\boldsymbol{b}_2=sin\phi\boldsymbol{b}_{q1}+cos\phi\boldsymbol{b}_{q2}$$

$$\begin{bmatrix}\boldsymbol{t}\\ \boldsymbol{n}\\ \boldsymbol{b}_1\\ \boldsymbol{b}_2\end{bmatrix}=\begin{bmatrix}1 & 0 & 0 & 0\\ 0 & 1 & 0 & 0\\ 0 & 0 & cos\phi & \sin\phi\\ 0 & 0 & -sin\phi & \cos\phi\end{bmatrix}\begin{bmatrix}\boldsymbol{t}\\ \boldsymbol{n}_q\\ \boldsymbol{b}_{q1}\\ \boldsymbol{b}_{q2}\end{bmatrix}$$

is written from here. In the equation (10), the expression $\boldsymbol{n}_q$ is expanded with $sin\theta$ and the expression $\mathbf{b}_{q2}$ is expanded with $cos\theta$, and if these expressions are added side by side, the equality

$$\boldsymbol{b}_2=sin\theta\boldsymbol{n}_q+cos\theta\boldsymbol{b}_{q2}$$

is reached. In a similar manner, if the $\boldsymbol{n}_q$ expression is expanded with $cos\theta$ and the $\mathbf{b}_{q2}$ expression is expanded with (-$sin\theta$), and these expressions are added side by side, the equality

$$\boldsymbol{n} = cos\theta \boldsymbol{n}_q - sin\ \theta \boldsymbol{b}_{q2}$$

is reached.

$$\begin{bmatrix} \boldsymbol{t} \\ \boldsymbol{n} \\ \boldsymbol{b}_1 \\ \boldsymbol{b}_2 \end{bmatrix} = \begin{bmatrix} 1 & 0 & 0 & 0 \\ 0 & cos\theta & 0 & -\sin\theta \\ 0 & 0 & 1 & 0 \\ 0 & sin\theta & 0 & \cos\theta \end{bmatrix} \begin{bmatrix} \boldsymbol{t} \\ \boldsymbol{n}_q \\ \boldsymbol{b}_{q1} \\ \boldsymbol{b}_{q2} \end{bmatrix}$$

is written from here. In equations (11), the expression $\boldsymbol{n}_q$ is expanded with $cos\psi$ and the expression $\boldsymbol{b}_{q1}$ is expanded with ($-sin\psi$); if these expressions are summed side by side, the equality

$$\boldsymbol{n} = cos\psi \boldsymbol{n}_q - sin\psi \boldsymbol{b}_{q1}$$

is reached. Smilarly, if the expression $\boldsymbol{n}_q$ is expanded with $sin\psi$ and the expression $\boldsymbol{b}_{q1}$ is expanded with $cos\psi$, and if these expressions are added side by side, the equality

$$\boldsymbol{b}_{q1} = sin\psi \boldsymbol{n}_q + cos\psi \boldsymbol{b}_{q1}$$

is reached.

$$\begin{bmatrix} \boldsymbol{t} \\ \boldsymbol{n} \\ \boldsymbol{b}_1 \\ \boldsymbol{b}_2 \end{bmatrix} = \begin{bmatrix} 1 & 0 & 0 & 0 \\ 0 & cos\psi & -\sin\psi & 0 \\ 0 & \sin\psi & cos\psi & 0 \\ 0 & 0 & 0 & 1 \end{bmatrix} \begin{bmatrix} \boldsymbol{t} \\ \boldsymbol{n}_q \\ \boldsymbol{b}_{q1} \\ \boldsymbol{b}_{q2} \end{bmatrix}$$

is written from here. Accordingly, the inverse transformation matrix is written as

$$M^{-1} = \begin{bmatrix} 1 & 0 & 0 & 0 \\ 0 & cos\psi & -\sin\psi & 0 \\ 0 & \sin\psi & cos\psi & 0 \\ 0 & 0 & 0 & 1 \end{bmatrix} \left(\begin{bmatrix} 1 & 0 & 0 & 0 \\ 0 & cos\theta & 0 & -\sin\theta \\ 0 & 0 & 1 & 0 \\ 0 & sin\theta & 0 & \cos\theta \end{bmatrix} \begin{bmatrix} 1 & 0 & 0 & 0 \\ 0 & 1 & 0 & 0 \\ 0 & 0 & cos\phi & -\sin\phi \\ 0 & 0 & sin\phi & \cos\phi \end{bmatrix} \right)$$

such that $M\ M^{-1} = I$. From here,

$$M^{-1} = \begin{bmatrix} 1 & 0 & 0 & 0 \\ 0 & cos\theta\cos\psi & -sin\theta\sin\phi cos\psi - sin\psi cos\phi & -sin\theta\cos\phi cos\psi + sin\psi sin\phi \\ 0 & sin\psi cos\theta & -sin\theta sin\phi sin\psi + cos\psi cos\phi & -sin\theta\cos\phi sin\psi - sin\phi cos\psi \\ 0 & sin\theta & sin\phi cos\theta & cos\theta\cos\phi \end{bmatrix}$$

is found. The relationship between the Frenet frame and the quasi-frame can then be expressed as

$$\begin{bmatrix} \boldsymbol{t} \\ \boldsymbol{n} \\ \boldsymbol{b}_1 \\ \boldsymbol{b}_2 \end{bmatrix} = M^{-1} \begin{bmatrix} \boldsymbol{t} \\ \boldsymbol{n}_q \\ \boldsymbol{b}_{q1} \\ \boldsymbol{b}_{q2} \end{bmatrix}$$

with M^{-1} represents the inverse of the transformation matrix.

Theorem 3 For the curve $\alpha(s)$, $||\alpha'(s)|| = 1$, the angle θ is normal and quasi-normal, the angle ϕ is first binormal and first quasi-binormal, and the angle ψ is given as the angles between the second binormal and second quasi-binormal vectors, in the form of the relationships between the quasi-curvatures and Frenet curvatures belonging to the space curve $\alpha(s)$

$$\begin{aligned} k_{q1} = \;& k_1 cos\theta\cos\psi \\ k_{q2} = \;& k_1(sin\theta\sin\phi cos\psi + sin\psi cos\phi) \\ k_{q3} = \;& (sin\phi d\theta) + (cos\phi cos\theta d\psi) + k_2(cos\theta cos\phi) \\ & + k_3(sin\psi sin\phi - sin\theta\cos\phi cos\psi) \\ k_{q4} = \;& (d\phi) + (sin\theta d\psi) + k_2(sin\theta) + k_3(cos\theta cos\psi) \end{aligned}$$

Proof First, to find the curvature k_{q1}, if the derivative of $\boldsymbol{n}_q$ in expression (10) is taken it becomes

$$\begin{aligned} \boldsymbol{n}_q &= (cos\theta cos\psi)\boldsymbol{n} + (cos\,\theta\, sin\psi)\boldsymbol{b}_1 + (sin\,\theta)\boldsymbol{b}_2 \\ \boldsymbol{n}_q{}' &= (-sin\theta cos\psi d\theta)\boldsymbol{n} - (cos\,\theta\, sin\psi d\psi)\boldsymbol{n} \\ &\quad + (cos\,\theta cos\psi)\boldsymbol{n}' + (cos\,\theta\, d\theta)\boldsymbol{b}_2 + (sin\theta)\boldsymbol{b}_2{}' \\ &\quad - (sin\,\theta sin\psi d\theta)\boldsymbol{b}_1 + (cos\,\theta cos\psi\, d\psi)\boldsymbol{b}_1 \\ &\quad + (cos\theta sin\psi)\boldsymbol{b}_1{}' \end{aligned}$$

and if the Frenet formulas given by equality (7) are substituted into the above expression,

$$\begin{aligned}\boldsymbol{n_q}' &= (-sin\theta cos\psi d\theta)\boldsymbol{n} - (cos\,\theta\, sin\psi d\psi)\boldsymbol{n} - (sin\theta)(k_3\,\boldsymbol{b}_1)\\ &\quad +(cos\,\theta cos\psi)(-k_1\,\boldsymbol{t} + k_2\,\boldsymbol{b}_1) + (cos\theta d\theta)\boldsymbol{b}_2\\ &\quad -(sin\,\theta sin\psi d\theta)\boldsymbol{b}_1 + (cos\,\theta cos\psi\, d\psi)\boldsymbol{b}_1\\ &\quad +(cos\theta sin\psi)(-k_2\boldsymbol{n} + k_3\boldsymbol{b}_2)\end{aligned}$$

If this expression is multiplied by $\boldsymbol{t}$, it becomes

$$k_{q1} = -<\boldsymbol{t}, \boldsymbol{n_q}'> = k_1\, cos\,\theta cos\psi.$$

To find the k_{q2} curvature now, if we take the derivative of $\boldsymbol{b}_{q1}$ in expression (10), it is found as

$$\begin{aligned}\boldsymbol{b_{q1}}' &= (-cos\phi d\phi sin\theta)\boldsymbol{n} + (sin\phi sin\psi d\psi\, sin\,\theta)\boldsymbol{n}\\ &\quad -(sin\phi cos\psi cos\theta d\theta)\,\boldsymbol{n} - (sin\phi cos\psi sin\theta)\,\boldsymbol{n}'\\ &\quad -(cos\psi d\psi cos\phi)\,\boldsymbol{n} + (sin\psi sin\phi d\phi)\boldsymbol{n} - (sin\psi cos\phi)\boldsymbol{n}'\\ &\quad -(sin\psi cos\phi d\psi)\,\boldsymbol{b}_1 - (sin\phi cos\psi d\phi)\boldsymbol{b}_1 + (cos\psi cos\phi)\boldsymbol{b_1}'\\ &\quad -(cos\phi sin\theta sin\psi d\phi)\,\boldsymbol{b}_1 - (sin\phi cos\theta d\theta sin\psi)\boldsymbol{b}_1\\ &\quad -(sin\phi sin\theta cos\psi d\psi)\,\boldsymbol{b}_1 - (sin\theta sin\psi sin\phi)\boldsymbol{b_1}'\\ &\quad -(sin\phi sin\theta d\theta)\,\boldsymbol{b}_2 + (cos\theta cos\phi d\phi)\boldsymbol{b}_2 + (sin\phi cos\theta)\,\boldsymbol{b_2}'\end{aligned}$$

since it is

$$\begin{aligned}\boldsymbol{b}_{q1} &= (-sin\phi cos\psi sin\theta - sin\psi cos\phi)\boldsymbol{n}\\ &\quad +(cos\psi cos\phi - sin\phi sin\theta sin\psi)\boldsymbol{b}_1 + (cos\theta sin\phi)\boldsymbol{b}_2\end{aligned}$$

If the Frenet formulas given by (7) are substituted and the necessary simplifications are made, it becomes

$$\begin{aligned}\boldsymbol{b_{q1}}' &= (-cos\phi cos\psi\, sin\,\theta d\phi)\boldsymbol{n} + (sin\psi\, sin\,\theta\, sin\phi d\psi)\boldsymbol{n}\\ &\quad -(cos\theta sin\phi cos\psi d\theta)\,\boldsymbol{n} + (sin\theta cos\psi sin\phi)\,(k_1\,\boldsymbol{t} + k_2\,\boldsymbol{b}_1)\\ &\quad +(sin\phi cos\psi d\psi)\,\boldsymbol{n} + (sin\psi cos\phi d\phi)\boldsymbol{n} - (cos\psi cos\phi d\psi)\boldsymbol{n}\\ &\quad -(sin\psi cos\phi d\psi)\,\boldsymbol{b}_1 - (sin\phi cos\psi d\phi)\boldsymbol{b}_1\\ &\quad -(cos\psi cos\phi)\boldsymbol{b}_2\,(k_2\boldsymbol{n} + k_3\boldsymbol{b}_2) - (sin\theta cos\phi sin\psi d\phi)\boldsymbol{b}_1\\ &\quad -(cos\theta sin\psi sin\phi d\theta)\,\boldsymbol{b}_1 - (sin\phi sin\theta cos\psi d\psi)\boldsymbol{b}_1\\ &\quad +(cos\theta cos\phi d\phi)\,\boldsymbol{b}_2 - (cos\theta sin\phi)(k_3\boldsymbol{b}_1)\end{aligned}$$

If the above expression is multiplied by $\boldsymbol{t}$ and the necessary adjustments are made

$$k_{q2} =< \boldsymbol{t}, \boldsymbol{b}_{q1}{}' >= k_1\,(sin\,\theta cos\psi\, sin\phi + sin\psi cos\phi)$$

is obtained.

Now, to find the k_{q3} curvature, if the $\boldsymbol{n}_q{}'$ and $\boldsymbol{b}_{q1}$ vectors are multiplied scalar-wise and the necessary simplifications are made, it is calculated as

$$\begin{aligned} < \boldsymbol{n}_q{}', \boldsymbol{b}_{q1} >= \quad & (sin\phi d\theta) + (cos\theta cos\phi d\psi) + (k_2 cos\theta cos\phi) \\ & +(k_3 sin\theta cos\psi cos\phi) + (k_3 sin\psi sin\phi) \end{aligned}$$

and

$$\begin{aligned} k_{q3} = \quad & (sin\phi d\theta) + (cos\theta cos\phi d\psi) \\ & +k_2(cos\theta cos\phi) + k_3(sin\psi sin\phi - sin\theta cos\psi cos\phi) \end{aligned}$$

Finally, to find the k_{q4} curvature, $\boldsymbol{b}_{q1}{}'$ and $\boldsymbol{b}_{q2}$ in expression (10) are multiplied by a scalar, and if necessary simplifications are made,

$$\begin{aligned} < \boldsymbol{b}_{q1}{}', \boldsymbol{b}_{q2} >= & (cos^2\phi d\phi) + (sin\theta d\psi) + (k_2 sin\theta) + (sin^2\phi d\phi) \\ & + (k_3 cos\psi cos\theta) \end{aligned}$$

is obtained. Then it'll be

$$k_{q4} = d\phi + (sin\theta d\psi) + (k_2 sin\theta) + (k_3 cos\psi cos\theta).$$

Corollary In this theorem, if the angle ϕ in the space covered by the first quasi-binormal $\boldsymbol{b}_{q1}$ and the second quasi-binormal $\boldsymbol{b}_{q2}$ and the normal vector $\boldsymbol{n}$, as well as the angle ψ in the space covered by the first quasi-binormal $\boldsymbol{b}_{q1}$, are taken as zero, then relations between quasi curvatures and Frenet curvatures in 3-dimensional space given by (7) is found.

Example 1 Let $\alpha(s)$ represent a central curve with the Frenet frame of a tubular surface in E^4, defined as

$$\alpha(s) = \frac{\sqrt{2}}{2}(\cos s\,, \sin s\,, \frac{1}{2}\cos 2s\,, \frac{1}{2}\sin 2s)$$

Since $\|\alpha(s)\| = 1$, it follows that the Frenet vectors are

$$\begin{aligned}
\boldsymbol{t} &= \frac{\sqrt{2}}{2}(-\sin s, \cos s, -\sin 2s, \cos 2s) \\
\boldsymbol{n} &= \frac{\sqrt{5}}{5}(-\cos s, -\sin s, -2\cos 2s, -2\sin 2s) \\
\boldsymbol{b}_2 &= \frac{\sqrt{5}}{5}(2\cos s, 2\sin s, -2\cos^2 s + 1, -\sin 2s) \\
\boldsymbol{b}_1 &= \frac{\sqrt{2}}{2}(\sin s, -\cos s, -\sin 2s, 2\cos^2 s - 1)
\end{aligned}$$

and from equation (2), Frenet curvatures are given as

$$k_1(s) = \tfrac{\sqrt{10}}{2},\ k_2(s) = \tfrac{-3\sqrt{10}}{10} \text{ and } k_3(s) = \tfrac{2\sqrt{10}}{5}.$$

If quasi frame vectors are calculated using $\mathbf{k}_x = (1,0,0,0)$ and $\mathbf{k}_y = (0,1,0,0)$ projection vectors, it becomes

$$\begin{aligned}
\boldsymbol{t} &= \frac{\sqrt{2}}{2}(-\sin s, \cos s, -\sin 2s, \cos 2s) \\
\boldsymbol{n}_q &= (0,0,\cos 2s, \sin 2s) \\
\boldsymbol{b}_{q2} &= (-\cos s, -\sin s, 0, 0) \\
\boldsymbol{b}_{q1} &= \frac{\sqrt{2}}{2}(\sin s, -\cos s, -\sin 2s, 2\cos^2 s - 1).
\end{aligned}$$

If the quasi-curvatures are calculated with the help of (8),

$$k_{q1} = -\sqrt{2},\ k_{q2} = 0,\ k_{q3} = \sqrt{2} \text{ and } k_{q4} = \tfrac{-\sqrt{2}}{2}$$

The curves in the projection spaces *xyz* and *xyt* and the normal and quasi-normal plane vectors at the points taken on them are plotted in Figure 4, respectively.

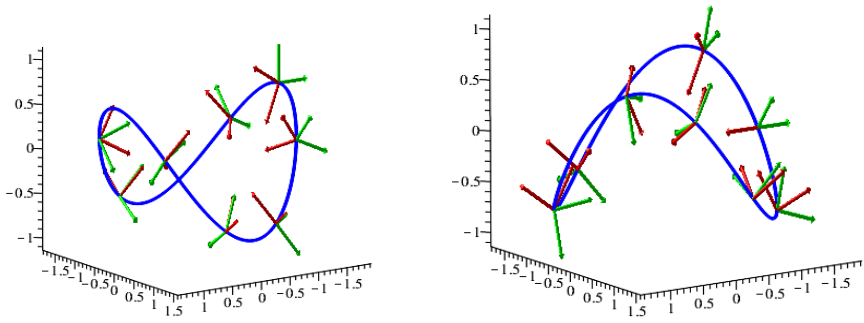

Figure 4 Frenet vectors $\boldsymbol{n}$ and $\boldsymbol{b}$ (red), quasi vectors $\boldsymbol{n}_q$ and $\boldsymbol{b}_q$ (green)

The curves in the projection spaces *xzt* and y*zt* and the normal and quasi-normal plane vectors at the points taken on them are plotted in Figure 5, respectively.

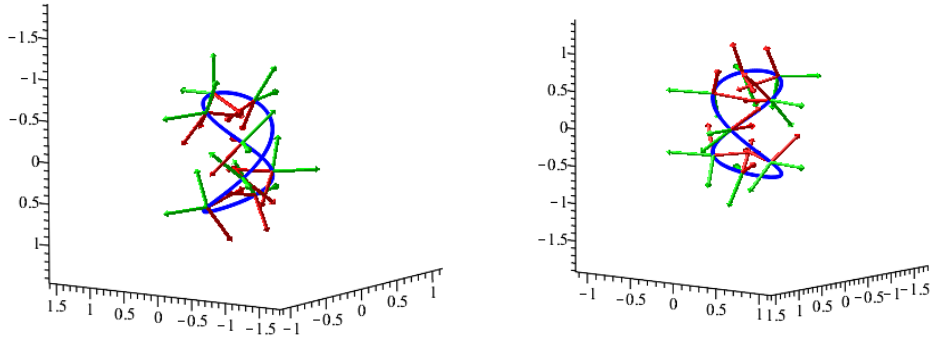

Figure 5 Frenet vectors $\boldsymbol{n}$ and $\boldsymbol{b}$ (red), quasi vectors $\boldsymbol{n}_q$ and $\boldsymbol{b}_q$ (green)

Example 2 Let $\alpha(s)$ represent a central curve with the Frenet frame of a tubular surface in E^4, defined as

$$\alpha(s) = (\sin\frac{s}{\sqrt{2}}, \cos\frac{s}{\sqrt{2}}, \frac{1}{\sqrt{2}}\sin s, \frac{1}{\sqrt{2}}\cos s)$$

Since $\|\alpha(s)\| = 1$, it follows that the Frenet vectors are

$$\begin{aligned}
\boldsymbol{t} &= \frac{1}{\sqrt{2}}\left(cos\frac{s}{\sqrt{2}}, -sin\frac{s}{\sqrt{2}}, cos\, s, -sin\, s\right)\\
\boldsymbol{n} &= \frac{-1}{\sqrt{3}}\left(sin\frac{s}{\sqrt{2}}, cos\frac{s}{\sqrt{2}}, \sqrt{2}\, sin\, s, \sqrt{2}\, cos\, s\right)\\
\boldsymbol{b}_2 &= \frac{-1}{\sqrt{3}}\left(-\sqrt{2}\, sin\frac{s}{\sqrt{2}}, -\sqrt{2}\, cos\frac{s}{\sqrt{2}}, sin\, s, cos\, s\right)\\
\boldsymbol{b}_1 &= -\frac{1}{\sqrt{2}}\left(cos\frac{s}{\sqrt{2}}, -sin\frac{s}{\sqrt{2}}, -cos\, s, sin\, s\right)
\end{aligned}$$

and from equation (2), Frenet curvatures are given as

$$k_1(s) = \frac{\sqrt{3}}{2},\ k_2(s) = -\frac{\sqrt{3}}{6} \text{ and } k_3(s) = \frac{\sqrt{6}}{3}. \tag{12}$$

If quasi frame vectors are calculated using $\mathbf{k}_x = (1,0,0,0)$ and $\mathbf{k}_y = (0,1,0,0)$ projection vectors, it becomes

$$\begin{aligned}
\boldsymbol{t} &= \frac{1}{\sqrt{2}}\left(cos\frac{s}{\sqrt{2}}, -sin\frac{s}{\sqrt{2}}, cos\, s, -sin\, s\right)\\
\boldsymbol{n_q} &= (0,0,-sin\, s, -cos\, s)\\
\boldsymbol{b}_{q2} &= \left(sin\frac{s}{\sqrt{2}}, cos\frac{s}{\sqrt{2}}, 0,0\right)\\
\boldsymbol{b}_{q1} &= -\frac{1}{\sqrt{2}}\left(cos\frac{s}{\sqrt{2}}, -sin\frac{s}{\sqrt{2}}, -cos\, s, sin\, s\right)
\end{aligned} \tag{13}$$

If the quasi-curvatures are calculated with the help of (8),

$$k_{q1}(s) = \frac{1}{\sqrt{2}},\ k_{q2}(s) = 0,\ k_{q3} = -\frac{1}{\sqrt{2}} \text{ and } k_{q4} = \frac{1}{2}$$

The curves in the projection spaces *xyz* and *xyt* and the normal and quasi-normal plane vectors at the points taken on them are plotted in Figure 6, respectively.

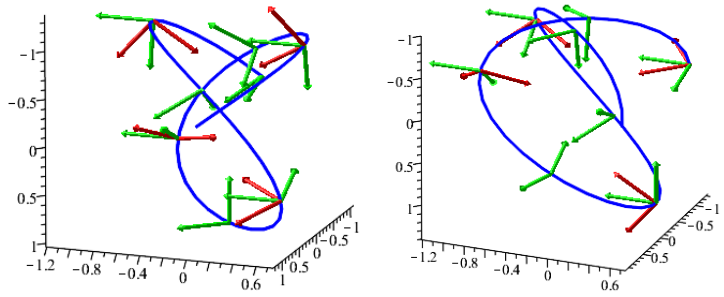

Figure 6 Frenet vectors $\boldsymbol{n}$ and $\boldsymbol{b}$ (red), quasi vectors $\boldsymbol{n}_q$ and $\boldsymbol{b}_q$ (green)

The curves in the projection spaces *xzt* and yz*t* and the normal and quasi-normal plane vectors at the points taken on them are plotted in Figure 7, respectively.

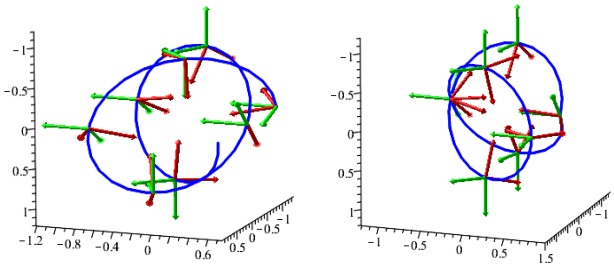

Figure 7 Frenet vectors $\boldsymbol{n}$ and $\boldsymbol{b}$ (red), quasi vectors $\boldsymbol{n}_q$ and $\boldsymbol{b}_q$ (green)

If the angles $\psi,\ \phi\ and\ \theta$ in the matrix given in Theorem 1 are specially chosen such that $\psi = 0,\ \phi = 2\pi$ and $\theta = arccos\frac{\sqrt{2}}{\sqrt{3}}$, then

$$\begin{bmatrix} \boldsymbol{t} \\ \boldsymbol{n}_q \\ \boldsymbol{b}_{q1} \\ \boldsymbol{b}_{q2} \end{bmatrix} = \begin{bmatrix} 1 & 0 & 0 & 0 \\ 0 & \frac{\sqrt{2}}{\sqrt{3}} & 0 & \frac{1}{\sqrt{3}} \\ 0 & 0 & 1 & 0 \\ 0 & -\frac{1}{\sqrt{3}} & 0 & \frac{\sqrt{2}}{\sqrt{3}} \end{bmatrix} \begin{bmatrix} \boldsymbol{t} \\ \boldsymbol{n} \\ \boldsymbol{b}_1 \\ \boldsymbol{b}_2 \end{bmatrix}.$$

is found with the help of the matrix M. If Frenet frame vectors are substituted in this equation, quasi frame vectors are obtained as

$$
\begin{aligned}
\boldsymbol{t} = & \frac{1}{\sqrt{2}}\left(cos\frac{s}{\sqrt{2}}, -sin\frac{s}{\sqrt{2}}, cos\, s\, , -sin\, s\right)\\
\boldsymbol{n_q} = & -\frac{\sqrt{2}}{3}\left(sin\frac{s}{\sqrt{2}}, cos\frac{s}{\sqrt{2}}, \sqrt{2}\, sin\, s\, , \sqrt{2}\, cos\, s\right)\\
& -\frac{1}{3}\left(-\sqrt{2}\, sin\frac{s}{\sqrt{2}}, -\sqrt{2}\, cos\frac{s}{\sqrt{2}}, sin\, s, cos\, s\right)\\
= & (0,0, -sin\, s, -cos\, s)\\
\boldsymbol{b}_{q2} = & \frac{1}{3}\left(sin\frac{s}{\sqrt{2}}, cos\frac{s}{\sqrt{2}}, \sqrt{2}\, sin\, s\, , \sqrt{2}\, cos\, s\right)\\
& -\frac{\sqrt{2}}{3}\left(-\sqrt{2}\, sin\frac{s}{\sqrt{2}}, -\sqrt{2}\, cos\frac{s}{\sqrt{2}}, sin\, s, cos\, s\right)\\
= & (sin\frac{s}{\sqrt{2}}, cos\frac{s}{\sqrt{2}}, 0,0)\\
\boldsymbol{b}_{q1} = & -\frac{1}{\sqrt{2}}(cos\frac{s}{\sqrt{2}}, -sin\frac{s}{\sqrt{2}}, -cos\, s\, , sin\, s)
\end{aligned}
$$

respectively. They are the same as the vectors given above (13). In a similar way, by substituting the given angle values into the Frenet curvatures given by (12) in the equations in Theorem 3, the quasi-curvatures are obtained as

$$
\begin{aligned}
k_{q1} = & \quad k_1 cos\theta cos\psi = \left(\frac{\sqrt{3}}{2}\right)\left(\frac{\sqrt{2}}{\sqrt{3}}\right) = \frac{1}{\sqrt{2}}\\
k_{q2} = & \quad k_1(sin\theta sin\phi cos\psi + sin\psi cos\phi) = 0\\
k_{q3} = & \quad (sin\phi d\theta) + (cos\phi cos\theta d\psi) + k_2(cos\theta cos\phi)\\
& \quad +k_3(sin\psi sin\phi - sin\theta cos\phi cos\psi)\\
= & \quad \left(-\frac{\sqrt{3}}{6}\right)\frac{\sqrt{2}}{\sqrt{3}} + \frac{\sqrt{6}}{3}(-\frac{1}{\sqrt{3}}) = -\frac{\sqrt{2}}{6} - \frac{\sqrt{2}}{3} = -\frac{1}{\sqrt{2}}\\
k_{q4} = & \quad (d\phi) + (sin\theta d\psi) + k_2(sin\theta) + k_3(cos\theta cos\psi)\\
= & \quad \left(-\frac{\sqrt{3}}{6}\right)\left(\frac{1}{\sqrt{3}}\right) + \left(\frac{\sqrt{6}}{3}\right)\left(\frac{\sqrt{2}}{\sqrt{3}}\right) = \frac{1}{2}.
\end{aligned}
$$

This value is the same as the above (19) quasi-curvature values.
All the figures in this study were created by using Maple programme.

CONCLUSION

In four-dimensional Euclidean space, we first defined the quasi frame and quasi curvatures with Frenet vectors. We emphasised the importance of the quasi frame in that it can be calculated easily and with the same accuracy even in the absence of the second derivative of the curve. We found the transition matrices between the quasi frame and the Frenet frame for a space curve in 4-dimensional space. We gave the relations between the curvatures of the two frames. We also took a curve for which we will calculate these two frame vectors and exemplified its images in projection spaces.

ACKNOWLEDGEMENT

This paper is derived from the thesis written in Eskisehir Osmangazi University by Buket Gezer.

REFERENCES

Alessio, O. (2009). Differential geometry of intersection curves in E^4 of three implicit surfaces, Comput. Aided Geom. Des., 26, 455.471.

Ateş, F., Gök, İ., Ekmekci, F.N. & Yaylı Y. (2019). Characterizations of inclined curves according to parallel transport frame in E^4 and Bishop Frame in E3 Konuralp Journal of Mathematics, 7, 16-24.

Bishop R., (1975). There is more than one way to frame a curve, in: The American Mathematical Monthly March, pp. 246.252 .

Bloomenthal, J. (1990). Calculation of reference frames along a space curve, In Graphics Gems., 567.571.

Coquillart, S. (1987). Computing offsets of B-spline curves, Computer-Aided Design, 19(6), pp. 305.309.

Çelik, F., Bozkurt Z., Gök, İ., Ekmekçi F.N. & YaylıY. (2014). Parallel transport frame in 4-dimensional euclidean space E^4, Caspian J. Math. Sci. (CJMS) 3 (1) 91.103 .

Dede, M., Ekici C. & Tozak H. (2015). Directional Tubular Surfaces, Int. J. of Alg., 9: 527-535.

Ekici Coşkun, A., & Akça, Z. (2023). The Ruled Surfaces Generated By Quasi-Vectors in E^4 Space. Hagia Sophia Journal of Geometry, 5(2), 6-17.

Elsayied, H.K., Tawfiq, A.M. & Elsharkawy, A. (2021). Special Smarandach curves according to the quasi frame in 4-dimensional Euclidean space E^4, Houston J. Math 47 (2), 467-482.

Gezer, B. & Ekici, C. (2023). On space curve with quasi frame in E^4. 4th International Black Sea Modern Scientific Research Congress (p. 1951-1962).

Hanson, A.J. & Ma, H. (1995). Parallel Transport Approach to Curve Framing, Tech. Math. Rep. 425, Indiana University Computer science Department.

Klok, F. (1986). Two moving coordinate frames for sweeping along a 3D trajectory, Comput Aided GeomD, 3, pp. 217.229.

Körpınar, T. & Turhan, E. (2013) Biharmonic curves according to parallel transport frame in E4, Bol. Soc. Paran. Mat., 31(2), 213-217,https://doi.org/10.5269/bspm.v31i2.17669.

Magden, A. & Yılmaz, S. (2014). On the curves of constant breadth in four dimensional Galilean space, Int. Math. Forum, 9(25), 1229.1236.

O.Neil, B. (1983). Semi-Riemannian Geometry with Applications to Relativity, Academic Press: London.

Özdemir. Z., Gök İ., Ekmekçi, F.N, & Yaylı, Y. (2015) A new approach on type-3 slant helix in E4, Gen. Math. Notes, 28(1), 40-49.

Öztürk, U., Öztürk E.B.K., İlarslan K. & Nesovic E. (2014). On Smarandache curves lying in lightcone in Minkowski 3-space, J. Dyn. Syst. Geom. Theor. 12(1), 81.91.

Turgut, M. (2009). Smarandache breadth pseudo null curves in Minkowski space-time, Int. J.Math. Combin., 1, 46.49 .

Turgut, M. & Yilmaz S. (2008). Smarandache curves in Minkowski space-time, Int. J.Math. Combin., 3, 51.55 .

Wang, W., Jüttler, B., Zheng, D. & Liu, Y. (2008). Computation of rotation minimizing frame, ACM Transactions on Graphics, 27(1), 1-18.

Yağbasan, B., Ekici, C., & Tozak, H. (2023). Directional Tube Surface in Euclidean 4-Space. Hagia Sophia Journal of Geometry, 5(2), 18-30.

Chapter 3

On New Structures Hardy-Hilbert-Type Inequalities with Diamond$-\propto$ Calculus

Yusuf ZEREN[1]

[1] Prof. Dr.; Yıldız Technical University Department of Mathematics
yzeren@yildiz.edu.tr ORCID No:0000-0001-8346-2208

INTRODUCTION

Overall, dynamic inequalities and their different forms are important in harmonic analysis and other application areas. The most well-known of these are the Hardy and Hilbert inequalities. These integral inequalities also play an important role in time scales combining continuous and discrete state forms. At the same time, these integral inequalities are the cornerstones of applied mathematics. Before starting our work, we think giving some information about these inequalities would be useful. The reader can refer to the references section at the end of this work for more detailed information.

In [1], the theorems we give below are well-known classical statements about Hilbert's inequality.

Theorem 1.1. Let $p, q > 1$, $\frac{1}{p} + \frac{1}{q} \leq 1$, and $0 < w = 2 - \frac{1}{p} - \frac{1}{q} = \frac{1}{p'} + \frac{1}{q'} \leq 1$, then

$$\sum_{j=1}^{\infty}\sum_{i=1}^{\infty}\frac{f_j g_i}{(j+i)^w} \leq D\left(\sum_{j=1}^{\infty} f_j^p\right)^{\frac{1}{p}}\left(\sum_{i=1}^{\infty} g_i^q\right)^{\frac{1}{q}}, \tag{1}$$

where $D = D(p, q)$.

Theorem 1.2. Let $f \in L^p(0,\infty)$, $g \in L^q(0,\infty)$, and let p, q, p', q', w be as in Theorem 1.1, then

$$\int_0^{\infty}\int_0^{\infty}\frac{f(x)g(y)}{(x+y)^w}\,dx\,dy \leq D\left(\int_0^{\infty} f^p(x)dx\right)^{\frac{1}{p}}\left(\int_0^{\infty} g^q(y)dy\right)^{\frac{1}{q}}, \tag{2}$$

where $D = D(p, q)$.

In [2], Zhao et al. introduced a new inequality that is compatible with the structure of Theorem 1.2.

Theorem 1.3. Let $\frac{1}{p_i}+\frac{1}{q_i}=1$ with $p_i>1,\ \pi_i\geq 1$. Let differentiable function $f_i(\theta_i)$ on $[0,k_i)$, where $k_i\in(0,\infty)$. Assume $f_i(0)=0$ for $(i=1,\dots,n)$. Then

$$\int_0^{k_1}\int_0^{k_2}\dots\int_0^{k_n}\frac{\prod_{i=1}^{n}|f_i^{\pi_i}(\theta_i)|}{\left(\sum_{i=1}^{n}\frac{\theta_i}{q_i}\right)^{\sum_{i=1}^{n}\frac{1}{q_i}}}d\theta_n d\theta_{n-1}\dots d\theta_1\leq D\prod_{i=1}^{n}\left(\int_0^{k_i}(k_i-\theta_i)\left|f_i^{\pi_i-1}(\theta_i)f_i'(\theta_i)\right|^{p_i}d\theta_i\right)^{\frac{1}{p_i}},$$

where $D=\left(n-\sum_{i=1}^{n}\frac{1}{p_i}\right)^{\sum_{i=1}^{n}\frac{1}{p_i}-n}\prod_{i=1}^{n}\pi_i k_i^{\frac{1}{q_i}}$.

In [3], Zhao and Chung introduced the following inequality.

Theorem 1.4. Let $\frac{1}{p_i}+\frac{1}{q_i}=1$ with $p_i>1,\ p_i$ are constants. Let $f_i(\delta_{1i},\dots,\delta_{ni})$ be real-valued $n-th$ differential functions defined on $[0,k_{1i})\times\dots\times[0,k_{ni})$, where $\delta_{ji}\in(0,\infty)$ and $0\leq k_{ji}\leq\delta_{ji},(j,i=1,\dots,n)$. Assume that

$$f_i(k_{1i},\dots,k_{ni})=\int_0^{k_{1i}}\dots\int_0^{k_{ni}}\frac{\partial^n}{\partial_{k_{1i}}\dots\partial_{k_{ni}}}f_i(\delta_{1i},\dots,\delta_{ni})d_{\delta_{ni}}\dots d_{\delta_{1i}},$$

then

$$\int_0^{\epsilon_{11}}\dots\int_0^{\epsilon_{n1}}\int_0^{\epsilon_{12}}\dots\int_0^{\epsilon_{n2}}\dots\int_0^{\epsilon_{1n}}\dots\int_0^{\epsilon_{nn}}\frac{\prod_{i=1}^{n}\left(\int_0^{k_{1i}}\dots\int_0^{k_{ni}}\left|\frac{\partial^n}{\partial_{k_{1i}}\dots\partial_{k_{ni}}}f_i(\delta_{1i},\dots,\delta_{ni})\right|^{p_i}d_{\delta_{ni}}\dots d_{\delta_{1i}}\right)^{\frac{1}{p_i}}}{\left(\sum_{i=1}^{n}\frac{(k_{1i}\dots k_{ni})}{q_i}\right)^{\sum_{i=1}^{n}\frac{1}{q_i}}}$$

$$d_{k_{11}}\dots d_{k_{n1}}d_{k_{12}}\dots d_{k_{n2}}\dots d_{k_{1n}}\dots d_{k_{nn}}$$

$$\leq M\prod_{i=1}^{n}\left(\int_0^{\epsilon_{1i}}\dots\int_0^{\epsilon_{ni}}\prod_{j=1}^{n}(\epsilon_{ji}-k_{ji})\left|\frac{\partial^n}{\partial_{k_{1i}}\dots\partial_{k_{ni}}}f_i(k_{1i},\dots,k_{ni})\right|^{p_i}d_{k_{ni}}\dots d_{k_{1i}}\right)^{\frac{1}{p_i}},\tag{3}$$

Where $M=\left(n-\sum_{i=1}^{n}\frac{1}{p_i}\right)^{\sum_{i=1}^{n}\frac{1}{p_i}-n}\prod_{i=1}^{n}(\epsilon_{1i}\dots\epsilon_{ni})^{\frac{1}{q_i}}$.

For more detailed information on inequalities, time scales, and fractional calculus, see monographs [4-27, 52-61].

AUXILIARY STATEMENTS AND PRELIMINARIES

Although the history of time scale calculation is not very long, it has positioned itself in the field of mathematics and other disciplines of science. It owes this position to the unification of continuous and discrete cases in mathematics. Due to this situation, scientists in almost every field have integrated this field into their field of study and have contributed many innovations to the literature. Analytical solutions of differential equations in applied mathematics and mathematical modeling in economics are just a few examples of these application areas. Those who want more general information can look at references [28, 42-51]. $\mathbb{T}$ is a time scale that arbitrary non-empty closed subset of real numbers ($\mathbb{R}$). In our study, we will take this situation of $(0,\infty)_{\mathbb{T}} = (0,\infty) \cap \mathbb{T}$ into consideration.

Now let's briefly give the basic concepts about the diamond-alpha derivative.

$\sigma, \rho: \mathbb{T} \to \mathbb{T}$ are defined by $\sigma(t) = inf\{s \in \mathbb{T}: s > t\}$, $\rho(t) = sup\{s \in \mathbb{T}: s > t\}$ for $t \in \mathbb{T}$. $\sigma(t)$ is the jump operator (forward), and $\rho(t)$ is the jump operator (backward), respectively. Let $\sigma(t) > t$, then t is rs (right-scattered), and let $\sigma(t) = t$, then t is called rd (right-dense). Let $\rho(t) < t$, then t is ls (left-scattered), and let $\rho(t) = t$, then t is called ld (left-dense).

Let $\mu, \vartheta: \mathbb{T} \to \mathbb{R}^+$ such that $\mu(t) = \sigma(t) - t$, $\vartheta(t) = t - \rho(t)$. μ(t) and $\vartheta(t)$ are called gm (graininess mappings).

If the time scale $\mathbb{T}$ has a ls (left-scattered) maximum m, then $\mathbb{T}^k = \mathbb{T} - \{m\}$. Otherwise $\mathbb{T}^k = \mathbb{T}$.

$\mathbb{T}^k$ is defined as follows

$$\mathbb{T}^k = \begin{cases} \mathbb{T} \setminus (\rho\, sup\, \mathbb{T}, sup\, \mathbb{T}], & if \quad sup\, \mathbb{T} < \infty \\ \mathbb{T}, & if \quad sup\, \mathbb{T} = \infty, \end{cases}$$

and

$$\mathbb{T}_k = \begin{cases} \mathbb{T} \setminus [inf\, \mathbb{T}, \sigma(inf\, \mathbb{T})], & |inf\, \mathbb{T}| < \infty \\ \mathbb{T}, & inf\, \mathbb{T} = -\infty. \end{cases}$$

Assume that $h: \mathbb{T} \to \mathbb{R}$ is a function. Let t be right-dense.

i) Let π be delta differentiable at t $(t \in \mathbb{T}^k (t \neq min\mathbb{T}))$, then π is continuous at t.

ii) Let π be lc (left continuous) at t, and t is rs (right-scattered), then π is delta differentiable at t,

$$\pi^{\Delta}(t) = \frac{\pi^{\sigma}(t) - \pi(t)}{\mu(t)}$$

iii) Let π be delta differentiable at t and $\lim_{s\to t}\frac{\pi(t)-\pi(s)}{t-s}$, then

iv)

$$\pi^{\Delta}(t)=\lim_{s\to t}\frac{\pi(t)-\pi(s)}{t-s}.$$

v) Let π be delta differentiable at t, then $\pi^{\sigma}(t)=\pi(t)+\mu(t)\pi^{\Delta}(t)$.

Let $\mathbb{T}=\mathbb{R}$, then $\pi^{\Delta}(t)=\pi'(t)$, and Let $\mathbb{T}=\mathbb{Z}$, then $\pi^{\Delta}(t)$ reduces to $\Delta\pi(t)$. Let $K:\mathbb{T}\to\mathbb{R}$ is defined as a delta antiderivative of $\pi:\mathbb{T}\to\mathbb{R}$, then $K^{\Delta}=\pi(t)$ holds for all $t\in\mathbb{T}$, and we define the delta integral of π by

$$\int_{s}^{t}\pi(\tau)\Delta\tau=K(t)-K(s),$$

for all $s,t\in\mathbb{T}$.

Suppose $\pi:\mathbb{R}\to\mathbb{R}$ is a continuous function and delta differentiable on $\mathbb{T}$. If $\varphi:\mathbb{R}\to\mathbb{R}$ is continuously differentiable, then we have

$$(\varphi\circ\pi)^{\Delta}(s)=\varphi'\big(\pi(m)\big)\pi^{\Delta}(s),\quad m\in[s,\sigma(s)].$$

Let's now give some definitions for the nabla integral.

Let $\pi:\mathbb{T}_k\to\mathbb{R}$ is called nabla differentiable at $t\in\mathbb{T}_k$. If $\varepsilon>0$, then the following inequality is provided

$$\big|\pi\big(\rho(t)\big)-\pi(s)-\pi^{\nabla}(t)(\rho(t)-s)\big|\le\varepsilon|\rho(t)-s|,$$

for all $s\in V$.

Let $K:\mathbb{T}\to\mathbb{R}$ is called a nabla antiderivative of $\pi:\mathbb{T}\to\mathbb{R}$, then we define

$$\int_{s}^{t}\pi(\tau)\nabla\tau=K(t)-K(s),$$

for all $s,t\in\mathbb{T}$.

In [50], Let $\vartheta(t)$ be diamond alpha differentiable on $\mathbb{T}$ for all $\propto, t \in \mathbb{T}$, then we define $\vartheta^{\diamond\propto}(t)$ by

$$\vartheta^{\diamond\propto}(t) = \propto \vartheta^{\Delta}(t) + (1-\propto)\vartheta^{\nabla}(t)$$

for $0 \leq \propto \leq 1$.

Theorem 2.1 [50] Let $\vartheta, h: \mathbb{T} \to \mathbb{R}$ be diamond alpha differentiable for all $\propto, t \in \mathbb{T}$ and $0 \leq \propto \leq 1$.

(i) Let $(\vartheta + h): \mathbb{T} \to \mathbb{R}$ be diamond alpha differentiable for all $t \in \mathbb{T}$, then

$$(\vartheta + h)^{\diamond\propto}(t) = \vartheta^{\diamond\propto}(t) + h^{\diamond\propto}(t).$$

(ii) Let $k\vartheta: \mathbb{T} \to \mathbb{R}$ be diamond alpha differentiable for all $\propto, t \in \mathbb{T}$, then

$$(k\vartheta)^{\diamond\propto}(t) = k\vartheta^{\diamond\propto}(t),$$

where t,$k \in \mathbb{R}$.

(iii) Let $\vartheta, h: \mathbb{T} \to \mathbb{R}$ be diamond alpha differentiable for all $\propto, t \in \mathbb{T}$, then

$$(\vartheta h)^{\diamond\propto}(t) = \vartheta^{\diamond\propto}(t)h(t) + \propto \vartheta^{\sigma}(t)h^{\Delta}(t) + (1-\propto)\vartheta^{\rho}(t)h^{\nabla}(t).$$

Definition 2.2 [50] If $\vartheta: \mathbb{T} \to \mathbb{R}$ is $\diamond_{\propto}-$integrable for all $\propto, b, t \in \mathbb{T}$, then

$$\int_b^t \vartheta(\delta) \diamond_{\propto} \delta = \propto \int_b^t \vartheta(\delta)\Delta\delta + (1-\propto) \int_b^t \vartheta(\delta)\nabla\delta$$

for $0 \leq \propto \leq 1$.

Definition 2.3 [46, 52] Let $\vartheta \in C_{rd}(\mathbb{T}, \mathbb{R})$, $t \in \mathbb{T}^k$ and let $\vartheta: \mathbb{T} \to \mathbb{R}$ be diamond alpha integrable, then

$$\int_t^{\sigma(t)} \vartheta(\tau) \diamond_{\propto} \tau = \mu(t)\vartheta(t).$$

The partial integration formula on the time scale is given by

$$\int_x^y u(s)w^{\diamond\alpha}(s)\,\diamond_\alpha s = u(s)w(s)\mathrm{I}_x^y - \int_x^y u^{\diamond\alpha}(s)w^{\sigma}(s)\,\diamond_\alpha s$$

for $0 \leq \alpha \leq 1$.

Definition 2.4 [25, 51] (Conformable diamond-alpha derivative) Given $\vartheta: \mathbb{T} \to \mathbb{R}$ and $\beta \in \mathbb{T}$, ϑ is (λ, β) −diamond alpha differentiable at $\eta > \beta$, if it's diamond alpha differentiable at η, and its (λ, β) −diamond alpha derivative is defined by

$$\diamond_{\alpha\beta}^{\lambda}\,\vartheta(\eta) = \Lambda_{1-\lambda}(\eta,\beta)\vartheta^{\diamond\alpha}(\eta) \qquad \eta > \beta, \tag{4}$$

Definition 2.5 [25, 51] (Conformable diamond-alpha integral) Suppose that $\beta, \eta_1, \eta_2 \in \mathbb{T}$, $\vartheta \in C(\mathbb{T}), 0 < \lambda \leq 1, \beta \leq \eta_1 \leq \eta_2$, and the function ϑ is called (λ, β) −diamond alpha integrable on $[\eta_1, \eta_2]$ if

$$\diamond_{\alpha\beta}^{\lambda}\,\vartheta(\eta) = \int_{\eta_1}^{\eta_2} \vartheta(\eta)\,\diamond_{\alpha\beta}^{\lambda}\,\eta = \int_{\eta_1}^{\eta_2} \vartheta(\eta)\Lambda_{1-\lambda}(\sigma^{1-\lambda}(\eta),\beta)\,\diamond_\alpha \eta, \tag{5}$$

Lemma 2.6 [14] If $f, \varepsilon \in CC_{rd}^1([\omega,p]_{\mathbb{T}} \times [\omega,p]_{\mathbb{T}}, \mathbb{R})$ are diamond alpha integrable functions and $\frac{1}{p} + \frac{1}{q} = 1$ with $p > 1$ and let $\omega, p \in \mathbb{T}$ with $\omega < p$, then

$$\int_\omega^p \int_\omega^p |f(t,\epsilon)\varepsilon(t,\epsilon)|\,\diamond_\alpha{}^{\lambda,\beta}\, t\,\diamond_\alpha{}^{\lambda,\beta}\,\epsilon$$

$$\leq \left(\int_\omega^p \int_\omega^p |f(t,\epsilon)|^p\,\diamond_\alpha{}^{\lambda,\beta}\, t\,\diamond_\alpha{}^{\lambda,\beta}\,\epsilon\right)^{\frac{1}{p}} \times \left(\int_\omega^p \int_\omega^p |\varepsilon(t,\epsilon)|^q\,\diamond_\alpha{}^{\lambda,\beta}\, t\,\diamond_\alpha{}^{\lambda,\beta}\,\epsilon\right)^{\frac{1}{q}}. \tag{5}$$

In this study, we prove a new fractional inequality of Hilbert-type on time scales using the properties of Theorem 1.3 mentioned above. We also obtain discrete cases of Hilbert-type inequalities related to some special cases of our results.

Main Result

Theorem 3.1 Let $\epsilon_0, k_{ij}, \delta_{ij}, \epsilon_{ij} \in \mathbb{T}$, $(i, j = 1, \dots, n)$. Let $p_i, q_i > 1$ be constants and $\frac{1}{p_i} + \frac{1}{q_i} = 1$ and let $f_i(\delta_{1j}, \dots, \delta_{nj})$ be $\diamond_\propto^{\lambda,\beta}-$differentiable functions and also defined on $[\epsilon_0, k_{1i})_{\mathbb{T}} \times \dots \times [\epsilon_0, k_{ni})_{\mathbb{T}}$, where $\epsilon_{ji} \in (0, \infty)$ and $\epsilon_0 \leq k_{ji} \leq \epsilon_{ji}, (j, i = 1, \dots, n)$. Assume that

$$f_i(k_{1i}, \dots, k_{ni}) = \int_{\epsilon_0}^{k_{1i}} \dots \int_{\epsilon_0}^{k_{ni}} \frac{\partial^n}{\diamond_\propto^{\lambda,\beta}\, \delta_{1i} \dots \diamond_\propto^{\lambda,\beta}\, \delta_{ni}} f_i(\delta_{1i}, \dots, \delta_{ni}) \diamond_\propto^{\lambda,\beta} \delta_{ni} \dots \diamond_\propto^{\lambda,\beta} \delta_{1i},$$

then

$$\int_{\epsilon_0}^{\epsilon_{11}} \dots \int_{\epsilon_0}^{\epsilon_{n1}} \int_{\epsilon_0}^{\epsilon_{12}} \dots \int_{\epsilon_0}^{\epsilon_{n2}} \dots \int_{\epsilon_0}^{\epsilon_{1n}} \dots \int_{\epsilon_0}^{\epsilon_{nn}} \square$$

$$\frac{\prod_{i=1}^n \left(\int_{\epsilon_0}^{k_{1i}} \dots \int_{\epsilon_0}^{k_{ni}} \left| \frac{\partial^n}{\diamond_\propto^{\lambda,\beta}\, \delta_{1i} \dots \diamond_\propto^{\lambda,\beta}\, \delta_{ni}} f_i(\delta_{1i}, \dots, \delta_{ni}) \right|^{p_i} \diamond_\propto^{\lambda,\beta} \delta_{ni} \dots \diamond_\propto^{\lambda,\beta} \delta_{1i} \right)^{\frac{1}{p_i}}}{\left(\sum_{i=1}^n \frac{(k_{1i} - \epsilon_0) \dots (k_{ni} - \epsilon_0)}{q_i} \right)^{\sum_{i=1}^n \frac{1}{q_i}}}$$

$$\diamond_\propto^{\lambda,\beta} k_{11} \dots \diamond_\propto^{\lambda,\beta} k_{n1} \dots \diamond_\propto^{\lambda,\beta} k_{12} \dots \diamond_\propto^{\lambda,\beta} k_{n2} \dots \diamond_\propto^{\lambda,\beta} k_{1n} \dots \diamond_\propto^{\lambda,\beta} k_{nn}$$

$$\leq M \prod_{i=1}^n \left(\int_{\epsilon_0}^{\epsilon_{1i}} \dots \int_{\epsilon_0}^{\epsilon_{ni}} \prod_{j=1}^n (h(\epsilon_{ji}) - k_{ji}) \left| \frac{\partial^n}{\diamond_\propto^{\lambda,\beta}\, k_{1i} \dots \diamond_\propto^{\lambda,\beta}\, k_{ni}} f_i(k_{1i}, \dots, k_{ni}) \right|^{p_i} \diamond_\propto^{\lambda,\beta} k_{1i} \dots \diamond_\propto^{\lambda,\beta} k_{ni} \right)^{\frac{1}{p_i}} \quad (6)$$

Where $M = M(\epsilon_{1i} \dots \epsilon_{ni}) \left(n - \sum_{i=1}^n \frac{1}{p_i} \right)^{\sum_{i=1}^n \frac{1}{p_i} - n} \prod_{i=1}^n ((\epsilon_{1i} - \epsilon_0) \dots (\epsilon_{ni} - \epsilon_0))^{\frac{1}{q_i}}$.

Proof. From Theorem 3.1, we obtain

$$f_i(k_{1i}, \dots, k_{ni}) \leq \int_{\epsilon_0}^{k_{1i}} \dots \int_{\epsilon_0}^{k_{ni}} \left| \frac{\partial^n}{\diamond_\propto^{\lambda,\beta}\, \delta_{1i} \dots \diamond_\propto^{\lambda,\beta}\, \delta_{ni}} f_i(\delta_{1i}, \dots, \delta_{ni}) \right| \diamond_\propto^{\lambda,\beta} \delta_{ni} \dots \diamond_\propto^{\lambda,\beta} \delta_{1i}. \quad (7)$$

On the other hand, by using Hölder's dynamic inequality and inequality

$$\left(\prod_{i=1}^{n} w_i^{\frac{1}{q_i}}\right)^{\frac{1}{\sum_{i=1}^{n}\frac{1}{q_i}}} \leq \frac{1}{\sum_{i=1}^{n}\frac{1}{q_i}}\sum_{i=1}^{n}\frac{w_i}{q_i}, \quad w_i > 0 \quad (i = 1, \dots, n),$$

we obtain

$$\prod_{i=1}^{n}|f_i(k_{1i}, \dots, k_{ni})| \leq \prod_{i=1}^{n}\int_{\epsilon_0}^{k_{1i}} \dots \int_{\epsilon_0}^{k_{ni}} \left|\frac{\partial^n}{\diamond_\alpha^{\lambda,\beta}\,\delta_{1i} \dots \diamond_\alpha^{\lambda,\beta}\,\delta_{ni}} f_i(\delta_{1i}, \dots, \delta_{ni})\right| \diamond_\alpha^{\lambda,\beta}\,\delta_{ni} \dots \diamond_\alpha^{\lambda,\beta}\,\delta_{1i}$$

$$\leq \prod_{i=1}^{n}((k_{1i} - \epsilon_0) \dots (k_{ni} - \epsilon_0))^{\frac{1}{q_i}}$$

$$\times \left(\int_{\epsilon_0}^{k_{1i}} \dots \int_{\epsilon_0}^{k_{ni}} \left|\frac{\partial^n}{\diamond_\alpha^{\lambda,\beta}\,\delta_{1i} \dots \diamond_\alpha^{\lambda,\beta}\,\delta_{ni}} f_i(\delta_{1i}, \dots, \delta_{ni})\right|^{p_i} \diamond_\alpha^{\lambda,\beta}\,\delta_{ni} \dots \diamond_\alpha^{\lambda,\beta}\,\delta_{1i}\right)^{\frac{1}{p_i}}$$

$$\leq \frac{\left(\sum_{i=1}^{n}\frac{(k_{1i} - \epsilon_0) \dots (k_{ni} - \epsilon_0)}{q_i}\right)^{\sum_{i=1}^{n}\frac{1}{q_i}}}{\left(n - \sum_{i=1}^{n}\frac{1}{p_i}\right)^{n-\sum_{i=1}^{n}\frac{1}{p_i}}}$$

$$\times \prod_{i=1}^{n}\left(\int_{\epsilon_0}^{k_{1i}} \dots \int_{\epsilon_0}^{k_{ni}} \left|\frac{\partial^n}{\diamond_\alpha^{\lambda,\beta}\,\delta_{1i} \dots \diamond_\alpha^{\lambda,\beta}\,\delta_{ni}} f_i(\delta_{1i}, \dots, \delta_{ni})\right|^{p_i} \diamond_\alpha^{\lambda,\beta}\,\delta_{ni} \dots \diamond_\alpha^{\lambda,\beta}\,\delta_{1i}\right)^{\frac{1}{p_i}}. \quad (8)$$

Divide (8) by $\left(\sum_{i=1}^{n}\frac{(k_{1i}-\epsilon_0)\dots(k_{ni}-\epsilon_0)}{q_i}\right)^{\sum_{i=1}^{n}\frac{1}{q_i}}$, then using dynamic Hölder inequality and $h(n)\geq n$, we have that

$$\int_{\epsilon_0}^{\epsilon_{11}}\dots\int_{\epsilon_0}^{\epsilon_{n1}}\int_{\epsilon_0}^{\epsilon_{12}}\dots\int_{\epsilon_0}^{\epsilon_{n2}}\dots\int_{\epsilon_0}^{\epsilon_{1n}}\dots\int_{\epsilon_0}^{\epsilon_{nn}}$$

$$\frac{\prod_{i=1}^{n}\left(\int_{\epsilon_0}^{k_{1i}}\dots\int_{\epsilon_0}^{k_{ni}}\left|\frac{\partial^n}{\diamond_\alpha^{\lambda,\beta}\,\delta_{1i}\dots\diamond_\alpha^{\lambda,\beta}\,\delta_{ni}}f_i(\delta_{1i},\dots,\delta_{ni})\right|^{p_i}\diamond_\alpha^{\lambda,\beta}\,\delta_{ni}\dots\diamond_\alpha^{\lambda,\beta}\,\delta_{1i}\right)^{\frac{1}{p_i}}}{\left(\sum_{i=1}^{n}\frac{(k_{1i}-\epsilon_0)\dots(k_{ni}-\epsilon_0)}{q_i}\right)^{\sum_{i=1}^{n}\frac{1}{q_i}}}$$

$$\diamond_\alpha^{\lambda,\beta}\,k_{11}\dots\diamond_\alpha^{\lambda,\beta}\,k_{n1}\dots\diamond_\alpha^{\lambda,\beta}\,k_{12}\dots\diamond_\alpha^{\lambda,\beta}\,k_{n2}\dots\diamond_\alpha^{\lambda,\beta}\,k_{1n}\dots\diamond_\alpha^{\lambda,\beta}\,k_{nn}$$

$$\leq\left(n-\sum_{i=1}^{n}\frac{1}{p_i}\right)^{\sum_{i=1}^{n}\frac{1}{p_i}-n}$$

$$\times\prod_{i=1}^{n}\int_{\epsilon_0}^{\epsilon_{1i}}\dots\int_{\epsilon_0}^{\epsilon_{ni}}\left(\int_{\epsilon_0}^{k_{1i}}\dots\int_{\epsilon_0}^{k_{ni}}\left|\frac{\partial^n}{\diamond_\alpha^{\lambda,\beta}\,\delta_{1i}\dots\diamond_\alpha^{\lambda,\beta}\,\delta_{ni}}f_i(\delta_{1i},\dots,\delta_{ni})\right|^{p_i}\diamond_\alpha^{\lambda,\beta}\,\delta_{ni}\dots\diamond_\alpha^{\lambda,\beta}\,\delta_{1i}\right)^{\frac{1}{p_i}}\diamond_\alpha^{\lambda,\beta}\,k_{ni}\dots\diamond_\alpha^{\lambda,\beta}\,k_{1i}$$

$$\leq\left(n-\sum_{i=1}^{n}\frac{1}{p_i}\right)^{\sum_{i=1}^{n}\frac{1}{p_i}-n}\prod_{i=1}^{n}((\epsilon_{1i}-\epsilon_0)\dots(\epsilon_{ni}-\epsilon_0))^{\frac{1}{q_i}}$$

$$\left(\int_{\epsilon_0}^{\epsilon_{1i}}\dots\int_{\epsilon_0}^{\epsilon_{ni}}\left(\int_{\epsilon_0}^{k_{1i}}\dots\int_{\epsilon_0}^{k_{ni}}\left|\frac{\partial^n}{\diamond_\alpha^{\lambda,\beta}\,\delta_{1i}\dots\diamond_\alpha^{\lambda,\beta}\,\delta_{ni}}f_i(\delta_{1i},\dots,\delta_{ni})\right|^{p_i}\diamond_\alpha^{\lambda,\beta}\,\delta_{ni}\dots\diamond_\alpha^{\lambda,\beta}\,\delta_{1i}\right)\diamond_\alpha^{\lambda,\beta}\,k_{ni}\dots\diamond_\alpha^{\lambda,\beta}\,k_{1i}\right)^{\frac{1}{p_i}}$$

$$=M\prod_{i=1}^{n}\left(\int_{\epsilon_0}^{\epsilon_{1i}}\dots\int_{\epsilon_0}^{\epsilon_{ni}}\prod_{j=1}^{n}(\epsilon_{ji}-k_{ji})\left|\frac{\partial^n}{\diamond_\alpha^{\lambda,\beta}\,k_{1i}\dots\diamond_\alpha^{\lambda,\beta}\,k_{ni}}f_i(k_{1i},\dots,k_{ni})\right|^{p_i}\diamond_\alpha^{\lambda,\beta}\,k_{ni}\dots\diamond_\alpha^{\lambda,\beta}\,k_{1i}\right)^{\frac{1}{p_i}}$$

$$\leq M\prod_{i=1}^{n}\left(\int_{\epsilon_0}^{\epsilon_{1i}}\dots\int_{\epsilon_0}^{\epsilon_{ni}}\prod_{j=1}^{n}(h(\epsilon_{ji})-k_{ji})\left|\frac{\partial^n}{\diamond_\alpha^{\lambda,\beta}\,k_{1i}\dots\diamond_\alpha^{\lambda,\beta}\,k_{ni}}f_i(k_{1i},\dots,k_{ni})\right|^{p_i}\diamond_\alpha^{\lambda,\beta}\,k_{ni}\dots\diamond_\alpha^{\lambda,\beta}\,k_{1i}\right)^{\frac{1}{p_i}}.$$

Remarks 3.2

i. In Theorem 3.1, let $\mathbb{T}=\mathbb{Z}, \propto=0$, and $\lambda=1$, then we see the results of Theorem 2.1 in [3].

ii. In Theorem 3.1, let $\mathbb{T}=\mathbb{R}, \propto=0$, and $\lambda=1$, then we see the results of Theorem 2.2 in [3].

Corollary 3.3 In Theorem 3.1, let $\propto = 0$, if we take $f_i(\theta_i)$ instead of $f_i(k_{1i}, \dots, k_{ni})$, then we see $f_i(\epsilon_0) = 0$,
and then we obtain

$$\int_{\epsilon_0}^{k_1}\int_{\epsilon_0}^{k_2}\dots\int_{\epsilon_0}^{k_n}\frac{\prod_{i=1}^{n}|f_i(\theta_i)|}{\left(\sum_{i=1}^{n}\frac{(\theta_i-\epsilon_0)}{q_i}\right)^{\sum_{i=1}^{n}\frac{1}{q_i}}}\diamond_{\propto}{}^{\lambda,\beta}\,\theta_n\diamond_{\propto}{}^{\lambda,\beta}\,\theta_{n-1}\dots\diamond_{\propto}{}^{\lambda,\beta}\,\theta_1$$

$$\leq S\prod_{i=1}^{n}\left(\int_{\epsilon_0}^{k_i}\left(h(k_i)-h(\theta_i)\right)\left|f_i{}^{\diamond_{\propto}{}^{\lambda,\beta}}(\theta_i)\right|^{p_i}\diamond_{\propto}{}^{\lambda,\beta}\,\delta_i\diamond_{\propto}{}^{\lambda,\beta}\,\theta_i\right)^{\frac{1}{p_i}}, \quad (9)$$

where $S = \left(n-\sum_{i=1}^{n}\frac{1}{p_i}\right)^{\sum_{i=1}^{n}\frac{1}{p_i}-n}\prod_{i=1}^{n}(k_i-\epsilon_0)^{\frac{1}{q_i}}$.

Remarks 3.4 Let $n = 2, \propto = 0$, in Corollary 3.3, if $p_1, p_2 > 1$ with $1/p_1 + 1/p_2 \geq 1$, and $0 < \lambda = 2 - 1/p_1 - 1/p_2 = 1/q_1 + 1/q_2 \leq 1$, inequality (9) reduces to inequality

$$\int_{\epsilon_0}^{k_1}\int_{\epsilon_0}^{k_2}\frac{|f_1(\theta_1)||f_2(\theta_2)|}{\left(q_2(\theta_1-\epsilon_0)+q_1(\theta_2-\epsilon_0)\right)^{w}}\diamond_{\propto}{}^{\lambda,\beta}\,\theta_2\diamond_{\propto}{}^{\lambda,\beta}\,\theta_1 \leq \frac{1}{(wq_1q_2)^{w}}(k_1-\epsilon_0)^{\frac{1}{q_1}}(k_2-\epsilon_0)^{\frac{1}{q_2}}$$

$$\times\left(\int_{\epsilon_0}^{k_1}\left(h(k_1)-h(\theta_1)\right)\left|f_1{}^{\diamond_{\propto}{}^{\lambda,\beta}}(\theta_1)\right|^{p_1}\diamond_{\propto}{}^{\lambda,\beta}\,\theta_1\right)^{\frac{1}{p_1}}\left(\int_{\epsilon_0}^{k_2}\left(h(k_2)-h(\theta_2)\right)\left|f_2{}^{\diamond_{\propto}{}^{\lambda,\beta}}(\theta_2)\right|^{p_2}\diamond_{\propto}{}^{\lambda,\beta}\,\theta_2\right)^{\frac{1}{p_2}}.$$

Conclusion

Hardy and Hilbert inequalities in different structures have been presented by researchers before. In this study, we have constructed new structures of Hardy-Hilbert inequalities in time scales for diamond alpha calculation. To be more precise, we have constructed a new form of Hardy-Hilbert inequality in time scales. The results we have obtained will be a source of motivation for our work in different fields.

REFERENCES

1. Hardy, G.H., Littlewood, J.E., Polya, G. (1952) Inequalities Cambridge Univ; Cambridge University Press: Cambridge, UK.
2. Zhao, C.-J., Chen, L.-Y., Cheung,W. (2011) On some new Hilbert-type inequalities. Math. Slovaca, 61, 15–28.
3. Zhao, C., Cheung, W. (2012) On Hilbert-type inequalities. J. Inequalities Appl. 2012, 145.
4. Pachpatte, B.G. (1998) A note on Hilbert type inequality. Tamkang J. Math., 29, 293–298.
5. Handley, G.D., Koliha, J.J., Pecaric, J. (2000) A Hilbert type inequality. Tamkang J. Math., 31, 311–316.
6. Akın, L., Zeren, Y. (2019). Some properties for higher order commutators of Hardy-type integral operator on Herz–Morrey spaces with variable exponent, Sigma J. Eng. & Nat. Sci.10(2), 157-163.
7. Akın, L. (2020) A Characterization of Boundedness of Fractional Maximal Operator with Variable Kernel on Herz-Morrey Spaces. Anal. Theory Appl., Vol. 36, No. 1, pp. 60-68.
8. Yang, B., Rassias, M.T., Raigorodskii, A. (2021) On an extension of a Hardy–Hilbert-type inequality with multi-parameters. Mathematics, 9, 2432.
9. Akin, L.(2018) A Characterization of Approximation of Hardy Operators in VLS, Celal Bayar University Journal of Science, Volume 14, Issue 3, pp:333-336.
10. Rassias, M.T. Yang, B. (2017) A half-discrete Hardy-Hilbert-type inequality with a best possible constant factor related to the hurwitz zeta function. In Progress in Approximation Theory and Applicable Complex Analysis: In Memory of QI Rahman; Springer: Cham, Switzerland, pp. 183–218.
11. Yang, B., Wu, S. Chen, Q. (2020) A new extension of Hardy-Hilbert's inequality containing a kernel of double power functions. Mathematics, 8, 894.
12. Yang, B., Wu, S., Wang, A. (2020) A new Hilbert-type inequality with positive homogeneous kernel and its equivalent forms. Symmetry, 12, 342.
13. Liao, J., Wu, S., Yang, B. (2020) On a new half-discrete Hilbert-type inequality involving the variable upper limit integral and partial sums. Mathematics, 8, 229.
14. Agarwal, R., O'Regan, D., Saker, S. (2014) Dynamic Inequalities on Time Scales; Springer: Cham, Switzerland.
15. Akin-Bohner, E., Bohner, M., Akin, F. (2005) Pachpatte inequalities on time scales. JIPAM J. Inequal. Pure Appl. Math., 6, 6.

16. Akın, L., Zeren, Y. (2023) On innovations of the multivariable fractional Hardy-type inequalities on time scales. Sigma J Eng Nat Sci;41(2):415−422.
17. Bohner, M., Matthews, T. (2008) Ostrowski inequalities on time scales. JIPAM J. Inequal. Pure Appl. Math., 9, 8.
18. Akın, L. (2024) On Some Inequalıtıes for Exponentıally Weighted Fractional Hardy Operators with Δ-Integral Calculus. Middle East Journal of Science 10(1):1-13.
19. Hilscher, R. (2002) A time scale version of a Wirtinger-type inequality and applications. J. Comput. Appl. Math., 141, 219–226.
20. Li, W.N. (2010) Some delay integral inequalities on time scales. Comput. Math. Appl., 59, 1929–1936.
21. Rehák, P. (2005) Hardy inequality on time scales and its application to half-linear dynamic equations. J. Inequal. Appl., 2005, 942973.
22. Agarwal, R.P., Lakshmikantham, V. (1993) Uniqueness and Nonuniqueness Criteria for Ordinary Differential Equations; Series in Real Analysis; World Scientific Publishing: Singapore,, Volume 6.
23. Li, J.D. (1992) Opial-type integral inequalities involving several higher order derivatives. J. Math. Anal. Appl., 167, 98–110.
24. Hilger, S. (1988) Ein Maßkettenkalkül mit Anwendung auf Zentrumsmannigfaltigkeiten. Ph.D. Thesis, Universität Würzburg, Würzburg, Germany.
25. Rahmat, M.R.S., Noorani, M.S.M. (2021) A new conformable nabla derivative and its application on arbitrary time scales. Adv. Differ. Equ., 2021, 238.
26. Akın, L. (2019) On a New Characterization of Some Class NonlinearEigenvalue Problem. Advances in Mathematical Physics, Volume 2019, Article ID 7865303, 1-7.
27. Pachpatte, B.G. (2000) Inequalities similar to certain extensions of Hilbert's inequality. J. Math. Anal. Appl., 243, 217–227.
28. Hilger, S. (1990). Analysis on measure chains-a unified approach to continuous and discrete calculus, Results Maths. 18(1-2) 18–56.
29. Hardy, G.H. (1920). Note on a theorem of Hilbert, Math. Z. 6(3–4), 314–317
30. Hardy, G.H.(1925). Notes on some points in the integral calculus, LX. An inequality between integrals, Mess. Math. 54,150–156.
31. Hardy, G.H., Littlewood, J.E. (1927). Elementary theorems concerning power series with positive coefficients and moment constants of positive functions, J. Reine Angew. Math. 157, 141–158.
32. Hardy, G.H. (1928). Notes on some points in the integral calculus, LXIV. Mess. Math. 57, 12–16.

33. Ahmad, W., Khan, K.A., Nosheen, A., Sultan, M.A. (2019). Copson, Leindler type inequalities for the function of several variables on time scales, Punjab Univ. J. of Math. 51(8),157–168.
34. Ashraf, M.S., Khan, K.A., Nosheen, A. (2019). Hardy-Copson type inequalities on time scales for the functions of n independent variables, Int. J. Anal. Appl. 17(2), 244–259.
35. Akın, L. (2019) Compactness of Fractional Maximal Operator in Weighted and Variable Exponent Spaces. Erzincan University Journal of Science and Technology, 12(1), 185-190
36. Nosheen, A., Nawaz, A., Khan, K.A., Awan, K.M. (in press) Multivariate Hardy and Littlewood inequalities on time scales, Arap Journal of Mathematical Science.
37. Saker, S.H., O'Regan, D. (2016) Hardy and Littlewood Inequalities on time scales, Bull. Malays. Math. Sci. Soc. 39(2) 527–543.
38. Li, W., Liu, D., Liu, J. (2019). Weighted inequalities for fractional Hardy operators and commutators, Journal of Inequalities and Applications 2019:158, 1-14.
39. Bradley, J. (1978). Hardy inequalities with mixed norms. Can. Math. Bull. 21(4), 405-408.
40. Kufner, A., Persson, L.E. (2003). Weighted Inequalities of Hardy Type. World Scientific, Singapore.
41. Opic, B., Kufner, A. (1990). Hardy-Type Inequalities. Pitman Research Notes in Mathematics Series, Longman Scientific and Technical, Harlow, Essex.
42. Akın, L. (2020). On some results of weighted Hölder type inequality on time scales. Middle East Journal of Science 6(1), 15-22.
43. Akın L.(2021). On innovations of n-dimensional integral-type inequality on time scales. Adv. Differ. Equ. 2021:148.
44. Bohner, M., Nosheen, A., Pecaric, J., Younas, A. (2014). Some dynamic Hardy type inequalities on time scales, J. Math. Inequal. 8(1), 185–199.
45. Agarwal, R.P., Bohner, M., O'Regan, D., Saker, S.H. (2011). Some Wirtinger-type inequalities on time scales and their applications, Pacific J. Math. 252, 1–26 (2011)
46. Akın, L. (2020). On the Fractional Maximal Delta Integral Type Inequalities on Time Scales. Fractal Fract. 4, 26, 1-10.
47. Bohner, M., Petereson, A. (2001). Dynamic Equations on Time Scales. An Introduction with Applications, Birkhauser, Boston.
48. Akın L. (2021). A New Approach for the Fractional Integral Operator in Time Scales with Variable Exponent Lebesgue Spaces. Fractal Fract. 5(7), 1-13.

49. Bohner, M., Georgiev, S.G. (2016). Sequences and Series of Functions. In: Multivariable Dynamic Calculus on Time Scales, Springer Int. Publ. Switzerland.
50. Akın, L. (2024) On generalized weighted dynamic inequalities for diamond−∝ integral on time scales calculus. Indian J Pure Appl Math 55, 363–376.
51. Anastassiou, G.A. Principles of delta fractional calculus on time scales and inequalities. Math. Comput. Model. 2010, 52, 556–566.
52. Akın, L. (2021) New Principles of Non-Linear Integral Inequalities on Time Scales. Applied Mathematics and Nonlinear Sciences, 6(2) (2021) 387–394.
53. Saker, S.H., El-Sheikh, M.M.A., Madian, A.M. (2021) Some new generalized weighted dynamic inequalities of Hardy's type on time scales, J. Math. Computer Sci., 23 (2021), 289–301.
54. Almarri, B., El-Deeb, A.A. (2023) Gamma-Nabla Hardy–Hilbert-Type Inequalities on Time Scales. Axioms, 12, 449.
55. Miller, K. B., Ross, B. (1993) An Introduction to the Fractional Calculus and Fractional Differential Equations. New York, Wiley.
56. Oldham, K. B., Spanier, J. (1974) The Fractional Calculus. New York and London: Academic Press.
57. Podlubny, I. (1999) Fractional Differential Equations. San Diego: Academic Press.
58. Herrmann, R. (2014) Fractional Calculus: an Introduction for Physicists[M]. Singapore: World Scientific.
59. Sabatier, J., Agrawal, O. P., Machado, J. A.T. (2007) Advances in Fractional Calculus: Theoretical Developments and Applications in Physics and Engineering[M]. Netherlands: Springer.
60. Tejado, I., Valerio, D., Valerio, N. (2015) Fractional Calculus in Economic Growth Modelling: the Spanish Case. Netherlands: Springer.
61. Meilanov, R. P., Magomedov. R. A. (2014) Thermodynamics in fractional calculus. J Eng Phys Thermophys, 87(6): 1521-1531.

Chapter 4

On n-Dimensional Hilbert-Type Inequalities on Time Scale

Lütfi AKIN[1]

[1] Doç. Dr.;Mardin Artuklu Üniversitesi İktisadi ve İdari Bilimler Fakültesi İşletme Bölümü.
lutfiakin@artuklu.edu.tr ORCID No: 0000-0002-5653-9393

INTRODUCTION

In general, inequalities and their different forms have a considerable place in harmonic analysis and other application areas. One of these is the well-known Hilbert inequality in mathematics. These integral inequalities also play an important role in calculating time scales, which combine continuous and different forms of cases. At the same time, these integral inequalities are one of the main cornerstones of applied mathematics. Before starting our work, we think giving some information about Hilbert's inequality will be useful. If the reader wants, he can look at the references section at the end of this work for more detailed information.

In [1], the theorems we give below are well-known classical statements about Hilbert's inequality.

Theorem 1.1. Let $p, q > 1$, $\frac{1}{p} + \frac{1}{q} \leq 1$, and $0 < w = 2 - \frac{1}{p} - \frac{1}{q} = \frac{1}{p'} + \frac{1}{q'} \leq 1$, then

$$\sum_{j=1}^{\infty}\sum_{i=1}^{\infty}\frac{f_j g_i}{(j+i)^w} \leq D\left(\sum_{j=1}^{\infty} f_j^p\right)^{\frac{1}{p}}\left(\sum_{i=1}^{\infty} g_i^q\right)^{\frac{1}{q}}, \tag{1}$$

where $D = D(p, q)$.

Theorem 1.2. Let $f \in L^p(0,\infty)$, $g \in L^q(0,\infty)$, and let p, q, p', q', w be as in Theorem 1.1, then

$$\int_0^{\infty}\int_0^{\infty}\frac{f(x)g(y)}{(x+y)^w}\,dx\,dy \leq D\left(\int_0^{\infty} f^p(x)dx\right)^{\frac{1}{p}}\left(\int_0^{\infty} g^q(y)dy\right)^{\frac{1}{q}}, \tag{2}$$

where $D = D(p, q)$.

In [2], Zhao et al. introduced a new inequality that is compatible with the structure of Theorem 1.2.

Theorem 1.3. Let $\frac{1}{p_i}+\frac{1}{q_i}=1$ with $p_i>1,\ \pi_i\geq 1$. Let differentiable function $f_i(\theta_i)$ on $[0,k_i)$, where $k_i\in(0,\infty)$. Assume $f_i(0)=0$ for $(i=1,\dots,n)$. Then

$$\int_0^{k_1}\int_0^{k_2}\dots\int_0^{k_n}\frac{\prod_{i=1}^{n}|f_i^{\pi_i}(\theta_i)|}{\left(\sum_{i=1}^{n}\frac{\theta_i}{q_i}\right)^{\sum_{i=1}^{n}\frac{1}{q_i}}}d\theta_n d\theta_{n-1}\dots d\theta_1\leq D\prod_{i=1}^{n}\left(\int_0^{k_i}(k_i-\theta_i)\left|f_i^{\pi_i-1}(\theta_i)f_i'(\theta_i)\right|^{p_i}d\theta_i\right)^{\frac{1}{p_i}},$$

where $D=\left(n-\sum_{i=1}^{n}\frac{1}{p_i}\right)^{\sum_{i=1}^{n}\frac{1}{p_i}-n}\prod_{i=1}^{n}\pi_i k_i^{\frac{1}{q_i}}$.

For more detailed information on Hilbert inequalities, see monographs [3-27, 52-61].

PRELIMINARIES

Although the history of time scale calculation is not very long, it has positioned itself not only in the field of mathematics but also in other disciplines of science. It owes this position to the unification of continuous and discrete cases in mathematics. Due to this situation, scientists in almost every field have integrated this field into their field of study and have contributed many innovations to the literature. Analytical solutions of differential equations in applied mathematics and mathematical modeling in economics are just a few examples of these application areas. Those who want to have more general information can look at references [28, 42, 43, 44, 45-51]. $\mathbb{T}$ is a time scale that arbitrary non-empty closed subset of real numbers ($\mathbb{R}$). In our study, we will take this situation of $(0,\infty)_{\mathbb{T}}=(0,\infty)\cap\mathbb{T}$ into consideration.

Now let's briefly give the basic concepts about the diamond-alpha derivative.

$\sigma,\rho:\mathbb{T}\to\mathbb{T}$ are defined by $\sigma(t)=inf\{s\in\mathbb{T}:s>t\}$, $\rho(t)=sup\{s\in\mathbb{T}:s>t\}$ for $t\in\mathbb{T}$. $\sigma(t)$ is the jump operator (forward), and $\rho(t)$ is the jump operator (backward), respectively. Let $\sigma(t)>t$, then t is rs (right-scattered), and let $\sigma(t)=t$, then t is called rd (right-dense). Let $\rho(t)<t$, then t is ls (left-scattered), and let $\rho(t)=t$, then t is called ld (left-dense).

Let $\mu,\vartheta:\mathbb{T}\to\mathbb{R}^+$ such that $\mu(t)=\sigma(t)-t,\ \vartheta(t)=t-\rho(t)$. $\mu(t)$ and $\vartheta(t)$ are called gm (graininess mappings).

If the time scale $\mathbb{T}$ has a ls (left-scattered) maximum m, then $\mathbb{T}^k = \mathbb{T} - \{m\}$. Otherwise $\mathbb{T}^k = \mathbb{T}$.

$\mathbb{T}^{\mathrm{k}}$ is defined as follows

$$\mathbb{T}^k = \begin{cases} \mathbb{T} \setminus (\rho\, sup\, \mathbb{T}, sup\, \mathbb{T}], & if \quad sup\, \mathbb{T} < \infty \\ \mathbb{T}, & if \quad sup\, \mathbb{T} = \infty, \end{cases}$$

and

$$\mathbb{T}_k = \begin{cases} \mathbb{T} \setminus [inf\, \mathbb{T}, \sigma(inf\, \mathbb{T})], & |inf\, \mathbb{T}| < \infty \\ \mathbb{T}, & inf\, \mathbb{T} = -\infty. \end{cases}$$

Assume that $h: \mathbb{T} \to \mathbb{R}$ is a function. Let t be right-dense.

i) Let π be delta differentiable at t $(t \in \mathbb{T}^k (t \neq min\mathbb{T}))$, then π is continuous at t.
ii) Let π be lc (left continuous) at t, and t is rs (right-scattered), then π is delta differentiable at t,

$$\pi^{\Delta}(t) = \frac{\pi^{\sigma}(t) - \pi(t)}{\mu(t)}$$

iii) Let π be delta differentiable at t and $\lim_{s \to t} \frac{\pi(t) - \pi(s)}{t - s}$, then

$$\pi^{\Delta}(t) = \lim_{s \to t} \frac{\pi(t) - \pi(s)}{t - s}.$$

iv) Let π be delta differentiable at t, then $\pi^{\sigma}(t) = \pi(t) + \mu(t)\pi^{\Delta}(t)$.

Let $\mathbb{T} = \mathbb{R}$, then $\pi^{\Delta}(t) = \pi'(t)$, and Let $\mathbb{T} = \mathbb{Z}$, then $\pi^{\Delta}(t)$ reduces to $\Delta\pi(t)$.

Let $K: \mathbb{T} \to \mathbb{R}$ is defined as a delta antiderivative of $\pi: \mathbb{T} \to \mathbb{R}$, then $K^{\Delta} = \pi(t)$ holds for all $t \in \mathbb{T}$, and we define the delta integral of π by

$$\int_s^t \pi(\tau)\Delta\tau = K(t) - K(s),$$

for all $s, t \in \mathbb{T}$.

Suppose $\pi: \mathbb{R} \to \mathbb{R}$ is a continuous function and delta differentiable on $\mathbb{T}$. If $\varphi: \mathbb{R} \to \mathbb{R}$ is continuously differentiable, then we have

$$(\varphi \circ \pi)^{\Delta}(s) = \varphi'\big(\pi(m)\big)\pi^{\Delta}(s), \quad m \in [s, \sigma(s)].$$

Let's now give some definitions for the nabla integral.

Let $\pi: \mathbb{T}_k \to \mathbb{R}$ is called nabla differentiable at $t \in \mathbb{T}_k$. If $\varepsilon > 0$, then the following inequality is provided

$$\big|\pi\big(\rho(t)\big) - \pi(s) - \pi^{\nabla}(t)(\rho(t) - s)\big| \leq \varepsilon|\rho(t) - s|,$$

for all $s \in V$.

Let $K: \mathbb{T} \to \mathbb{R}$ is called a nabla antiderivative of $\pi: \mathbb{T} \to \mathbb{R}$, then we define

$$\int_s^t \pi(\tau)\nabla\tau = K(t) - K(s),$$

for all $s, t \in \mathbb{T}$.

In [50], Let $\vartheta(t)$ be diamond alpha differentiable on $\mathbb{T}$ for all $\propto, t \in \mathbb{T}$, then we define $\vartheta^{\diamond\propto}(t)$ by

$$\vartheta^{\diamond\propto}(t) = \propto \vartheta^{\Delta}(t) + (1-\propto)\vartheta^{\nabla}(t)$$

for $0 \leq \propto \leq 1$.

Theorem 2.1 [50] Let $\vartheta, h: \mathbb{T} \to \mathbb{R}$ be diamond alpha differentiable for all $\propto, t \in \mathbb{T}$ and $0 \leq \propto \leq 1$.

(i) Let $(\vartheta + h): \mathbb{T} \to \mathbb{R}$ be diamond alpha differentiable for all $t \in \mathbb{T}$, then

$$(\vartheta + h)^{\diamond\propto}(t) = \vartheta^{\diamond\propto}(t) + h^{\diamond\propto}(t).$$

(ii) Let $k\vartheta: \mathbb{T} \to \mathbb{R}$ be diamond alpha differentiable for all $\propto, t \in \mathbb{T}$, then

$$(k\vartheta)^{\diamond\propto}(t) = k\vartheta^{\diamond\propto}(t),$$

where t,$k \in \mathbb{R}$.

(iii) Let $\vartheta, h: \mathbb{T} \to \mathbb{R}$ be diamond alpha differentiable for all $\propto, t \in \mathbb{T}$, then

$$(\vartheta h)^{\diamond\propto}(t) = \vartheta^{\diamond\propto}(t)h(t) + \propto \vartheta^{\sigma}(t)h^{\Delta}(t) + (1-\propto)\vartheta^{\rho}(t)h^{\nabla}(t).$$

Definition 2.2 [50] If $\vartheta: \mathbb{T} \to \mathbb{R}$ is $\diamond_{\propto}-$integrable for all $\propto, b, t \in \mathbb{T}$, then

$$\int_{b}^{t} \vartheta(\delta) \diamond_{\propto} \delta = \propto \int_{b}^{t} \vartheta(\delta)\Delta\delta + (1-\propto) \int_{b}^{t} \vartheta(\delta)\nabla\delta$$

for $0 \leq \propto \leq 1$.

Definition 2.3 [46, 52] Let $\vartheta \in C_{rd}(\mathbb{T}, \mathbb{R})$, $t \in \mathbb{T}^{k}$ and let $\vartheta: \mathbb{T} \to \mathbb{R}$ be diamond alpha integrable, then

$$\int_{t}^{\sigma(t)} \vartheta(\tau) \diamond_{\propto} \tau = \mu(t)\vartheta(t).$$

The partial integration formula on the time scale is given by

$$\int_{x}^{y} u(s)w^{\diamond\propto}(s) \diamond_{\propto} s = u(s)w(s)\mathrm{I}_{x}^{y} - \int_{x}^{y} u^{\diamond\propto}(s)w^{\sigma}(s) \diamond_{\propto} s$$

for $0 \leq \propto \leq 1$.

Definition 2.4 [25, 51] (Conformable diamond-alpha derivative) Given $\vartheta: \mathbb{T} \to \mathbb{R}$ and $\beta \in \mathbb{T}$, ϑ is $(\lambda, \beta)-$diamond alpha differentiable at $\eta > \beta$, if it's diamond alpha differentiable at η, and its $(\lambda, \beta)-$diamond alpha derivative is defined by

$$\diamond_{\propto}^{\lambda}{}_{\beta} \vartheta(\eta) = \Lambda_{1-\lambda}(\eta, \beta)\vartheta^{\diamond\propto}(\eta) \qquad \eta > \beta, \tag{3}$$

Definition 2.5 [25, 51] (Conformable diamond-alpha integral) Suppose that $\beta, \eta_1, \eta_2 \in \mathbb{T}$, $\vartheta \in C(\mathbb{T}), 0 < \lambda \leq 1, \beta \leq \eta_1 \leq \eta_2$, and the function ϑ is called $(\lambda, \beta)-$diamond alpha integrable on $[\eta_1, \eta_2]$ if

$$\diamond_{\propto}{}_{\beta}^{\lambda}\,\vartheta(\eta)=\int_{\eta_1}^{\eta_2}\vartheta(\eta)\,\diamond_{\propto}{}_{\beta}^{\lambda}\,\eta=\int_{\eta_1}^{\eta_2}\vartheta(\eta)\Lambda_{1-\lambda}(\sigma^{1-\lambda}(\eta),\beta)\,\diamond_{\propto}\eta, \qquad (4)$$

Lemma 2.6 [14] If $f,\varepsilon\in CC_{rd}^{1}([\omega,p]_{\mathbb{T}}\times[\omega,p]_{\mathbb{T}},\mathbb{R})$ are diamond alpha integrable functions and $\frac{1}{p}+\frac{1}{q}=1$ with $p>1$ and let $\omega,p\in\mathbb{T}$ with $\omega<p$, then

$$\int_{\omega}^{p}\int_{\omega}^{p}|f(t,\epsilon)\varepsilon(t,\epsilon)|\,\diamond_{\propto}{}^{\lambda,\beta}\,t\,\diamond_{\propto}{}^{\lambda,\beta}\,\epsilon$$

$$\leq\left(\int_{\omega}^{p}\int_{\omega}^{p}|f(t,\epsilon)|^{p}\,\diamond_{\propto}{}^{\lambda,\beta}\,t\,\diamond_{\propto}{}^{\lambda,\beta}\,\epsilon\right)^{\frac{1}{p}}\times\left(\int_{\omega}^{p}\int_{\omega}^{p}|\varepsilon(t,\epsilon)|^{q}\,\diamond_{\propto}{}^{\lambda,\beta}\,t\,\diamond_{\propto}{}^{\lambda,\beta}\,\epsilon\right)^{\frac{1}{q}}. \qquad (5)$$

In this study, we prove a new fractional inequality of Hilbert-type on time scales using the properties of Theorem 1.3 mentioned above. We also obtain discrete cases of Hilbert-type inequalities related to some special cases of our results.

Main Result

Theorem 3.1 Let $\epsilon_0,\tau_i,k_i,\theta_i,\epsilon_i\in\mathbb{T}$, $(i=1,\dots,n)$. Let $p_i,q_i>1,\pi_i\geq1$ be constants and $\frac{1}{p_i}+\frac{1}{q_i}=1$ and let $\diamond_{\propto}{}^{\lambda,\beta}-$differentiable functions and $f_i(\theta_i,\epsilon_i)$ be decreasing on $[\epsilon_0,k_i)_{\mathbb{T}}\times[\epsilon_0,\tau_i)_{\mathbb{T}}$ and $f_i(\epsilon_0,\epsilon_i)=f_i(\theta_i,\epsilon_0)=0$ (i=1,…,n). Let $f_i{}^{\diamond_{\propto_1}^{\lambda,\beta}}$, $f_i{}^{\diamond_{\propto_2}^{\lambda,\beta}}$, $f_i{}^{\diamond_{\propto_{12}}^{\lambda,\beta}}=f_i{}^{\diamond_{\propto_{21}}^{\lambda,\beta}}$ partial derivatives of f_i f and let

$$\left(f_i^{\pi_i}(\theta_i,\epsilon_i)\right)^{\diamond_{\propto_1}^{\lambda,\beta}\diamond_{\propto_2}^{\lambda,\beta}}\leq\left(\pi_i f_i^{\pi_i-1}(\theta_i,\epsilon_i)f_i{}^{\diamond_{\propto_1}^{\lambda,\beta}}(\theta_i,\epsilon_i)\right)^{\diamond_{\propto_2}^{\lambda,\beta}}=f_i{}^{\diamond_{\propto_{12}}^{\lambda,\beta}}(\theta_i,\epsilon_i),$$

then

$$\int_{\epsilon_0}^{k_1}\int_{\epsilon_0}^{\tau_1}\dots\int_{\epsilon_0}^{k_n}\int_{\epsilon_0}^{\tau_n}\frac{\prod_{i=1}^{n}|f_i^{\pi_i}(\theta_i,\epsilon_i)|}{\left(\sum_{i=1}^{n}\frac{(\theta_i-\epsilon_0)(\epsilon_i-\epsilon_0)}{q_i}\right)^{\sum_{i=1}^{n}\frac{1}{q_i}}}\,\diamond_{\propto}^{\lambda,\beta}\,\epsilon_n\,\diamond_{\propto}^{\lambda,\beta}\,\theta_n\dots\diamond_{\propto}^{\lambda,\beta}\,\epsilon_1\,\diamond_{\propto}^{\lambda,\beta}\,\theta_1$$

$$\leq B\prod_{i=1}^{n}\left(\int_{\epsilon_0}^{k_i}\int_{\epsilon_0}^{\tau_i}(h(k_i)-h(\theta_i))\,(h(\tau_i)-h(\epsilon_i))\left|f_i^{\diamond_{\propto_{12}}^{\lambda,\beta}}(\theta_i,\epsilon_i)\right|^{p_i}\diamond_{\propto}^{\lambda,\beta}\,\epsilon_i\,\diamond_{\propto}^{\lambda,\beta}\,\theta_i\right)^{\frac{1}{p_i}}, \tag{6}$$

where $B=B(k_1\tau_1,\dots,k_n\tau_n)=\left(n-\sum_{i=1}^{n}\frac{1}{p_i}\right)^{\sum_{i=1}^{n}\frac{1}{p_i}-n}\prod_{i=1}^{n}[(k_i-\epsilon_0)(\tau_i-\epsilon_0)]^{\frac{1}{q_i}}$.

Proof. We can write the following inequality

$$f_i^{\pi_i}(\theta_i,\epsilon_i)=f_i^{\pi_i}(\theta_i,\epsilon_i)-f_i^{\pi_i}(\epsilon_0,\epsilon_i)-f_i^{\pi_i}(\theta_i,\epsilon_0)f_i^{\pi_i}(\epsilon_0,\epsilon_0)$$

$$=\int_{\epsilon_0}^{\theta_i}\left(f_i^{\pi_i}(\eta_i,\epsilon_i)\right)^{\diamond_{\propto_1}^{\lambda,\beta}}\diamond_{\propto_1}^{\lambda,\beta}\,\eta_i-\int_{\epsilon_0}^{\theta_i}\left(f_i^{\pi_i}(\eta_i,\epsilon_0)\right)^{\diamond_{\propto_1}^{\lambda,\beta}}\diamond_{\propto_1}^{\lambda,\beta}\,\eta_i$$

$$=\int_{\epsilon_0}^{\theta_i}\left[\left(f_i^{\pi_i}(\eta_i,\epsilon_i)\right)^{\diamond_{\propto_1}^{\lambda,\beta}}-\left(f_i^{\pi_i}(\eta_i,\epsilon_0)\right)^{\diamond_{\propto_1}^{\lambda,\beta}}\right]\diamond_{\propto}^{\lambda,\beta}\,\eta_i$$

$$\leq\int_{\epsilon_0}^{\theta_i}\int_{\epsilon_0}^{\epsilon_i}\left[\pi_i f_i^{\pi_i-1}(\eta_i,\varphi_i)f_i^{\diamond_{\propto_1}^{\lambda,\beta}}(\eta_i,\varphi_i)\right]^{\diamond_{\propto_2}^{\lambda,\beta}}\diamond_{\propto}^{\lambda,\beta}\,\eta_i\,\diamond_{\propto}^{\lambda,\beta}\,\varphi_i$$

$$=\int_{\epsilon_0}^{\theta_i}\int_{\epsilon_0}^{\epsilon_i}f_i^{\diamond_{\propto_{12}}^{\lambda,\beta}}(\eta_i,\varphi_i)\diamond_{\propto}^{\lambda,\beta}\,\varphi_i\,\diamond_{\propto}^{\lambda,\beta}\,\eta_i. \tag{7}$$

Applying (5), we have

$$\prod_{i=1}^{n} f_i^{\pi_i}(\theta_i,\epsilon_i) \le \prod_{i=1}^{n} \int_{\epsilon_0}^{\theta_i}\int_{\epsilon_0}^{\epsilon_i} f_i^{\circ_{\propto_{12}}^{\lambda,\beta}}(\eta_i,\varphi_i) \diamond_{\propto}^{\lambda,\beta} \varphi_i \diamond_{\propto}^{\lambda,\beta} \eta_i$$

$$\le \prod_{i=1}^{n}\left((\theta_i-\epsilon_0)(\epsilon_i-\epsilon_0)\right)^{\frac{1}{q_i}}\left(\int_{\epsilon_0}^{\theta_i}\int_{\epsilon_0}^{\epsilon_i} f_i^{\circ_{\propto_{12}}^{\lambda,\beta}}(\eta_i,\varphi_i) \diamond_{\propto}^{\lambda,\beta} \varphi_i \diamond_{\propto}^{\lambda,\beta} \eta_i\right)^{\frac{1}{p_i}}. \quad (8)$$

Applying the following inequality

$$\left(\prod_{i=1}^{n} w_i^{\frac{1}{q_i}}\right)^{\frac{1}{\sum_{i=1}^{n}\frac{1}{q_i}}} \le \frac{1}{\sum_{i=1}^{n}\frac{1}{q_i}}\sum_{i=1}^{n}\frac{w_i}{q_i}, \quad w_i > 0 \quad (i=1,\dots,n),$$

we find

$$\frac{\prod_{i=1}^{n}|f_i^{\pi_i}(\theta_i,\epsilon_i)|}{\left(\sum_{i=1}^{n}\frac{(\theta_i-\epsilon_0)(\epsilon_i-\epsilon_0)}{q_i}\right)^{\sum_{i=1}^{n}\frac{1}{q_i}}}$$

$$\le \left(n-\sum_{i=1}^{n}\frac{1}{p_i}\right)^{\sum_{i=1}^{n}\frac{1}{p_i}-n}\prod_{i=1}^{n}\left(\int_{\epsilon_0}^{\theta_i}\int_{\epsilon_0}^{\epsilon_i} f_i^{\diamond_{\propto_{12}}^{\lambda,\beta}}(\eta_i,\varphi_i) \diamond_{\propto}^{\lambda,\beta} \varphi_i \diamond_{\propto}^{\lambda,\beta} \eta_i\right)^{\frac{1}{p_i}}. \quad (9)$$

From inequality (5) and Fubini's theorem, we see that

$$\int_{\epsilon_0}^{k_1}\int_{\epsilon_0}^{\tau_1}\cdots\int_{\epsilon_0}^{k_n}\int_{\epsilon_0}^{\tau_n}\frac{\prod_{i=1}^{n}|f_i^{\pi_i}(\theta_i,\epsilon_i)|}{\left(\sum_{i=1}^{n}\frac{(\theta_i-\epsilon_0)(\epsilon_i-\epsilon_0)}{q_i}\right)^{\sum_{i=1}^{n}\frac{1}{q_i}}}\,\diamond_{\propto}{}^{\lambda,\beta}\,\epsilon_n\,\diamond_{\propto}{}^{\lambda,\beta}\,\theta_n\ldots\diamond_{\propto}{}^{\lambda,\beta}\,\epsilon_1\,\diamond_{\propto}{}^{\lambda,\beta}\,\theta_1$$

$$\leq\left(n-\sum_{i=1}^{n}\frac{1}{p_i}\right)^{\sum_{i=1}^{n}\frac{1}{p_i}-n}\times\prod_{i=1}^{n}\left(\int_{\epsilon_0}^{k_i}\int_{\epsilon_0}^{\tau_i}\left(\int_{\epsilon_0}^{\theta_i}\int_{\epsilon_0}^{\epsilon_i}\left|f_i^{\diamond_{\propto_{12}}^{\lambda,\beta}}(\eta_i,\varphi_i)\right|^{p_i}\diamond_{\propto}{}^{\lambda,\beta}\,\varphi_i\,\diamond_{\propto}{}^{\lambda,\beta}\,\eta_i\right)^{\frac{1}{p_i}}\diamond_{\propto}{}^{\lambda,\beta}\,\epsilon_i\,\diamond_{\propto}{}^{\lambda,\beta}\,\theta_i\right)$$

$$\leq\left(n-\sum_{i=1}^{n}\frac{1}{p_i}\right)^{\sum_{i=1}^{n}\frac{1}{p_i}-n}$$

$$\times\prod_{i=1}^{n}((k_i-\epsilon_0)(\tau_i-\epsilon_0))^{\frac{1}{q_i}}\left(\int_{\epsilon_0}^{k_i}\int_{\epsilon_0}^{\tau_i}\left(\int_{\epsilon_0}^{\theta_i}\int_{\epsilon_0}^{\epsilon_i}\left|f_i^{\diamond_{\propto_{12}}^{\lambda,\beta}}(\eta_i,\varphi_i)\right|^{p_i}\diamond_{\propto}{}^{\lambda,\beta}\,\varphi_i\,\diamond_{\propto}{}^{\lambda,\beta}\,\eta_i\right)\diamond_{\propto}{}^{\lambda,\beta}\,\epsilon_i\,\diamond_{\propto}{}^{\lambda,\beta}\,\theta_i\right)^{\frac{1}{p_i}}$$

$$=B\prod_{i=1}^{n}\left(\int_{\epsilon_0}^{k_i}\int_{\epsilon_0}^{\tau_i}(k_i-\theta_i)(\tau_i-\epsilon_i)\left|f_i^{\diamond_{\propto_{12}}^{\lambda,\beta}}(\theta_i,\epsilon_i)\right|^{p_i}\diamond_{\propto}{}^{\lambda,\beta}\,\epsilon_i\,\diamond_{\propto}{}^{\lambda,\beta}\,\theta_i\right)^{\frac{1}{p_i}}. \tag{10}$$

Using $k_i\leq h(k_i)$, we obtain

$$\int_{\epsilon_0}^{k_1}\int_{\epsilon_0}^{\tau_1}\cdots\int_{\epsilon_0}^{k_n}\int_{\epsilon_0}^{\tau_n}\frac{\prod_{i=1}^{n}|f_i^{\pi_i}(\theta_i,\epsilon_i)|}{\left(\sum_{i=1}^{n}\frac{(\theta_i-\epsilon_0)(\epsilon_i-\epsilon_0)}{q_i}\right)^{\sum_{i=1}^{n}\frac{1}{q_i}}}\,\diamond_{\propto}{}^{\lambda,\beta}\,\epsilon_n\,\diamond_{\propto}{}^{\lambda,\beta}\,\theta_n\ldots\diamond_{\propto}{}^{\lambda,\beta}\,\epsilon_1\,\diamond_{\propto}{}^{\lambda,\beta}\,\theta_1$$

$$\leq B\prod_{i=1}^{n}\left(\int_{\epsilon_0}^{k_i}\int_{\epsilon_0}^{\tau_i}\big(h(k_i)-h(\theta_i)\big)\big(h(\tau_i)-h(\epsilon_i)\big)\left|f_i^{\diamond_{\propto_{12}}^{\lambda,\beta}}(\theta_i,\epsilon_i)\right|^{p_i}\diamond_{\propto}{}^{\lambda,\beta}\,\epsilon_i\,\diamond_{\propto}{}^{\lambda,\beta}\,\theta_i\right)^{\frac{1}{p_i}}.$$

Remarks 3.2

i. In Theorem 3.1, let $\mathbb{T}=\mathbb{Z},\propto=0,\lambda=1$, and $\pi_i=1$, then we see the results of (Theorem 1.2, [2]).
ii. In Theorem 3.1, let $\mathbb{T}=\mathbb{R},\propto=0,\lambda=1$, then we see the results of (Theorem 1.4, [2]).

Corollary 3.3 In Theorem 3.1, let $n = 2, \pi_1 = \pi_2 = 1$. Also let $f_1{}^{\circ_{\alpha_{12}}^{\lambda,\beta}}(\theta_1, \epsilon_1) = f^{\circ_{\alpha_2}^{\lambda,\beta}\circ_{\alpha_1}^{\lambda,\beta}}(\theta_1, \epsilon_1)$, $f_2{}^{\circ_{\alpha_{12}}^{\lambda,\beta}}(\theta_1, \epsilon_1) = f^{\circ_{\alpha_2}^{\lambda,\beta}\circ_{\alpha_1}^{\lambda,\beta}}(\theta_2, \epsilon_2)$.

If $p_1, p_2 > 1$ are such that $\frac{1}{p_1} + \frac{1}{p_2} \geq 1$ and $0 < w = 2 - \frac{1}{p_1} - \frac{1}{p_2} = \frac{1}{q_1} + \frac{1}{q_2} \leq 1$, inequality (6) reduces to

$$\int_{\epsilon_0}^{k_1}\int_{\epsilon_0}^{\tau_1}\left(\int_{\epsilon_0}^{k_2}\int_{\epsilon_0}^{\tau_2}\frac{|f_1(\theta_1,\epsilon_1)||f_2(\theta_2,\epsilon_2)|}{\left(f_1(\theta_1-\epsilon_0)(\epsilon_1-\epsilon_0)+q_1(\theta_1-\epsilon_0)(\epsilon_2-\epsilon_0)\right)^w}\circ_{\alpha}^{\lambda,\beta}\ \theta_2\circ_{\alpha}^{\lambda,\beta}\ \epsilon_2\right)\circ_{\alpha}^{\lambda,\beta}\ \theta_1\circ_{\alpha}^{\lambda,\beta}\ \epsilon_1$$

$$\leq \frac{1}{(wq_1q_2)^w}\left((k_1-\epsilon_0)(\tau_1-\epsilon_0)\right)^{\frac{1}{q_1}}\left((k_2-\epsilon_0)(\tau_2-\epsilon_0)\right)^{1-\frac{1}{q_1}}$$

$$\times\left(\int_{\epsilon_0}^{k_1}\int_{\epsilon_0}^{\tau_1}(h(k_1)-h(\theta_1))(h(\tau_1)-h(\epsilon_1))\left|f^{\circ_{\alpha_2}^{\lambda,\beta}\circ_{\alpha_1}^{\lambda,\beta}}(\theta_1,\epsilon_1)\right|^{p_1}\circ_{\alpha}^{\lambda,\beta}\ \theta_1\circ_{\alpha}^{\lambda,\beta}\ \epsilon_1\right)^{\frac{1}{p_1}}$$

$$\cdot\left(\int_{\epsilon_0}^{k_2}\int_{\epsilon_0}^{\tau_2}(h(k_2)-h(\theta_1))(h(\tau_2)-h(\epsilon_1))\left|f^{\circ_{\alpha_2}^{\lambda,\beta}\circ_{\alpha_1}^{\lambda,\beta}}(\theta_2,\epsilon_2)\right|^{p_2}\circ_{\alpha}^{\lambda,\beta}\ \theta_2\circ_{\alpha}^{\lambda,\beta}\ \epsilon_2\right)^{\frac{1}{p_2}}. \tag{11}$$

Remarks 3.4

i. Let $\mathbb{T} = \mathbb{R}, \alpha = 0, \lambda = 1$ in (11), then inequality (11) reduces to

ii.

$$\int_0^{k_1}\int_0^{\tau_1}\left(\int_0^{k_2}\int_0^{\tau_2}\frac{|f_1(\theta_1,\epsilon_1)||f_2(\theta_2,\epsilon_2)|}{(p_1\theta_1\epsilon_1+q_1\theta_2\epsilon_2)^w}d\,\theta_2 d\,\epsilon_2\right)d\,\theta_1 d\,\epsilon_1 \leq \frac{1}{(wq_1q_2)^w}(k_1\tau_1)^{\frac{1}{q_1}}(k_2\tau_2)^{1-\frac{1}{q_1}}$$

$$\times\left(\int_0^{k_1}\int_0^{\tau_1}(k_1-\theta_1))(\tau_1-\epsilon_1)|C_1C_2f_1(\theta_1,\epsilon_1)|^{p_1}d\,\theta_1 d\,\epsilon_1\right)^{\frac{1}{p_1}}$$

$$\cdot\left(\int_0^{k_2}\int_0^{\tau_2}(k_2-\theta_2))(\tau_2-\epsilon_2)|C_1C_2f_2(\theta_2,\epsilon_2)|^{p_2}d\,\theta_2 d\,\epsilon_2\right)^{\frac{1}{p_2}}. \tag{12}$$

iii. Let $\mathbb{T} = \mathbb{Z}, \alpha = 0, \lambda = 1$ in (11), then inequality (11) reduces to

$$\sum_{\theta_1=1}^{m_1}\sum_{\epsilon_1=1}^{n_1}\left(\sum_{\theta_2=1}^{m_2}\sum_{\epsilon_2=1}^{n_2}\frac{|\beta_1(\theta_1,\epsilon_1)||\beta_2(\theta_2,\epsilon_2)|}{(p_1\theta_1\epsilon_1+q_1\theta_2\epsilon_2)^w}\right)\le\frac{1}{(wq_1q_2)^w}(m_1n_1)^{\frac{1}{q_1}}(m_2n_2)^{1-\frac{1}{q_1}}$$

$$\times\left(\sum_{\theta_1=1}^{m_1}\sum_{\epsilon_1=1}^{n_1}(n_1-\epsilon_1)(m_1-\theta_1)\left|{}_{\circ}\alpha_1^{\lambda,\beta}\,{}_{\circ}\alpha_2^{\lambda,\beta}\,\beta_1(\theta_1,\epsilon_1)\right|^{p_1}\right)^{\frac{1}{p_1}}$$

$$\cdot\left(\sum_{\theta_2=1}^{m_2}\sum_{\epsilon_2=1}^{n_2}(n_2-\epsilon_2)(m_2-\theta_2)\left|{}_{\circ}\alpha_1^{\lambda,\beta}\,{}_{\circ}\alpha_2^{\lambda,\beta}\,\beta_2(\theta_2,\epsilon_2)\right|^{p_2}\right)^{\frac{1}{p_2}}. \tag{13}$$

Corollary 3.5 In Corollary 3.3, if we take $w=1, p_1=q_2$, and $p_2=q_1$ with $\frac{1}{p_1}+\frac{1}{p_2}=\frac{1}{q_1}+\frac{1}{q_2}=1$ then inequality (11) reduces to

$$\int_{\epsilon_0}^{k_1}\int_{\epsilon_0}^{\tau_1}\left(\int_{\epsilon_0}^{k_2}\int_{\epsilon_0}^{\tau_2}\frac{|f_1(\theta_1,\epsilon_1)||f_2(\theta_2,\epsilon_2)|}{(f_1(\theta_1-\epsilon_0)(\epsilon_1-\epsilon_0)+q_1(\theta_2-\epsilon_0)(\epsilon_2-\epsilon_0))}\,{}_{\circ}\alpha^{\lambda,\beta}\,\theta_2\,{}_{\circ}\alpha^{\lambda,\beta}\,\epsilon_2\right){}_{\circ}\alpha^{\lambda,\beta}\,\theta_1\,{}_{\circ}\alpha^{\lambda,\beta}\,\epsilon_1$$

$$\le\frac{1}{p_1q_1}\left((k_1-\epsilon_0)(\tau_1-\epsilon_0)\right)^{1-\frac{1}{p_1}}\left((k_2-\epsilon_0)(\tau_2-\epsilon_0)\right)^{1-\frac{1}{q_1}}$$

$$\times\left(\int_{\epsilon_0}^{k_1}\int_{\epsilon_0}^{\tau_1}(\pi(k_1)-\pi(\theta_1))(\pi(\tau_1)-\pi(\epsilon_1))\left|f^{{}_{\circ}\alpha_2^{\lambda,\beta}\,{}_{\circ}\alpha_1^{\lambda,\beta}}(\theta_1,\epsilon_1)\right|^{p_1}\,{}_{\circ}\alpha^{\lambda,\beta}\,\theta_1\,{}_{\circ}\alpha^{\lambda,\beta}\,\epsilon_1\right)^{\frac{1}{p_1}}$$

$$\cdot\left(\int_{\epsilon_0}^{k_2}\int_{\epsilon_0}^{\tau_2}(\pi(k_2)-\epsilon_0)(\pi(\tau_2)-\epsilon_0)\left|f^{{}_{\circ}\alpha_2^{\lambda,\beta}\,{}_{\circ}\alpha_1^{\lambda,\beta}}(\theta_2,\epsilon_2)\right|^{p_2}\,{}_{\circ}\alpha^{\lambda,\beta}\,\theta_2\,{}_{\circ}\alpha^{\lambda,\beta}\,\epsilon_2\right)^{\frac{1}{p_2}}. \tag{14}$$

Remarks 3.6

i. In Corollary 3.5, If we take $\mathbb{T}=\mathbb{R}, \alpha=0, \lambda=1$, we have Theorem 4 in [27].
ii. In Corollary 3.5, If we take $\mathbb{T}=\mathbb{Z}, \alpha=0, \lambda=1$, we have Theorem 3 in [27].

Conclusion

The inequality of Hilbert's in the different structures has been presented before. In this study, we have taken n-dimensional Hilbert inequalities on time scales for diamond alpha calculation and have created new inequalities of the results presented in previous studies. To be more precise, we have created a new form of inequality of Hilbert's on time scales. The results we have obtained will motivate us to work in different areas.

REFERENCES

1. Hardy, G.H., Littlewood, J.E., Polya, G. (1952) Inequalities Cambridge Univ; Cambridge University Press: Cambridge, UK.
2. Zhao, C.-J., Chen, L.-Y., Cheung,W. (2011) On some new Hilbert-type inequalities. Math. Slovaca, 61, 15–28.
3. Zhao, C., Cheung, W. (2012) On Hilbert type inequalities. J. Inequalities Appl. 2012, 145.
4. Pachpatte, B.G. (1998) A note on Hilbert type inequality. Tamkang J. Math., 29, 293–298.
5. Handley, G.D., Koliha, J.J., Pecaric, J. (2000) A Hilbert type inequality. Tamkang J. Math., 31, 311–316.
6. Zhao, C., Cheung, W. (2006) Inverses of new Hilbert-Pachpatte-type inequalities. J. Inequalities Appl., 2006, 97860.
7. Pachpatte, B.G. (1998) On some new inequalities similar to Hilbert's inequality. J. Math. Anal. Appl., 226, 166–179.
8. Yang, B., Rassias, M.T., Raigorodskii, A. (2021) On an extension of a Hardy–Hilbert-type inequality with multi-parameters. Mathematics, 9, 2432.
9. Rassias, M.T., Yang, B. (2016) On a Hardy-Hilbert-type inequality with a general homogeneous kernel. Int. J. Nonlinear Anal. Appl., 7, 249–269.
10. Rassias, M.T. Yang, B. (2017) A half-discrete Hardy-Hilbert-type inequality with a best possible constant factor related to the hurwitz zeta function. In Progress in Approximation Theory and Applicable Complex Analysis: In Memory of QI Rahman; Springer: Cham, Switzerland, pp. 183–218.
11. Yang, B., Wu, S. Chen, Q. (2020) A new extension of Hardy-Hilbert's inequality containing kernel of double power functions. Mathematics, 8, 894.
12. Yang, B., Wu, S., Wang, A. (2020) A new Hilbert-type inequality with positive homogeneous kernel and its equivalent forms. Symmetry, 12, 342.
13. Liao, J., Wu, S., Yang, B. (2020) On a new half-discrete Hilbert-type inequality involving the variable upper limit integral and partial sums. Mathematics, 8, 229.
14. Agarwal, R., O'Regan, D., Saker, S. (2014) Dynamic Inequalities on Time Scales; Springer: Cham, Switzerland.
15. Akin-Bohner, E., Bohner, M., Akin, F. (2005) Pachpatte inequalities on time scales. JIPAM J. Inequal. Pure Appl. Math., 6, 6.
16. Bohner, M., Matthews, T. (2007) The Grüss inequality on time scales. Commun. Math. Anal., 3, 1–8.

17. Bohner, M., Matthews, T. (2008) Ostrowski inequalities on time scales. JIPAM J. Inequal. Pure Appl. Math., 9, 8.
18. Dinu, C. (2008) Hermite-Hadamard inequality on time scales. J. Inequal. Appl., 2008, 287947.
19. Hilscher, R. (2002) A time scales version of a Wirtinger-type inequality and applications. J. Comput. Appl. Math., 141, 219–226.
20. Li, W.N. (2010) Some delay integral inequalities on time scales. Comput. Math. Appl., 59, 1929–1936.
21. Rehák, P. (2005) Hardy inequality on time scales and its application to half-linear dynamic equations. J. Inequal. Appl., 2005, 942973.
22. Agarwal, R.P., Lakshmikantham, V. (1993) Uniqueness and Nonuniqueness Criteria for Ordinary Differential Equations; Series in Real Analysis; World Scientific Publishing: Singapore,, Volume 6.
23. Li, J.D. (1992) Opial-type integral inequalities involving several higher order derivatives. J. Math. Anal. Appl., 167, 98–110.
24. Hilger, S. (1988) Ein Maßkettenkalkül mit Anwendung auf Zentrumsmannigfaltigkeiten. Ph.D. Thesis, Universität Würzburg, Würzburg, Germany.
25. Rahmat, M.R.S., Noorani, M.S.M. (2021) A new conformable nabla derivative and its application on arbitrary time scales. Adv. Differ. Equ., 2021, 238.
26. Cloud, M.J., Drachman, B.C., Lebedev, L. (1998) Inequalities; Springer: Berlin/Heidelberg, Germany.
27. Pachpatte, B.G. (2000) Inequalities similar to certain extensions of Hilbert's inequality. J. Math. Anal. Appl., 243, 217–227.
28. Hilger, S. (1990). Analysis on measure chains-a unified approach to continuous and discrete calculus, Results Maths. 18(1-2) 18–56.
29. Hardy, G.H. (1920). Note on a theorem of Hilbert, Math. Z. 6(3–4), 314–317
30. Hardy, G.H.(1925). Notes on some points in the integral calculus, LX. An inequality between integrals, Mess. Math. 54,150–156.
31. Hardy, G.H., Littlewood, J.E. (1927). Elementary theorems concerning power series with positive coefficients and moment constants of positive functions, J. Reine Angew. Math. 157, 141–158.
32. Hardy, G.H. (1928). Notes on some points in the integral calculus, LXIV. Mess. Math. 57, 12–16.
33. Ahmad, W., Khan, K.A., Nosheen, A., Sultan, M.A. (2019). Copson, Leindler type inequalities for function of several variables on time scales, Punjab Univ. J. of Math. 51(8),157–168.

34. Ashraf, M.S., Khan, K.A., Nosheen, A. (2019). Hardy-Copson type inequalities on time scales for the functions of n independent variables, Int. J. Anal. Appl. 17(2), 244–259.
35. Baric, J., Bibi, R., Bohner, M., Nosheen, A., Pecaric, J. (2015). Jensen inequalities and their applications on time scales, Element, Zagreb, Croatia
36. Nosheen, A., Nawaz, A., Khan, K.A., Awan, K.M. (in press) Multivariate Hardy and Littlewood inequalities on time scales, Arap Journal of Mathematical Science.
37. Saker, S.H., O'Regan, D. (2016) Hardy and Littlewood Inequalities on time scales, Bull. Malays. Math. Sci. Soc. 39(2) 527–543.
38. Li, W., Liu, D., Liu, J. (2019). Weighted inequalities for fractional Hardy operators and commutators, Journal of Inequalities and Applications 2019:158, 1-14.
39. Bradley, J. (1978). Hardy inequalities with mixed norms. Can. Math. Bull. 21(4), 405-408.
40. Kufner, A., Persson, L.E. (2003). Weighted Inequalities of Hardy Type. World Scientific, Singapore.
41. Opic, B., Kufner, A. (1990). Hardy-Type Inequalities. Pitman Research Notes in Mathematics Series, Longman Scientific and Technical, Harlow, Essex.
42. Akın, L. (2020). On some results of weighted Hölder type inequality on time scales. Middle East Journal of Science 6(1), 15-22.
43. Akın L.(2021). On innovations of n-dimensional integral-type inequality on time scales. Adv. Differ. Equ. 2021:148.
44. Bohner, M., Nosheen, A., Pecaric, J., Younas, A. (2014). Some dynamic Hardy type inequalities on time scales, J. Math. Inequal. 8(1), 185–199.
45. Agarwal, R.P., Bohner, M., O'Regan, D., Saker, S.H. (2011). Some Wirtinger-type inequalities on time scales and their applications, Pacific J. Math. 252, 1–26 (2011)
46. Akın, L. (2020). On the Fractional Maximal Delta Integral Type Inequalities on Time Scales. Fractal Fract. 4, 26, 1-10.
47. Bohner, M., Petereson, A. (2001). Dynamic Equations on Time Scales. An Introduction with Applications, Birkhauser, Boston.
48. Akın L. (2021). A New Approach for the Fractional Integral Operator in Time Scales with Variable Exponent Lebesgue Spaces. Fractal Fract. 5(7), 1-13.

49. Bohner, M., Georgiev, S.G. (2016). Sequences and Series of Functions. In: Multivariable Dynamic Calculus on Time Scales, Springer Int. Publ. Switzerland.
50. Akın, L. (2024) On generalized weighted dynamic inequalities for diamond−∝ integral on time scales calculus. Indian J Pure Appl Math 55, 363–376.
51. Anastassiou, G.A. Principles of delta fractional calculus on time scales and inequalities. Math. Comput. Model. 2010, 52, 556–566.
52. Kac, V., Cheung, P. (2002) Quantum Calculus. Universitext Springer, New York.
53. Saker, S.H., El-Sheikh, M.M.A., Madian, A.M. (2021) Some new generalized weighted dynamic inequalities of Hardy's type on time scales, J. Math. Computer Sci., 23 (2021), 289–301.
54. Almarri, B., El-Deeb, A.A. (2023) Gamma-Nabla Hardy–Hilbert-Type Inequalities on Time Scales. Axioms, 12, 449.
55.Miller, K. B., Ross, B. (1993) An Introduction to the Fractional Calculus and Fractional Differential Equations . New York, Wiley.
56. Oldham, K. B., Spanier, J. (1974) The Fractional Calculus. New York and London: Academic Press.
57. Podlubny, I. (1999) Fractional Differential Equations. San Diego: Academic Press.
58. Herrmann, R. (2014) Fractional Calculus: an Introduction for Physicists[M]. Singapore: World Scientific.
59. Sabatier, J., Agrawal, O. P., Machado, J. A.T. (2007) Advances in Fractional Calculus: Theoretical Developments and Applications in Physics and Engineering[M]. Netherlands: Springer.
60. Tejado, I., Valerio, D., Valerio, N. (2015) Fractional Calculus in Economic Growth Modelling: the Spanish Case. Netherlands: Springer.
61. Meilanov, R. P., Magomedov. R. A. (2014) Thermodynamics in fractional calculus. J Eng Phys Thermophys, 87(6): 1521-1531.

Chapter 5

Define The Frontlines of The Battle Against Breast Cancer with Immune Warriors

Kübra SOLAK[1, 2]
Yağmur ÜNVER[3]

[1] : Department of Molecular Biology and Genetics, Faculty of Science, Erzurum Technical University, Erzurum, Türkiye. ORCID ID: 0000-0001-6643-3368
[2] : Department of Nanoscience and Nanoengineering, Institute of Science and Technology, Atatürk University, Erzurum, Türkiye.
[3] : Department of Molecular Biology and Genetics, Faculty of Science, Atatürk University, Erzurum, Türkiye. ORCID ID: 0000-0003-1497-081X

1. Introduction

Breast cancer is a highly heterogeneous disease with significant variability in morphologic and pathologic features. Breast cancer, like skin and lung cancer, is a risky type of cancer that can metastasize to other organs (Den Oudsten, der Steeg, A., & De, 2012; Leone & Leone, 2015). Genetic and epigenetic changes in genes regulating mammary epithelial cell proliferation, survival, polarity, and differentiation likely initiate breast carcinogenesis.

Breast cancer has different molecular subtypes based on gene expression profiles (Mota et al., 2017; Yee, Borgia, Semenova, Campbell, & Booth, 2023). The most common molecular subtypes are luminal A, luminal B, HER2-positive (human epidermal growth factor receptor 2), and triple-negative (TNBC) cancers (Harbeck et al., 2019; Iqbal Memon, Din Ujjan, & Masroor Bhatti, 2023). Luminal A cancer comprises estrogen receptor-positive (ER+) and progesterone receptor-positive (PR+) cells. This type of cancer has a lower cell division rate than other molecular subtypes and generally has a better prognosis. Luminal B cancer consists of ER-positive cells but may not be PR+. This type of cancer is more aggressive and has a higher cell division rate than the luminal A type. HER2+ cancer cells produce extreme amounts of HER2 protein. This type of cancer requires a different treatment approach than other molecular subtypes. The TNBC consists of negative cells for both ER and PR receptors and does not have HER2 protein. This type of cancer can be more aggressive than other molecular subtypes, and treatment options are limited (Den Oudsten et al., 2012). Having HER2, activation of ER and/or PR receptors, as well as BRCA (breast cancer gene) mutations, which are among the molecular characteristics of breast cancer, determines the propensity of the disease (Harbeck et al., 2019). These molecular subtypes of breast cancer are essential for its diagnosis, prognosis, and treatment.

Recently, the focus of research has shifted from the tumor mass to the biological character of the tumor, with the molecular level of cancer disease elucidated. In this respect, it is known that the success rate of an individualized cancer treatment that focuses on the cell in the tumor mass that appears in the patient increases. In addition, since breast cancer is a heterogeneous disease in general, multidisciplinary approaches should not be ignored when aiming for an effective treatment. Breast cancer is 70-80% curable if it is diagnosed early and is not metastatic (Harbeck et al., 2019).

Cancer treatments consist of various methods used to destroy or control its growth. Determining a treatment strategy depends on the type and stage of cancer, as well as the condition of the patient's health. Cancer treatments include chemotherapy, radiotherapy, surgery, and immunotherapy. Currently, two major approaches are used to control breast cancer: regional intervention (surgery and

radiation therapy) and systemic treatment. The molecular character of the tumor greatly influences which treatment approach is chosen, such as chemotherapy, anti-HER2 therapy for HER2+ patients, endocrine therapy, and immunotherapy (Harbeck et al., 2019). However, current therapies are not fully adequate for the treatment of invasive breast cancer. In such patients, current therapies aim to control symptoms, improve the patient's life quality, and prolong survival, even to some extent (Iqbal Memon et al., 2023). These goals accompany the planning of numerous ongoing studies.

Multiple therapies, proposed as a combination of therapeutic approaches, improve the clinical management of diseases (Farokhzad & Langer, 2006). Especially in the fight against a multifaceted and treatment-resistant disease such as cancer, the ability to strike the disease from many angles at once increases the effectiveness of treatment. For example, combining hyperthermia, which aims to treat by increasing the temperature in the target tissue, and immunotherapy, which uses the patient's defense system, with other treatments (chemotherapy, radiotherapy, etc.) increases the effectiveness of treatments. Immunotherapy boosts the efficacy of surgery, chemotherapy, hyperthermia, radiotherapy, or targeted therapies used in cancer treatment (Chen & Mellman, 2013).

2. Passive immunity for breast cancer

The immune system plays an extremely important role in cancer development and in response to chemotherapy and clinical outcomes. Metastatic breast cancer is a heterogeneous disease that influences immune cells in the bloodstream and might lead to systemic immune anomalies. Tumor-infiltrating lymphocytes (TILs) are associated with a high pathological response to neoadjuvant chemotherapy in aggressive breast cancer (Poncin et al., 2021; Wagner et al., 2019). Circulating immune cells, including neutrophils, lymphocytes, and eosinophils, affect responses to chemotherapy and cancer outcomes. On the other hand, TILs are crucial in improving the chemotherapy response and clinical outcomes in all breast cancer subtypes.

To form a tumor mass, cancer cells can escape the immune system through a decrease in antigen presentation, a diminution of immune effector cells, and an increase in the expression of checkpoint molecules. The presence of TILs is reduced in ER+ breast cancer. TILs are more common in HER-2+ and TNBC, but also in hormone receptor-positive breast cancer. A study on immune cells related to ductal carcinoma found that 28% of cases were TIL-high (Agahozo et al., 2020). In this study, it has been reported that cases with ER+ HER2+ subtype have a higher proportion of CD8+ T cells than TNBC cases. The increase in ER expression may be responsible for this effect. This creates a Th2 immune

environment and lowers the number of MHC class II molecules in breast cancer cells. Classical HLA molecules (-A, -B, and -C) are down-regulated in 30-40% of higher-grade breast tumors (Nicolini, Rossi, & Ferrari, 2023). In contrast, non-classical HLA-E, HLA-F, and HLA-G molecules promote immune escape. TNBCs have lymphocyte-predominant tumors, benefiting from a 10% increase in TIL (Stanton & Disis, 2016). HER2+ breast cancers have similar immune infiltrate levels (Hwang et al., 2019). Hormone receptor-positive HER2-negative tumors have the minimum immune infiltrate but show a worse prognosis with increased FOXP3 (forkhead box P3, a protein from the FOX family) regulatory T-cell infiltrates.

Immune evasion may occur via the involvement of molecules in antigen presentation and mutations in interferon (IFN) response genes (Gatti-Mays et al., 2019). Pathway changes that promote cancer growth, such as mutations in the PI3K (phosphoinositide 3-kinases) pathway, are essential for suppressing or inhibiting the activation of T cells. Elevated frequencies of programmed cell death ligand 1 positive (PD-L1+) tumor-associated macrophages and depleted T lymphocytes with exhaustion were seen in high-grade ER+ and ER− cancers (Wagner et al., 2019). Another study demonstrated that the HER2+ subgroup had the lowest PD-L1-SP142 expression on tumor cells, indicating a more robust antitumor immune response in HER2+ ductal carcinoma *in situ* (Agahozo et al., 2020). Also, HER2-negative metastatic breast cancer caused elevated monocyte levels and reduced CD4+ T cells (Chauhan et al., 2024).

Tumor cells could increase the production of indoleamine-pyrrole 2,3 dioxygenase (IDO) in response to interferon-gamma and ER signaling. Cancers classified as ER+ exhibit elevated levels of IDO compared to ER cancers (Nicolini et al., 2023). A study examining the expression and distribution levels of FoxP3 and CD8 in breast carcinoma found that overexpression of FoxP3 and a high FoxP3+/CD8+ ratio were associated with adverse outcomes in terms of both overall survival and disease-free survival (Peng et al., 2019). The CD8+ cytotoxic T lymphocytes (CTLs) and FoxP3+ regulatory T (Treg) cells might behavior as prognostic markers for breast cancer patients. Patients with metastatic breast cancer who exhibit systemic immunological markers have an immune-suppressed environment, which is associated with persistent chronic inflammation. However, in a normal process, Treg cells maintain immune homeostasis in the body by suppressing excessive immune system reactions. In contrast, in cancer like breast cancer, this role reverses to promoting tumor development and growth (Liang et al., 2015). The immunosuppressive effect of increasing Treg cells in the tumor microenvironment contributes to cancer progression, which diminishes immune responses to cancer. In breast cancer, a

significantly higher number of Treg cells has been considered as the marker of a poor prognosis (Hashemi et al., 2020). Treg cells suppress the activity of antitumoral immune cells, such as CD8+ cytotoxic T cells and NK cells (Hashemi et al., 2020; Togashi, Shitara, & Nishikawa, 2019). This suppression is usually mediated by molecules such as CTLA-4, IL-10, and TGF-β. These molecules inhibit the activation of T cells and limit antigen presentation by impairing the function of dendritic cells (DCs). In these ways, Treg cells resist immunotherapies, creating resistance to therapies and reducing their effectiveness in cancer treatments. Hence, therapeutic strategies that inhibit function of Treg cells enhance immunotherapies' effectiveness (Shan, Somasundaram, Bruno, Workman, & Vignali, 2022).

On the other hand, tumor-promoting immune cells, including Treg cells and myeloid-derived suppressor cells (MDSCs), perform an essential function in maintaining immune homeostasis and peripheral tolerance (Binnewies et al., 2018; X. Lei et al., 2020; Sadeghi, Dehnavi, Sharifat, Amiri, & Khodadadi, 2024). Granulocytic or polymorphonuclear MDSCs (PMN-MDSCs) and monocytic MDSCs (M-MDSCs) are two types of tumor-promoting immune cells within the tumor microenvironment (TME) (Gatti-Mays et al., 2019; Zhao et al., 2018). They have the potential to increase angiogenesis, stimulate cancer cell migration towards endothelial cells, and facilitate metastasis. Inhibiting MDSC trafficking has been shown to enhance T cell-based immunotherapeutic efficacy.

To summarize, TILs, Treg cells, MDSCs, and some mediator molecules (IFNs, IDO, etc.) significantly impact the treatment response and prognosis of breast cancer. Oncogenic cells have mechanisms to evade the immune system, affecting treatment outcomes. Different breast cancer subtypes vary in their immune profiles, which influences treatment strategies. Finally, examining immune responses and immune-related molecules might serve as biomarkers for estimating the rate of breast cancer development and therapeutic efficacy.

3. Immune cells in the tumor microenvironment

In carcinogenesis, cancer development, and metastasis, the TME is an essential player. Additionally, immune cells play a crucial role in treating and preventing breast cancer (Figure 1). Effector T cells, DCs, natural killer (NK) cells, M1 polarized macrophages, and N1 polarized neutrophils are types of anti-tumor immune cells (X. Lei et al., 2020; Sadeghi et al., 2024). These cells recognize neoantigens and ligands, serving in chronic inflammation and immunosurveillance. CD8+ CTLs are the primary lymphocyte subset that eliminates cancer cells that express major histocompatibility complex class I molecules (MHC-I). Antigens presented by DCs can induce the transformation of CD8+ T cells into effector CD8+ T cells that possess cytotoxic capabilities (Sadeghi et al., 2024). Activated CTLs can move into the inflammatory environment as directed by chemokines, facilitated by the expression of CXCR3 (C-X-C Motif Chemokine Receptor 3). Besides, CD4+ T cells can stimulate the activation of DCs by delivering tumor antigens to CD8+ T cells or by triggering the synthesis of cytokines and co-stimulatory molecules, promoting the activation of DCs and enabling them to activate CD8+ T cells efficiently.

As breast cancer progresses, immune cells infiltrate an increase in tumor parenchyma and stroma, including DCs, B cells, CD4+ and CD8+ cytotoxic T cells, and macrophages. Adoptive transfer of breast TILs is one experimental approach that has the potential to reverse metastases and encourage the development of novel T-cell immunotherapy treatments. γδ T-cells and NK cells in the TME have also been associated with better prognosis in all breast cancer subtypes (Alaluf, Shalamov, & Sonnenblick, 2024; Sadeghi et al., 2024). Understanding these roles is essential for the prevention and treatment of breast cancer.

Although the exact function of B lymphocytes in the TME as tumor antagonizers is poorly understood, they have been associated with positive therapeutic results in breast cancer patients (Laumont, Banville, Gilardi, Hollern, & Nelson, 2022). According to some research, B cells may promote cancer by reducing CTL function, increasing angiogenesis, and attracting MDSCs through cytokines. It has been reported that Treg cells and Breg (B regulatory) cells are interdependent in the development of metastasis in breast cancer patients (Ishigami et al., 2019). The specific roles of various subsets of tumor-infiltrating B lymphocytes within the TME are expected to be revealed by future research.

Figure 1. Classification of cell types involved in the identification and destruction of cancer cells, as well as in immunosuppression, tumor growth facilitation, and immune evasion.

4. Immune-boosting vaccines and therapies for breast cancer

Immunotherapy targets tumors specifically while minimizing damage to healthy cells. Various strategies are employed to utilize the immune system for cancer treatment, including cancer vaccines (therapeutic peptide and protein-based, B cell-based, dendritic cell-based, and DNA/mRNA-based), immune checkpoint (PD-1, PD-L1, CTLA-4) inhibitors, directed monoclonal antibodies, antibody-drug conjugates, bispecific antibodies, adoptive cellular therapy, TLR agonists, autologous tumor cells, cytokine-based immunotherapy, γδ T cells, tumor-associated macrophages, oncolytic viruses, and immuno-metabolic targets (Alaluf et al., 2024; Davodabadi et al., 2022).

A study compared the effects of margetuximab and trastuzumab combined with chemotherapy on survival in patients with previously treated HER 2-positive breast cancer. Their research focused on polymorphic allelic variations (158V or 158F) of CD16A, suggesting enhanced survival for margetuximab in CD16A-158FF patients and trastuzumab in CD16A-158VV patients (Rugo et al., 2023). Another study uses murine HER2+ breast cancer models to test the effect of anti-HER2/neu and anti-4-1BB monoclonal antibody (mAb) combination therapy and found that adding anti-4-1BB mAb to anti-HER2/neu mAb potentiated the cytotoxic antitumor response. However, this combination therapy was shown not to evoke immune memory, and tumors recurred. It has been stated that this situation can be overcome with the dose regulation of anti-4-1BB mAb to 1 mg/kg (Kim et al., 2022).

However, T-cell activity is regulated by modulating the creation of costimulatory signals via several mechanisms. T cell activation encompasses (*i*) the primary signal, which comes from the binding of the T cell receptor (TCR) to the MHC molecule presented by an antigen-presenting cell (APC), and (*ii*) the costimulatory signal, which may result from several specific T cell-APC interactions (Chae et al., 2018). Several signaling pathways have been implicated in the modulation of T cell activity, including CTLA-4, PD-1, and PD-1/PD-L1 checkpoint inhibitors. In a study developing a tetravalent bispecific PD-1 x CTLA-4 molecule (MGD019) to achieve optimal co-blockade of PD-1 neutralization and maximal CTLA-4 inhibition, experiments were conducted in vitro in human cells, Cynomolgus monkeys and humans (Berezhnoy et al., 2020). In solid tumor cancer indications, such as breast cancer, combined immunotherapy using antibodies directed against PD-1 and CTLA-4 has shown better clinical effects than single pharmaceuticals.

Another cancer therapy involves the use of autologous tumor-infiltrating lymphocytes. In adaptive cellular therapy (ACT), a small number of anti-tumor cells with appropriate properties are taken from the individual, identified, and

then grown *ex vivo* for treatment (Rosenberg, Restifo, Yang, Morgan, & Dudley, 2008). There has been remarkable success in treating hematological malignancies with chimeric antigen receptor (CAR)-T cell therapy, leading to the development of new ACTs like CAR-macrophage, CAR-natural killer, CAR-natural killer T, and CAR-γδT (P. Zhang, Zhang, & Wan, 2023). In addition to cells, exosomes derived from CAR-T cells by secreting perforin and granzyme B have demonstrated efficacy in diminishing the development of triple-negative breast cancer without noticeable side effects *in vivo* (Yang et al., 2021).

Tumor-based cancer vaccines have several advantages, like ensuring more safety than chemotherapy and preventing malignant tumor recurrence through long-term immunological memories. Nanotechnology-based nanoparticles are used as adjuvants, immunogens, and delivery vehicles to activate the immune system (Davodabadi et al., 2022). A study uses nanoparticles to deliver a mRNA vaccine encoding tumor antigen MUC1 (type 1 transmembrane mucin) to DCs in lymph nodes, activating and expanding tumor-specific T cells (Liu et al., 2018). The NP-based vaccine successfully expresses tumor antigen, induces a robust and antigen-specific response against TNBC 4T1 cells, and enhances anti-tumor immune response.

Peptide-based vaccination has been explored as an alternative to treatments for tumors. Peptides are based on a region of the epidermal growth factor receptor (EGFR) extracellular domain IV, interrupting immune tolerance and stimulating immune response against cancer. It was mentioned that the EGFR p580 antiserum inhibited the growth of MDA-MB-453 breast cancer cells, which expresses HER2 but not EGFR (Doyle et al., 2018).

Lastly, bispecific antibodies, autologous tumor cells, TLR agonists, γδ T cells, tumor-associated macrophages, radiotherapy, oncolytic viruses, cytokine-based immunotherapy, and immuno-metabolic targeting are other modalities employed in the treatment of breast cancer.

Table 1. Immunotherapy approaches and therapeutic targets have been examined in various studies.

Immune Therapy	**Treatment**	**Targets**	**Reference**
Directed Monoclonal Antibodies	Trastuzumab and Margetuximab	Margetuximab-enhanced chemotherapy is a therapeutic option for patients with pretreated HER2+.	(Rugo et al., 2023)
	anti-HER2/neu and anti-4-1BB	Treatment with anti-4-1BB mAb causes different types of immunological memory in naive and activated CD8+ T cells.	(Kim et al., 2022)
Antibody-Drug Conjugates	Trastuzumab emtansine (T-DM1)	Clinical practice on HER2+ breast cancer patients. Trastuzumab: HER2-directed monoclonal antibody. Emtansine: Cytotoxic microtubule polymerization inhibitor.	(Michel, Bermejo, Gondos, Marmé, & Schneeweiss, 2015)
Immune Checkpoint Inhibitors (PD-1, PD-L1, CTLA-4)	Engineered tetravalent bispecific PD-1xCTLA-4 molecule (MGD019)	Dual PD-1 and CTLA-4 blockade.	(Berezhnoy et al., 2020)
Adaptive Cellular Therapy	Exosomes produced by mesothelin (MSLN)-targeted CAR-T cells	Mesothelin-expressing triple-negative breast cancer.	(Yang et al., 2021)
Cancer Vaccines	Therapeutic Peptide and Protein-Based	Iso-aspartyl (iso-Asp)-modified EGFR p580 immune sera inhibit the growth of EGFR-overexpressing human A431 and MDA-MB-453 tumor cells that express HER2 but not EGFR.	(Doyle et al., 2018)
	DNA/mRNA-Based	MUC1 (type 1 transmembrane mucin) to DCs in lymph nodes.	(Liu et al., 2018)

5. Immune approaches as adjunctive therapy to conventional therapies

Immune approaches as adjunctive therapies have gained significant attention in recent years, aiming to enhance the efficacy of conventional cancer treatments like chemotherapy, radiation, and surgery by strengthening the immune system in the body. These approaches include immune checkpoint inhibitors, oncolytic viruses, CAR-T cell therapy, cytokine therapies, cancer vaccines, ACTs, combination therapies, and personalized medicine approaches (Blattman & Greenberg, 2004; Blattman, Greenberg, Guth, & Dow, 2004; H. Zhang & Chen, 2018). Immune checkpoint inhibitors inhibit checkpoint proteins, while CAR-T cell therapy extracts genetically engineered T cells to target cancer cells. Cancer vaccines enhance the immune response against specific cancer antigens, whereas oncolytic viruses selectively target and eradicate cancer cells while eliciting an immunological response. Cytokine treatments enhance the immune response against cancer, and ACT infuses expanded and genetically modified immune cells to eliminate residual cancer cells and prevent recurrence. Combination therapies, such as chemotherapy and immunotherapy, radiation and immunotherapy, and surgery and immunotherapy, target residual disease and reduce the risk of recurrence. However, challenges include developing novel strategies for tumor resistance, managing immune-related adverse events, identifying predictive biomarkers, and optimizing therapy timing and sequence (Emens et al., 2024; Y. Lei, Li, Huang, Zheng, & Liu, 2021).

Treatment efficacy for TNBC is greatly improved when the mRNA-expressing tumor antigen MUC1 vaccination is administered in combination with an anti-CTLA-4 monoclonal antibody (Liu et al., 2018). Nanotechnology offers ideal tools for multi-therapy approaches. The research combines a drug combination methyltryptophan-paclitaxel (MP) by attaching the immunosuppressive enzyme indoleamine-2,3-dioxygenase (IDO) inhibitor to the chemotherapeutic agent paclitaxel (PTX) (Hu, Zheng, Xu, Gao, & Lu, 2020). MP binds to human serum albumin, enhancing the concentration of D-1-methyltryptophan (D-1MT) in tumors. MP NPs enhance the anti-tumor effect by strengthening the codelivery of PTX and D-1MT in tumors. MP NPs improve the immune environment, increasing effector CD8+ T cells and decreasing Treg cells.

New research has shown that γδ T cells are an immune effector subgroup that might be used to create innovative cancer immunotherapies. The genotype of mitochondrial DNA influences the composition of the gut microbiota, which demonstrates the connections of mitochondria with γδ17 T cells (Kawaguchi, Maeshima, & Toi, 2022).

6. Conclusion

In conclusion, breast cancer is a highly heterogeneous disease influenced by various molecular subtypes, genetic mutations, and interactions with the immune system. Breast cancer patients are cured via different treatment methods, such as surgery, chemotherapy, and radiation therapy, alongside advanced immunotherapy techniques. Understanding the TME and the immune system's involvement is critical in improving prognosis and treatment response. In breast cancer, TILs assist as prognostic indicators for chemotherapy response and survival. Immunotherapy such as immune checkpoint inhibitors, cancer vaccines, CAR-T cell therapy, and other adjunctive therapies have offered promise as an adjunct to the existing treatment regimens. Such agents, which harness the immune responses to eradicate cancer, have been shown to increase the survival rates of patients with especially very aggressive types of breast cancer like TNBC and HER2+. However, cancer treatment utilizing these therapies also presents challenges regarding tumor evasion, immune-mediated side effects, and the need for individualized strategy. Exploring potential cancer immunotherapy based on biomarkers, new targets for drug therapy, and methods for treatment personalization gives hope that effective and lasting control of malignancies will be possible.

References

Agahozo, M. C., van Bockstal, M. R., Groenendijk, F. H., van den Bosch, T. P. P., Westenend, P. J., & van Deurzen, C. H. M. (2020). Ductal carcinoma in situ of the breast: immune cell composition according to subtype. *Modern Pathology*, *33*(2). https://doi.org/10.1038/s41379-019-0331-8

Alaluf, E., Shalamov, M. M., & Sonnenblick, A. (2024). Update on current and new potential immunotherapies in breast cancer, from bench to bedside. *Frontiers in Immunology*, Vol. 15. https://doi.org/10.3389/fimmu.2024.1287824

Berezhnoy, A., Sumrow, B. J., Stahl, K., Shah, K., Liu, D., Li, J., … Moore, P. A. (2020). Development and Preliminary Clinical Activity of PD-1-Guided CTLA-4 Blocking Bispecific DART Molecule. *Cell Reports Medicine*, *1*(9). https://doi.org/10.1016/j.xcrm.2020.100163

Binnewies, M., Roberts, E. W., Kersten, K., Chan, V., Fearon, D. F., Merad, M., … Krummel, M. F. (2018). Understanding the tumor immune microenvironment (TIME) for effective therapy. *Nature Medicine*, *24*(5). https://doi.org/10.1038/s41591-018-0014-x

Blattman, J. N., & Greenberg, P. D. (2004). Cancer immunotherapy: a treatment for the masses. *Science (New York, N.Y.)*, *305*(5681), 200–205. https://doi.org/10.1126/science.1100369

Blattman, J. N., Greenberg, P. D., Guth, A. M., & Dow, S. (2004). Cancer Immunotherapy: A Treatment for the Masses. *Joseph N. Blattman Philip D. Greenberg*, *305*(5681), 200–205. https://doi.org/10.1016/B978-1-4377-2362-5.00013-X

Chae, Y. K., Arya, A., Iams, W., Cruz, M. R., Chandra, S., Choi, J., & Giles, F. (2018). Current landscape and future of dual anti-CTLA4 and PD-1/PD-L1 blockade immunotherapy in cancer; lessons learned from clinical trials with melanoma and non-small cell lung cancer (NSCLC). *Journal for ImmunoTherapy of Cancer*, Vol. 6. https://doi.org/10.1186/s40425-018-0349-3

Chauhan, S. K., Dunn, C., Andresen, N. K., Røssevold, A. H., Skorstad, G., Sike, A., … Kyte, J. A. (2024). Peripheral immune cells in metastatic breast cancer patients display a systemic immunosuppressed signature consistent with chronic inflammation. *Npj Breast Cancer*, *10*(1). https://doi.org/10.1038/s41523-024-00638-2

Chen, D. S., & Mellman, I. (2013). Oncology meets immunology: The cancer-immunity cycle. *Immunity*, *39*(1), 1–10. https://doi.org/10.1016/j.immuni.2013.07.012

Davodabadi, F., Sarhadi, M., Arabpour, J., Sargazi, S., Rahdar, A., & Díez-Pascual, A. M. (2022). Breast cancer vaccines: New insights into immunomodulatory and nano-therapeutic approaches. *Journal of Controlled Release*, Vol. 349. https://doi.org/10.1016/j.jconrel.2022.07.036

Den Oudsten, B. L., der Steeg, A. F. W. Van, A., J., & De, J. (2012). Changes in Body Image in Women with Early Stage Breast Cancer. In *Topics in Cancer Survivorship*. https://doi.org/10.5772/24628

Doyle, H. A., Koski, R. A., Bonafé, N., Bruck, R. A., Tagliatela, S. M., Gee, R. J., & Mamula, M. J. (2018). Epidermal growth factor receptor peptide vaccination induces cross-reactive immunity to human EGFR, HER2, and HER3. *Cancer Immunology, Immunotherapy*, *67*(10). https://doi.org/10.1007/s00262-018-2218-9

Emens, L. A., Romero, P. J., Anderson, A. C., Bruno, T. C., Capitini, C. M., Collyar, D., … Wargo, J. A. (2024). Challenges and opportunities in cancer immunotherapy: A Society for Immunotherapy of Cancer (SITC) strategic vision. *Journal for ImmunoTherapy of Cancer*, *12*(6). https://doi.org/10.1136/jitc-2024-009063

Farokhzad, O. C., & Langer, R. (2006). Nanomedicine: Developing smarter therapeutic and diagnostic modalities. *Advanced Drug Delivery Reviews*, Vol. 58, pp. 1456–1459. https://doi.org/10.1016/j.addr.2006.09.011

Gatti-Mays, M. E., Balko, J. M., Gameiro, S. R., Bear, H. D., Prabhakaran, S., Fukui, J., … Mittendorf, E. A. (2019). If we build it they will come: targeting the immune response to breast cancer. *Npj Breast Cancer*, Vol. 5. https://doi.org/10.1038/s41523-019-0133-7

Harbeck, N., Penault-Llorca, F., Cortes, J., Gnant, M., Houssami, N., Poortmans, P., … Cardoso, F. (2019). Breast cancer. *Nature Reviews Disease Primers*, *5*(1), 66. https://doi.org/10.1038/s41572-019-0111-2

Hashemi, V., Maleki, L. A., Esmaily, M., Masjedi, A., Ghalamfarsa, G., Namdar, A., … Jadidi-Niaragh, F. (2020). Regulatory T cells in breast cancer as a potent anti-cancer therapeutic target. *International Immunopharmacology*, Vol. 78. https://doi.org/10.1016/j.intimp.2019.106087

Hu, Z., Zheng, B., Xu, J., Gao, S., & Lu, W. (2020). An albumin-bound drug conjugate of paclitaxel and indoleamine-2,3-dioxygenase inhibitor for enhanced cancer chemo-immunotherapy. *Nanotechnology*, *31*(29). https://doi.org/10.1088/1361-6528/ab824d

Hwang, H. W., Jung, H., Hyeon, J., Park, Y. H., Ahn, J. S., Im, Y. H., … Cho, E. Y. (2019). A nomogram to predict pathologic complete response (pCR) and the value of tumor-infiltrating lymphocytes (TILs) for prediction of response to neoadjuvant chemotherapy (NAC) in breast cancer patients.

Breast Cancer Research and Treatment, Vol. 173. https://doi.org/10.1007/s10549-018-4981-x

Iqbal Memon, A., Din Ujjan, I., & Masroor Bhatti, A. (2023). Management of the Triple Negative Locally Advanced Breast Cancer. In *Breast Cancer Updates*. https://doi.org/10.5772/intechopen.110149

Ishigami, E., Sakakibara, M., Sakakibara, J., Masuda, T., Fujimoto, H., Hayama, S., … Otsuka, M. (2019). Coexistence of regulatory B cells and regulatory T cells in tumor-infiltrating lymphocyte aggregates is a prognostic factor in patients with breast cancer. *Breast Cancer*, *26*(2). https://doi.org/10.1007/s12282-018-0910-4

Kawaguchi, K., Maeshima, Y., & Toi, M. (2022). Tumor immune microenvironment and systemic response in breast cancer. *Medical Oncology*, Vol. 39. https://doi.org/10.1007/s12032-022-01782-0

Kim, H. Y., Choi, J. H., Haque, M. M., Park, J. H., Kim, I. H., Choi, B. K., … Park, S. G. (2022). Combined treatment with anti-HER2/neu and anti-4-1BB monoclonal antibodies induces a synergistic antitumor effect but requires dose optimization to maintain immune memory for protection from lethal rechallenge. *Cancer Immunology, Immunotherapy*, *71*(4). https://doi.org/10.1007/s00262-021-03120-1

Laumont, C. M., Banville, A. C., Gilardi, M., Hollern, D. P., & Nelson, B. H. (2022). Tumour-infiltrating B cells: immunological mechanisms, clinical impact and therapeutic opportunities. *Nature Reviews Cancer*, Vol. 22. https://doi.org/10.1038/s41568-022-00466-1

Lei, X., Lei, Y., Li, J. K., Du, W. X., Li, R. G., Yang, J., … Tan, H. B. (2020). Immune cells within the tumor microenvironment: Biological functions and roles in cancer immunotherapy. *Cancer Letters*, Vol. 470. https://doi.org/10.1016/j.canlet.2019.11.009

Lei, Y., Li, X., Huang, Q., Zheng, X., & Liu, M. (2021). Progress and Challenges of Predictive Biomarkers for Immune Checkpoint Blockade. *Frontiers in Oncology*, Vol. 11. https://doi.org/10.3389/fonc.2021.617335

Leone, J. P., & Leone, B. A. (2015). Breast cancer brain metastases: The last frontier. *Experimental Hematology and Oncology*, *4*(1), 1–10. https://doi.org/10.1186/s40164-015-0028-8

Liang, D., Xiao-Feng, H., Guan-Jun, D., Er-Ling, H., Sheng, C., Ting-Ting, W., … Ya-Yi, H. (2015). Activated STING enhances Tregs infiltration in the HPV-related carcinogenesis of tongue squamous cells via the c-jun/CCL22 signal. *Biochimica et Biophysica Acta - Molecular Basis of Disease*, *1852*(11). https://doi.org/10.1016/j.bbadis.2015.08.011

Liu, L., Wang, Y., Miao, L., Liu, Q., Musetti, S., Li, J., & Huang, L. (2018). Combination Immunotherapy of MUC1 mRNA Nano-vaccine and CTLA-4 Blockade Effectively Inhibits Growth of Triple Negative Breast Cancer. *Molecular Therapy*, *26*(1). https://doi.org/10.1016/j.ymthe.2017.10.020

Michel, L. L., Bermejo, J. L., Gondos, A., Marmé, F., & Schneeweiss, A. (2015). T-DM1 as a new treatment option for patients with metastatic HER2-positive breast cancer in clinical practice. *Anticancer Research*, *35*(9).

Mota, A. de L., Evangelista, A. F., Macedo, T., Oliveira, R., Scapulatempo-Neto, C., Vieira, R. A. da C., & Marques, M. M. C. (2017). Molecular characterization of breast cancer cell lines by clinical immunohistochemical markers. *Oncology Letters*, *13*(6). https://doi.org/10.3892/ol.2017.6093

Nicolini, A., Rossi, G., & Ferrari, P. (2023). Experimental and clinical evidence in favour of an effective immune stimulation in ER-positive, endocrine-dependent metastatic breast cancer. *Frontiers in Immunology*, Vol. 14. https://doi.org/10.3389/fimmu.2023.1225175

Peng, G. L., Li, L., Guo, Y. W., Yu, P., Yin, X. J., Wang, S., & Liu, C. P. (2019). CD8+ cytotoxic and FoxP3+ regulatory T lymphocytes serve as prognostic factors in breast cancer. *American Journal of Translational Research*, *11*(8).

Poncin, A., Onesti, C. E., Josse, C., Boulet, D., Thiry, J., Bours, V., & Jerusalem, G. (2021). Immunity and breast cancer: Focus on eosinophils. *Biomedicines*, Vol. 9. https://doi.org/10.3390/biomedicines9091087

Rosenberg, S. A., Restifo, N. P., Yang, J. C., Morgan, R. A., & Dudley, M. E. (2008). Adoptive cell transfer: A clinical path to effective cancer immunotherapy. *Nature Reviews Cancer*, Vol. 8. https://doi.org/10.1038/nrc2355

Rugo, H. S., Im, S. A., Cardoso, F., Cortes, J., Curigliano, G., Musolino, A., … Gradishar, W. J. (2023). Margetuximab Versus Trastuzumab in Patients with Previously Treated HER2-Positive Advanced Breast Cancer (SOPHIA): Final Overall Survival Results from a Randomized Phase 3 Trial. *Journal of Clinical Oncology*, *41*(2). https://doi.org/10.1200/JCO.21.02937

Sadeghi, M., Dehnavi, S., Sharifat, M., Amiri, A. M., & Khodadadi, A. (2024). Innate immune cells: Key players of orchestra in modulating tumor microenvironment (TME). *Heliyon*, Vol. 10. https://doi.org/10.1016/j.heliyon.2024.e27480

Shan, F., Somasundaram, A., Bruno, T. C., Workman, C. J., & Vignali, D. A. A. (2022). Therapeutic targeting of regulatory T cells in cancer. *Trends in Cancer*, Vol. 8. https://doi.org/10.1016/j.trecan.2022.06.008

Stanton, S. E., & Disis, M. L. (2016). Clinical significance of tumor-infiltrating lymphocytes in breast cancer. *Journal for ImmunoTherapy of Cancer*, Vol. 4. https://doi.org/10.1186/s40425-016-0165-6

Togashi, Y., Shitara, K., & Nishikawa, H. (2019). Regulatory T cells in cancer immunosuppression — implications for anticancer therapy. *Nature Reviews Clinical Oncology*, Vol. 16. https://doi.org/10.1038/s41571-019-0175-7

Wagner, J., Rapsomaniki, M. A., Chevrier, S., Anzeneder, T., Langwieder, C., Dykgers, A., … Bodenmiller, B. (2019). A Single-Cell Atlas of the Tumor and Immune Ecosystem of Human Breast Cancer. *Cell*, *177*(5). https://doi.org/10.1016/j.cell.2019.03.005

Yang, P., Cao, X., Cai, H., Feng, P., Chen, X., Zhu, Y., … Jie, J. (2021). The exosomes derived from CAR-T cell efficiently target mesothelin and reduce triple-negative breast cancer growth. *Cellular Immunology*, *360*. https://doi.org/10.1016/j.cellimm.2020.104262

Yee, N. S., Borgia, J. A., Semenova, E., Campbell, C. J., & Booth, B. W. (2023). The Influence of the Normal Mammary Microenvironment on Breast Cancer Cells. *Cancers 2023, Vol. 15, Page 576*, *15*(3), 576. https://doi.org/10.3390/CANCERS15030576

Zhang, H., & Chen, J. (2018). Current status and future directions of cancer immunotherapy. *Journal of Cancer*, *9*(10), 1773–1781. https://doi.org/10.7150/jca.24577

Zhang, P., Zhang, G., & Wan, X. (2023). Challenges and new technologies in adoptive cell therapy. *Journal of Hematology and Oncology*, Vol. 16. https://doi.org/10.1186/s13045-023-01492-8

Zhao, Y., Shao, Q., Zhu, H., Xu, H., Long, W., Yu, B., … Su, Z. (2018). Resveratrol ameliorates Lewis lung carcinoma-bearing mice development, decreases granulocytic myeloid-derived suppressor cell accumulation and impairs its suppressive ability. *Cancer Science*, *109*(9). https://doi.org/10.1111/cas.13720

Chapter 6

Therapeutic Effect Of Magnetic Field On Cancer

Şeyda Nur KALIN[1]
Yağmur ÜNVER[2]

[1] Dr. Şeyda Nur KALIN, Erzincan Binali Yıldırım University, Faculty of Science and Arts, Department of Chemistry, 24002, Erzincan, Turkey. seydanurcakir32@gmail.com, ORCID ID: 0000-0002-2594-2489
[2] Assoc. Prof. Dr. Yağmur ÜNVER, Atatürk University, Science Faculty, Department of Molecular Biology and Genetics, 25240, Erzurum, Turkey. yunver@atauni.edu.tr, ORCID ID: 0000-0003-1497-081X

1. Introduction

Cancer is a significant disease that threatens human health worldwide. Despite significant advancements in cancer treatment, the morbidity and mortality rates remain highly prevalent, according to the 2022 global cancer statistics (Bray et al., 2018, 2024). In cancer treatment, although traditional methods such as surgery, chemotherapy, and radiotherapy are used, each of these methods has its own unique limitations in terms of efficacy, cost, and undesirable side effects. In this regard, the need for novel and more effective treatment methods to address these deficiencies has increased. Magnetic fields have been widely suggested as a potential therapeutic modality due to their high efficacy, low side effects, wide range of applications, and low cost advantages, and their effects on biological systems are being closely studied by scientists (L. Zhang et al., 2017).

Magnetic fields are commonly used in industrial and agricultural production, science and technology medicine, and other applications. A magnetic field can have an effect on a wide range of biological metabolism and processes in cells and organisms. In the literature, magnetic fields have been reported to have anti-carcinogenic potential both *in vivo* and *in vitro*, additionally, that magnetic treatment has potential for pain reduction, wound healing support, osteonecrosis, regulation of muscle functions, peripheral nerve regeneration, and anti-inflammation (Ding et al., 2011; Eccles, 2005; Jing et al., 2010; Kiss et al., 2013; Schuster & Rapoport, 2016; Shang et al., 2019; Strauch et al., 2007; Suszyński et al., 2014; Zhao et al., 2017; Zhu et al., 2017). Compared to existing treatments, magnetic fields hold an important place in cancer therapy due to their reliability, high efficiency, low cost, non-invasive nature and absence of scarring and infection risks. Magnetic fields are known to suppress angiogenesis of tumor and enhance the immune response in living organisms. Magnetic fields have an effect on biological functions at the cellular level by affecting, cell cycle, cell morphology, mitochondrial function, and cell membrane structure. The effect of the magnetic field observed at the molecular level leads to tumor suppression by interfering with DNA synthesis, reactive oxygen species (ROS) levels, epidermal growth factor receptor orientation, and the transmission of second messenger molecules (G. Zhang et al., 2023a). This review aims at summarising current knowledge of magnetic field therapy on cancer and its underlying mechanisms, as well as future prospects of magnetic field therapy.

2. Magnetic and Electromagnetic Fields

Magnetic field (MF) is the force field that forms around magnets or a moving electric charge (Prša & Kasaš-Lažetić, 2018). The magnetic field produced by natural magnets is generated by the alignment and mutual reinforcement of the

magnetic moments of atoms in a certain order. Electromagnetic fields (EMF) are generated by electromagnets or current-carrying wires and produce a magnetic field that varies over time (A. Xu et al., 2021b).

In the magnetic field, the international unit Tesla (T) is the unit of magnetic flux density. One Tesla is equal to one Weber per square meter, which is equal to 10^4 gauss (G), which is the unit of magnetic field in the centimeter-gram-second system. So, 1 G = 100 μT. The magnetic flux density is proportionate to the magnetic permeability of the magnetic field and the magnetic field strength (Maffei, 2022b). The magnetic flux density can be calculated by the following formula:

$$B = \mu \times H$$

B: magnetic flux density (tesla)
μ: magnetic permeability (henry/meterkilogram-second squared)
H: magnetic field strength (amperes/meterkilogram)

Frequency refers to the rate of change over time of a periodic quantity, such as the instantaneous field strength of a low-frequency electric or magnetic field. The unit of frequency, a measure of the number of cycles per unit of time, is the Hertz (Hz) (Anonymous, 2024). The power flux density of the electromagnetic field (S), consisting of the energetic fractions of the magnetic field and electric components, is measured in watts per square meter (W m^{-2}) (Maffei, 2022a).

2.1. Classification of Magnetic Field

Magnetic fields (MF) are categorised into two types according to their properties: constant magnetic field (CMF) or dynamic magnetic field (DMF) (Y. Liu et al., 2024a). CMF can be generated by permanent magnets or solenoids with unidirectional currents, also called as magnetostatic field (MSF) or static magnetic field (SMF) (G. Zhang et al., 2023b). DMF can be categorised according to the mode of magnetic field generation, which varies with time: geomagnetic field (GMF), pulsating magnetic field (PuMF), pulsed magnetic field (PMF), and alternating magnetic field (AMF) (Hildebrandt, 2002; A. Xu et al., 2021a; G. Zhang et al., 2023b). AMFs are produced either by a regularly moving magnet or by an electromagnetic coil with a current of a given frequency. PMFs are generated by electromagnetic coils fuelled by current pulses, PuMFs by electromagnetic coils fuelled by current from rectifier data and GMFs by the Earth and the ionosphere (Guo et al., 2024; Maffei, 2022a).

SMFs are classified according to the magnetic field intensity as low MFs (<1 mT), medium MFs (1 mT - 1 T), high MFs (1 T - 5 T) and ultrahigh MFs (>5 T)

(Hunt et al., 2009; Y. Liu et al., 2024b; Van Huizen et al., 2019b). According to frequency, magnetic fields can be subdivided into low frequency MF, radio-frequency MF, medium frequency MF and high frequency MFs (Figure 1) (Y. Liu et al., 2024b). The treatment of magnetic fields involves two mechanisms: non-thermal effect (non-ionising radiation, NI) and thermal effect (ionising radiation).

Figure 1. Classification of magnetic field types.

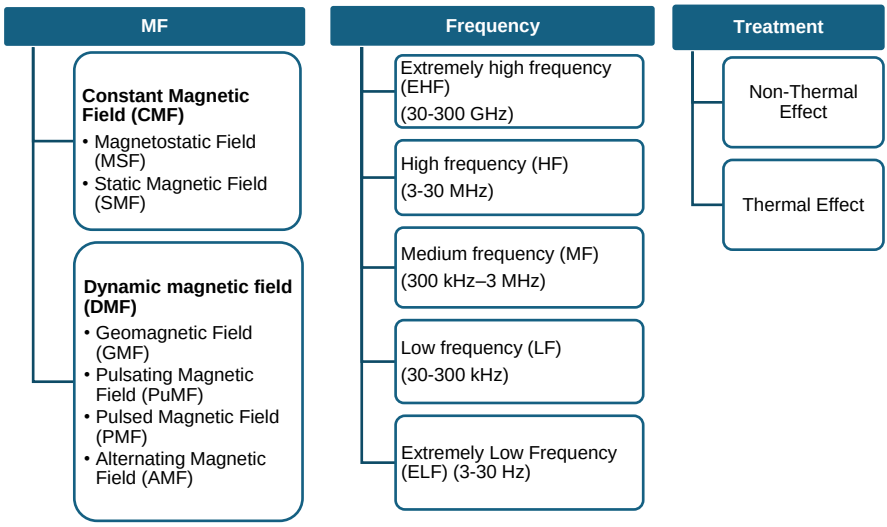

2.2. Use of Magnetic Field in Biological Systems

Magnetic fields have been known to have biologically effects on living organisms since the mid-19th century through the induction of electric fields and currents (Gaffey & Tenforde, 1981). Specific magnetic properties, so-called biomagnetism, are known to exist in different tissues and organs in organisms (G. Zhang et al., 2023b). In the literature, it has been reported that the magnetic susceptibilities of cellular lipid protein, and water components in living organisms differ (Zablotskii et al., 2018). Shin *et al*. reported that investigating brain microstructural information based on magnetic susceptibility differences of iron and myelin can be used as a useful tool to improve understanding of disease pathogenesis and lesion characterization, as they are involved in normal brain function and are important biomarkers of neurological disorders (Shin et al., 2021). Thus, the application of biomagnetism differences between biological components in disease detection and diagnosis is of interest in the medical field.

SMFs, which cause various physio-chemical effects because of the intrinsic magnetism of organisms, can alter the position, orientation and morphology of intracellular substructures and affect various biological metabolism and

processes, including structural adaptation, proliferation, and stress responses (Tao et al., 2019). Therefore, research into stimulating living cultures with different types of magnetic fields is also important. SMFs are widely used in many fields such as industrial and agricultural production, modern science and technology, especially in medicine and healthcare. The process of magnetic field generation and its accurate quantification as a factor that impacts cells, tissues and organisms is the most important research topic of magnetic fields in biotechnology. In the literature, it has been reported that magnetic resonance imaging resolution and imaging capabilities have improved with the increase in SMF intensity and 4-9.4 T research systems have been developed for clinical imaging applications (Tian et al., 2021). Effects of static or oscillating weak magnetic fields on stem cells, calcium concentration, electron transfer in cryptochrome, ROS, circadian clock, action potentials, anxiety, analgesia, development, neuronal activities, memory, DNA, genetics and many other functions have also been reported (Van Huizen et al., 2019a; Wang et al., 2022; J. Xu et al., 2021; Zadeh-Haghighi & Simon, 2022). The fact that the effects of SMFs used in medicine on biological systems and their underlying mechanisms have not yet been fully elucidated has led to the need for further investigation of magnetic fields (Table 1).

Table 1. The biological effects of magnetic fields

Tumor cells	Application conditions	Effect of application	Ref.
Human neuroblastoma (SH-SY5Y)	1 mT, 50 Hz DMF for 72 h	Increased ROS levels Induced apoptosis	(Benassi et al., 2016)
Human breast cancer (MCF-7)	10 mT SMF for 24 and 48 h	Decreased viability Decreased differentiation Increased ROS levels	(Hajipour Verdom et al., 2018)
Human breast cancer (MCF-7 and MDA-MB-231)	0.011 T, 8 Hz PMF for twice a day for 5 days	Decreased viability Inhibited cell proliferation Induced cell death Induced cellular senescence	(Pantelis et al., 2024)
MCF-7 and MDA-MB-231 cell lines	1 mT, 50 Hz ELF-MF for 24 h	Decreased viability Inhibited cell proliferation	(Elexpuru-Zabaleta et al., 2023)
Mouse breast cancer (4T1)	~150 mT SMF for 24 h	Inhibited cell migration Repressed telomerase activity	(Fan et al., 2020)
Jurkat Lymphoma cells	4.75 T SMF	Inhibited cell proliferation	(Aldinucci et al., 2003)
Human Epidermal Stem Cells (hESC)	5 mT, 50 Hz ELF-EMF for 7 days (30 min/day)	Promoted cell proliferation Increased cell growth Increased proportion of S-phase cells	(M. Zhang et al., 2013)
Prostate cancer (LNCaP, PC3, and DU145)	0.2 mT, 60 Hz MF	Decreased cell growth Induced apoptosis through ROS	(Koh et al., 2008)
Male Wistar rats	7 mT, 50 Hz ELF-MF for 24 h	Stimulated pro-inflammatory cytokines	(Wyszkowska et al., 2018)
Human leukaemia (U937)	6 mT SMFfor 72 h	Increased intracellular Ca^{2+} Mitochondria localized near nucleus	(Dini et al., 2009)

3. The Effect of Magnetic Fields in Cancer Therapy

Cancer cells can be affected by MFs to different degrees and this effect is known to be related to non-thermal (non-ionising radiation) and thermal (ionising radiation) mechanisms in the treatment of MFs. High-frequency MFs (gamma rays and X-rays, etc.) cause direct damage to DNA, while low-frequency MFs (LF-MFs) have a biochemical effect on the reactions of the cells (Diab, 2019). ELF-MFs have been found to have anticancer activity, to reduce the risk of certain tumors, and to have potential benefits in the healing process of cancer patients, according to numerous studies in the literature (Khan et al., 2021). As a result, MFs can be proposed as a strategy for cancer therapy.

3.1. Thermal Effects of Magnetic Field Therapy

Hyperthermia (HT) is a widely used anticancer treatment modality in combination with radiotherapy and chemotherapy to increase the body's tissue temperature, based on the application of heat (39-45 ◦C) to prevent the growth of cancerous cells and kill them (Chang et al., 2018; X. Liu et al., 2020; Peiravi et al., 2022). The aim is to increase the sensitivity of tumor tissues and, on the other hand, to affect the defence system (Chicheł et al., 2007). The increase in tissue temperature with HT can lead to oxygenation of the tumor by altering vascularity and increasing blood flow, as well as killing cells by affecting cell membranes, nucleic acid repair enzymes, proteins, and cellular structures. However, although this method triggers the death of tumor cells, it can cause serious side effects as it also affects healthy tissues (Peiravi et al., 2022). Therefore, it is recommended to use nanotechnological methods to increase the sensitivity of HT with a harmless, effective, and easy treatment approach. Studies have shown that nanoparticles (NPs) induce DNA damage and expression of heat shock proteins by applying heat only to tumor tissues in HT and direct cells to death (Szwed & Marczak, 2024).

Magnetic hyperthermia (MHT) is based on the principle of heat generation by increasing the hyperthermia efficiency of magnetic nanoparticles (MNPs) in the presence of AMF, and thus, with the widespread use of nanotechnology, MHT has been proposed as an alternative method in tumor therapy (Beik et al., 2016; GILCHRIST et al., 1957; Peiravi et al., 2022). The MNPs-mediated MHT (MNPs-MHT) therapeutic modality has a great advantage in that it allows the magnetic killing of cancer cells without the need for deep tissue penetration and without damaging the surrounding normal tissues (Kumar & Mohammad, 2011; Shubayev et al., 2009). MNPs-MHT enables the realization of intracellular hyperthermia by applying therapeutic heat directly to cancer cells and, as a result of these therapeutic advantages, MNPs-MHT-based cancer therapies have been

transferred from the laboratory stage to clinical studies and used in the treatment of breast, prostate, and glioblastoma cancer (Acar et al., 2022; Espinosa et al., 2018; Jordan et al., 1999). Though MNPs-MHT treatment has been applied in clinical trials, the obstacles limiting the efficacy of MNPs-MHT on cancer therapy need to be investigated to overcome the challenges of this therapeutic approach.

In MNPs-MHT treatment, one of the main aims is to synthesis multifunctional MNPs with appropriately functionalized surfaces that exhibit the highest possible saturation magnetization using antibodies, chemical compounds, and DNA probes allowing them to selectively bind to target tissues or cells. Furthermore, while the shape and size of MNPs are important for their therapeutic efficacy, surface modifications that help to maintain their stability and biocompatibility are also important (Rajan & Sahu, 2020). Polyethylene glycol (PEG), polyethyleneimine (PEI), polyvinyl alcohol (PVA), silica and polyvinylpyrrolidine (PVP) are the most commonly used biocompatible coating materials for MNPs (Cho et al., 2019). MNPs are used in bioimaging, cell labelling and targeted drug delivery, particularly in hyperthermia (Bañobre-López et al., 2013; Dey et al., 2017; Kolosnjaj-Tabi et al., 2013; F. Liu et al., 2011; Solak et al., 2021). The application of colloidal iron oxide and iron oxide-based core-shell nanostructures has shown promising potential in this field due to their high efficiency in carcinogenic cell destruction while showing limited toxicity to normal cells (Kossatz et al., 2014; Martinelli et al., 2019; Peiravi et al., 2022). In addition to being minimally invasive as it is injected intra-tumorally or intravenously, this method can provide sufficient thermal dosage to the targeted area while sparing healthy tissue. After the MNPs reach the target, the heat generated by the application of an external AMF is limited to the area covering the MNPs and is directed throughout the tissue (Peiravi et al., 2022). With this treatment method, it has been shown in the literature that the amount of iron-based nanoparticles will not cause toxicity in healthy cells and that most of the MNPs are evacuated by the body in a short time after treatment (Fukuda et al., 2012; Herring et al., 2013; Kim et al., 2011; LeBrun & Zhu*, 2018).

3.2. Non-Thermal Effects of Magnetic Field Therapy

Non-thermal effects of MF can be defined as their direct interaction with biological cells without relying on the principle of heat (Israel et al., 2013; A. Xu et al., 2021a). In addition to having antiproliferative, apoptotic, autophagic, angiogenic, and antimetastatic effects in cancer cells, MFs have also been reported to stop the cell cycle and improve the inflammatory response (Figure 2) (A. Xu et al., 2021a).

Figure 2. Potential anticancer effects of magnetic field

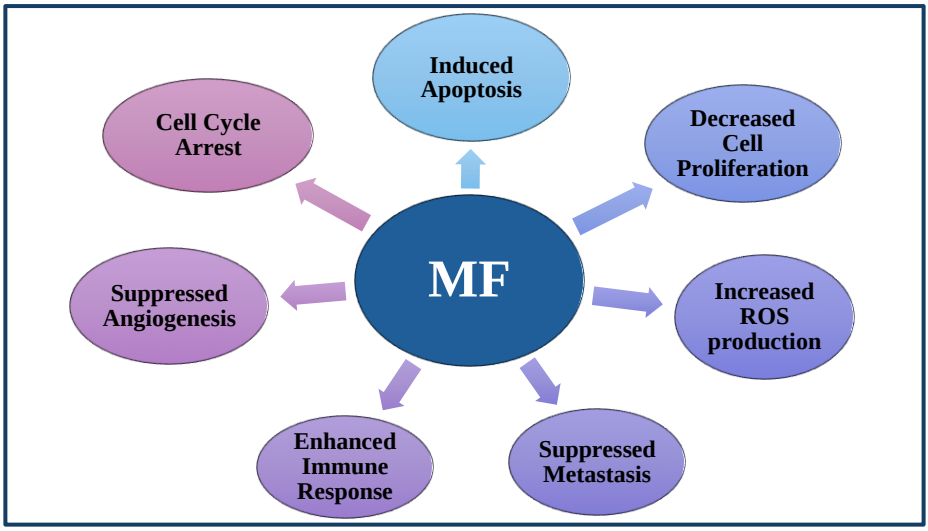

The cell cycle, which is closely associated with cell growth and death, includes G1, S, G2 and M phases and abnormal expression of cell cycle proteins in cancer cells may lead to uncontrolled cell proliferation (Otto & Sicinski, 2017). Most of the current chemotherapy and radiotherapy methods disrupt the integrity of DNA at cell cycle checkpoints, thereby inhibiting the proliferation of cancer cells and leading to their death. Therefore, targeting these cycle proteins is considered as a therapeutic strategy (Otto & Sicinski, 2017). The literature has described that MF suppresses the cell proliferation by keeping them in G2 phase (Miyakoshi, 2005). Chen *et al*. observed that exposure of human leukaemia (K562) cell line to SMFs (8.8 mT) caused DNA damage and arrest in G2/M phase and SMFs enhanced the anticancer effect of cisplatin (W.-F. Chen et al., 2010). Nie *et al*. demonstrated that exposure of melanoma cells (B16-F10) to LF-MF (7.5 Hz, 0.4 T, 43 days) induced an arrest of the cell cycle in the G2/M phase (Nie, Du, et al., 2013).

Apoptosis is mediated by mitochondrial (intrinsic) and cell death receptor (extrinsic) pathways (Mohammad et al., 2015). Targeting pro-apoptotic and anti-apoptotic proteins and mitochondrial membrane permeability, especially in the mitochondrial pathway, has become attractive in cancer therapies by contributing to the induction of apoptosis (Ko et al., 2007; Portt et al., 2011). Yuan *et al.* observed that exposure of nephroblastoma and neuroblastoma cells to LF-MF (50 Hz, 5.1 mT, 2 h per day) inhibited cell proliferation, induced apoptosis and increased cisplatin efficacy *in vivo* (Yuan et al., 2018). Gürhan *et al*. demonstrated that in human fibrosarcoma (HT-1080) cells exposed to SMFs, the

increase in intracellular ROS levels led to the release of cytochrome c into the cytoplasm, thereby triggering apoptotic cell death (Gurhan et al., 2021). Koh *et al*. reported that after MF (60 Hz, 48 h) exposure, intensity-dependent ROS accumulation occurred in prostate cancer (LNCaP, PC3, and DU145) cell lines and the cells were directed to apoptosis (Koh et al., 2008). So far, it has been established that miRNAs play a role in regulating a number of biological processes, such as autophagy and apoptosis (Yu et al., 2012). Xu *et al*. showed that LF-MFs inhibited growth of tumor and induced autophagic cell death by upregulating the expression level of miR-486, which plays a role in cell autophagy in lung cancer, in a Lewis Lung Cancer mouse model (Y. Xu et al., 2017). Although MF has been implicated in the induction of apoptosis and autophagy in a number of cancers, there are only a limited number of studies in this area and further research is needed.

Angiogenesis has become a therapeutic target in chronic inflammation and cancer because of its importance in embryonic development, tumor growth, and metastatic spread (Z.-L. Liu et al., 2023). The migration of vascular endothelial cells has a significant role in the progression of angiogenesis of tumor cells regulated by a variety of anti-angiogenic and pro-angiogenic molecules. Targeting vascular endothelial growth factor (VEGF-A, VEGF) and vascular endothelial growth factor receptor-2 (VEGFR-2) is particularly important in cancer therapy (Ferrara et al., 2003). In the literature, Strelczyk *et al*. showed that SMF of 600 mT for 10 days suppressed angiogenesis and delayed vascular maturation *in vivo* by reducing vessel diameter and functional vessel density (Strelczyk et al., 2009). Williams *et al*. showed that C3H/HeJ mice treated with a pulsating magnetic field of 120 pulses per second (0, 10 mT, 15 mT, or 20 mT for 10 minutes per day) significantly reduced tumor growth and vascularization (Williams et al., 2001). Monache *et al*. demonstrated that human umbilical vein endothelial cells (HUVEC) exposed to MF (50 Hz, 2mT) had decreased proliferative, migratory, and tube-like processes. Furthermore, MF treatment significantly downregulated the levels of VEGFR2 and decreased the ability of endothelial cells to form new vessels by affecting the VEGF signaling pathway (Delle Monache et al., 2013). Together, these findings suggest that MF therapy is a promising treatment modality that may have an impact on angiogenesis of tumor.

The immune function of the organism plays an important role in tumor initiation and metastatic spread. Therefore, effective strategies to re-model the immune system in tumors are becoming a key element of cancer immunotherapy (Finck et al., 2020). Nie *et al*. showed that tumor-bearing mice treated with MF (7.5 Hz, 0.4 T) increased lifetime, suppressed cytokine production, including

keratinocyte-derived chemokine (KC), granulocyte colony-stimulating factor (G-CSF), and interleukin-6 (IL-6) indicated that MF had an effect on improving immunity (Nie, Chen, et al., 2013). As for tumor metastasis, a leading cause of death in cancer patients, occurs when cancer cells spread beyond the source site of a tumor (Tracey A. Martin, Lin Ye, Andrew J. Sanders, Jane Lane, n.d.). Therefore, inhibition of metastasis has been an important target of cancer treatment modalities. Song *et al*. showed that SMF can inhibit cell metastasis in ovarian cancer in a ROS-dependent manner (Song et al., 2021). Tofani *et al*. indicated that MF (5.5 mT, 50 Hz) significantly inhibited tumor growth and metastasis in breast cancer MDA-MB-435 cell line (Tofani et al., 2002). Nie *et al.* found that metastasis was suppressed in melanoma B16-F10 cells after MF (0.4 T and 7.5 Hz) exposure (Nie, Du, et al., 2013). Song *et al*. stated that SMFs can suppress ovarian cancer metastasis *in vitro* and *in vivo* (Song et al., 2021).

4. Magnetic Fields in Combination Therapies

The fact that cancer-related mortality rates are still very high despite current cancer treatments has necessitated the development of new strategies that are cost-effective and highly effective. Combination therapy, one of such approaches, has an important role in cancer treatment as it is a treatment method that combines two or more therapeutic agents (Yap et al., 2013). Compared to the monotherapy approach, which targets actively proliferating cells in a non-selective manner (without discriminating between healthy and cancerous cells), the synergistic effect of combining anticancer agents increases the efficacy of treatment (Partridge et al., 2001). Combination therapies aim to reduce toxicity and side effects that occur as a result of drug resistance caused by chemotherapy-induced high dosage and long-term treatment (Albain et al., 2008). In addition to reducing drug resistance, this treatment method provides therapeutic benefits such as inducing apoptosis, reducing tumor growth, cancer stem cell populations and metastatic potential (Mokhtari et al., 2013). In summary, as shown in Table 2, MF can be applied as an adjuvant therapy to improve the effects of chemotherapeutic drugs by inducing cell cycle arrest, apoptosis, and DNA damage in cancer treatment.

Table 2. Combinational approaches with magnetic field for cancer therapy

Combinational approaches	Type of cancer	Application conditions	Effect of application	Ref.
SMF + Adriamycin	Human leukemia (K562)	8.8 mT SMF for 12 h, with Adriamycin (25 ng/ml)	Cytotoxic effect Arrested G2/M phase Increased DNA damage	(Hao et al., 2011)
SMF + Paclitaxel	K562 cell line	8.8 mT SMF for 24 h, with Paclitaxel (10 ng/ml, 24 h)	Inhibited the metabolic activity Arrested G2/M phase Increased cell membrane damage	(Sun et al., 2012)
SMF + Cisplatin	Ovarian carcinoma (Sensitive (A2780) and resistant (A2780CP))	15 mT SMF for 24, 48 and 96 h) with Cisplatin (IC_{50} values for 24, 48, and 96 h)	Increased DNA damage Genotoxicity Induced apoptosis Induced necrosis	(Zafari et al., 2024)
SMF + Cisplatin	Murine Lewis lung carcinomas (LLCs)	3 mT SMF for 35 min/day and cisplatin (3 mg/kg, i.p.)	Inhibited cell proliferation Longer survival time Cytotoxic effect	(Tofani, 2003)
SMF + Doxorubicin	Female B6C3F1 mice with transplanted mammary adenocarcinoma	110 mT SMF and doxorubicin (10 mg/kg, i.p.)	Tumor regression	(Gray et al., 2000)
SMF + Cisplatin	Human cervical cancer (HeLa)	10 mT SMF for 48 h and cisplatin (IC_{50} values)	Decreased cell viability Increased ROS production	(Kamalipooya et al., 2017)
PMF +Temozolomide	Human glioblastoma (T98G)	2 mT, 75 Hz PMF for 1 h/day and temozolomide (10 µM for 24 h)	Decreased cell proliferation Epigenetically influencing tumor suppressors and the regulation of oncogenes	(Pasi et al., 2016)
LF-MF +Temozolomide	Human glioblastoma (U87 and T98G)	10 mT, 100 Hz LF-MF for 144 h and temozolomide (100 µM)	Increased ROS production	(Akbarnejad et al., 2017)
LF-MF + 5-fluorouracil (5-FU)	MCF-7 cell line	1 mT, 50 Hz LF-MF for 12 h and 5-fluorouracil (5-FU) (5 µM for 24 h)	Decreased cell proliferation Cytotoxic effect Accumulation of cancer cells in S phase	(Han et al., 2018)

Extremely low-frequency electromagnetic field (ELF-EMF) + Folic acid-modified magnetic nanoparticles (FA-MNPs)	Human hepatoma (BEL-7402)	0.7 mT, 100 Hz ELF-EMF and FA-MNPs for 24 h	Inhibited cell proliferation Induced apoptosis	(B. Chen et al., 2014)
AMF+ Photothermal Therapy	Malignant cell lines (SKOV3, PC3, and A431)	12 mT, 110 kHz AC magnetic field, Iron oxide MNPs and laser irradiation 808 nm at 0.3 W/cm^2	Dual action yielded complete apoptosis-mediated cell death	(Espinosa et al., 2016)
AMF + Immune Therapy	4T1 (breast cancer) cell line	1.7 mT, CoFe2O4@MnFe2O4 NPs for 10 min at 50 °C (MHT) and α-PD-L1 treatment	The combined therapy demonstrated the great potentials in the fight against both primary and metastatic tumors	(Pan et al., 2020)

5. Conclusion

In conclusion, numerous studies have shown that different types of MF have different effects on tumor cells and that these effects are related to thermal and non-thermal mechanisms. This review discusses the potential of MFs in anti-tumor therapies to suppress cancer cell proliferation, arrest the cell cycle, inhibit neovascularization, suppress metastasis, and promote cell death in both *in vivo* and *in vitro* models. In addition, the synergistic potential of MFs in combination with chemotherapeutic agents, photothermal therapy or immunotherapy was discussed, which might be more effective in combined anticancer therapy. The potential of MF therapy in oncology needs to be systematically investigated and elucidated in more detail with further studies.

References

Acar, M., Solak, K., Yildiz, S., Unver, Y., & Mavi, A. (2022). Comparative heating efficiency and cytotoxicity of magnetic silica nanoparticles for magnetic hyperthermia treatment on human breast cancer cells. *3 Biotech*, *12*(11), 313. https://doi.org/10.1007/s13205-022-03377-y

Akbarnejad, Z., Eskandary, H., Dini, L., Vergallo, C., Nematollahi-Mahani, S. N., Farsinejad, A., Abadi, M. F. S., & Ahmadi, M. (2017). Cytotoxicity of temozolomide on human glioblastoma cells is enhanced by the concomitant exposure to an extremely low-frequency electromagnetic field (100 Hz, 100 G). *Biomedicine & Pharmacotherapy*, *92*, 254–264. https://doi.org/10.1016/j.biopha.2017.05.050

Albain, K. S., Nag, S. M., Calderillo-Ruiz, G., Jordaan, J. P., Llombart, A. C., Pluzanska, A., Rolski, J., Melemed, A. S., Reyes-Vidal, J. M., Sekhon, J. S., Simms, L., & O'Shaughnessy, J. (2008). Gemcitabine Plus Paclitaxel Versus Paclitaxel Monotherapy in Patients With Metastatic Breast Cancer and Prior Anthracycline Treatment. *Journal of Clinical Oncology*, *26*(24), 3950–3957. https://doi.org/10.1200/JCO.2007.11.9362

Aldinucci, C., Garcia, J. B., Palmi, M., Sgaragli, G., Benocci, A., Meini, A., Pessina, F., Rossi, C., Bonechi, C., & Pessina, G. P. (2003). The effect of strong static magnetic field on lymphocytes. *Bioelectromagnetics*, *24*(2), 109–117. https://doi.org/10.1002/bem.10071

Anonymous. (2024). *Electromagnetic fields*. https://www.bfs.de/EN/topics/emf/lff/introduction/introduction_node.html

Bañobre-López, M., Teijeiro, A., & Rivas, J. (2013). Magnetic nanoparticle-based hyperthermia for cancer treatment. *Reports of Practical Oncology & Radiotherapy*, *18*(6), 397–400. https://doi.org/10.1016/j.rpor.2013.09.011

Beik, J., Abed, Z., Ghoreishi, F. S., Hosseini-Nami, S., Mehrzadi, S., Shakeri-Zadeh, A., & Kamrava, S. K. (2016). Nanotechnology in hyperthermia cancer therapy: From fundamental principles to advanced applications. *Journal of Controlled Release*, *235*, 205–221. https://doi.org/10.1016/j.jconrel.2016.05.062

Benassi, B., Filomeni, G., Montagna, C., Merla, C., Lopresto, V., Pinto, R., Marino, C., & Consales, C. (2016). Extremely Low Frequency Magnetic Field (ELF-MF) Exposure Sensitizes SH-SY5Y Cells to the Pro-Parkinson's Disease Toxin MPP+. *Molecular Neurobiology*, *53*(6), 4247–4260. https://doi.org/10.1007/s12035-015-9354-4

Bray, F., Ferlay, J., Soerjomataram, I., Siegel, R. L., Torre, L. A., & Jemal, A. (2018). Global cancer statistics 2018: GLOBOCAN estimates of incidence and mortality worldwide for 36 cancers in 185 countries. *CA: A Cancer Journal for Clinicians*, *68*(6), 394–424. https://doi.org/10.3322/caac.21492

Bray, F., Laversanne, M., Sung, H., Ferlay, J., Siegel, R. L., Soerjomataram, I., & Jemal, A. (2024). Global cancer statistics 2022: GLOBOCAN estimates of incidence and mortality worldwide for 36 cancers in 185 countries. *CA: A Cancer Journal for Clinicians*, *74*(3), 229–263. https://doi.org/10.3322/caac.21834

Chang, D., Lim, M., Goos, J. A. C. M., Qiao, R., Ng, Y. Y., Mansfeld, F. M., Jackson, M., Davis, T. P., & Kavallaris, M. (2018). Biologically Targeted Magnetic Hyperthermia: Potential and Limitations. *Frontiers in Pharmacology*, *9*. https://doi.org/10.3389/fphar.2018.00831

Chen, B., Jiang, S., Chen, Z., Zhao, W., Yi, Y., Yang, R., & Wen, J. (2014). Apoptosis selectively induced in BEL-7402 cells by folic acid-modified magnetic nanoparticles combined with 100 Hz magnetic field. *International Journal of Nanomedicine*, 2043. https://doi.org/10.2147/IJN.S60457

Chen, W.-F., Qi, H., Sun, R.-G., Liu, Y., Zhang, K., & Liu, J.-Q. (2010). Static Magnetic Fields Enhanced the Potency of Cisplatin on K562 Cells. *Cancer Biotherapy and Radiopharmaceuticals*, *25*(4), 401–408. https://doi.org/10.1089/cbr.2009.0743

Chicheł, A., Skowronek, J., Kubaszewska, M., & Kanikowski, M. (2007). Hyperthermia – description of a method and a review of clinical applications. *Reports of Practical Oncology & Radiotherapy*, *12*(5), 267–275. https://doi.org/10.1016/S1507-1367(10)60065-X

Cho, H.-Y., Mavi, A., Chueng, S.-T. D., Pongkulapa, T., Pasquale, N., Rabie, H., Han, J., Kim, J. H., Kim, T.-H., Choi, J.-W., & Lee, K.-B. (2019). Tumor Homing Reactive Oxygen Species Nanoparticle for Enhanced Cancer Therapy. *ACS Applied Materials & Interfaces*, *11*(27), 23909–23918. https://doi.org/10.1021/acsami.9b07483

Delle Monache, S., Angelucci, A., Sanità, P., Iorio, R., Bennato, F., Mancini, F., Gualtieri, G., & Colonna, R. C. (2013). Inhibition of Angiogenesis Mediated by Extremely Low-Frequency Magnetic Fields (ELF-MFs). *PLoS ONE*, *8*(11), e79309. https://doi.org/10.1371/journal.pone.0079309

Dey, C., Baishya, K., Ghosh, A., Goswami, M. M., Ghosh, A., & Mandal, K. (2017). Improvement of drug delivery by hyperthermia treatment using magnetic cubic cobalt ferrite nanoparticles. *Journal of Magnetism and Magnetic Materials*, *427*, 168–174. https://doi.org/10.1016/j.jmmm.2016.11.024

Diab, K. A. (2019). *The Impact of the Low Frequency of the Electromagnetic Field on Human* (pp. 135–149). https://doi.org/10.1007/5584_2019_420

Ding, S., Peng, H., Fang, H.-S., Zhou, J.-L., & Wang, Z. (2011). Pulsed electromagnetic fields stimulation prevents steroid-induced osteonecrosis in rats. *BMC Musculoskeletal Disorders*, *12*(1), 215. https://doi.org/10.1186/1471-2474-12-215

Dini, L., Dwikat, M., Panzarini, E., Vergallo, C., & Tenuzzo, B. (2009). Morphofunctional study of 12- O -tetradecanoyl-13-phorbol acetate (TPA)-induced differentiation of U937 cells under exposure to a 6 mT static magnetic field. *Bioelectromagnetics*, *30*(5), 352–364. https://doi.org/10.1002/bem.20474

Eccles, N. K. (2005). A Randomized, Double-Blinded, Placebo-Controlled Pilot Study to Investigate the Effectiveness of a Static Magnet to Relieve Dysmenorrhea. *The Journal of Alternative and Complementary Medicine*, *11*(4), 681–687. https://doi.org/10.1089/acm.2005.11.681

Elexpuru-Zabaleta, M., Lazzarini, R., Tartaglione, M. F., Piva, F., Ciarapica, V., Marinelli Busilacchi, E., Poloni, A., Valentino, M., Santarelli, L., & Bracci, M. (2023). A 50 Hz magnetic field influences the viability of breast cancer cells 96 h after exposure. *Molecular Biology Reports*, *50*(2), 1005–1017. https://doi.org/10.1007/s11033-022-08069-7

Espinosa, A., Di Corato, R., Kolosnjaj-Tabi, J., Flaud, P., Pellegrino, T., & Wilhelm, C. (2016). Duality of Iron Oxide Nanoparticles in Cancer Therapy: Amplification of Heating Efficiency by Magnetic Hyperthermia and Photothermal Bimodal Treatment. *ACS Nano*, *10*(2), 2436–2446. https://doi.org/10.1021/acsnano.5b07249

Espinosa, A., Kolosnjaj-Tabi, J., Abou-Hassan, A., Plan Sangnier, A., Curcio, A., Silva, A. K. A., Di Corato, R., Neveu, S., Pellegrino, T., Liz-Marzán, L. M., & Wilhelm, C. (2018). Magnetic (Hyper)Thermia or Photothermia? Progressive Comparison of Iron Oxide and Gold Nanoparticles Heating in Water, in Cells, and In Vivo. *Advanced Functional Materials*, *28*(37). https://doi.org/10.1002/adfm.201803660

Fan, Z., Hu, P., Xiang, L., Liu, Y., He, R., & Lu, T. (2020). A Static Magnetic Field Inhibits the Migration and Telomerase Function of Mouse Breast Cancer Cells. *BioMed Research International*, *2020*, 1–9. https://doi.org/10.1155/2020/7472618

Ferrara, N., Gerber, H.-P., & LeCouter, J. (2003). The biology of VEGF and its receptors. *Nature Medicine*, *9*(6), 669–676. https://doi.org/10.1038/nm0603-669

Finck, A., Gill, S. I., & June, C. H. (2020). Cancer immunotherapy comes of age and looks for maturity. *Nature Communications*, *11*(1), 3325. https://doi.org/10.1038/s41467-020-17140-5

Fukuda, K., Fujieda, S., Shinoda, K., Suzuki, S., & Jeyadevan, B. (2012). Low temperature synthesis of FePt alloy nanoparticles by polyol process. *Journal of Physics: Conference Series*, *352*, 012020. https://doi.org/10.1088/1742-6596/352/1/012020

Gaffey, C. T., & Tenforde, T. S. (1981). Alterations in the rat electrocardiogram induced by stationary magnetic fields. *Bioelectromagnetics*, *2*(4), 357–370. https://doi.org/10.1002/bem.2250020407

GILCHRIST, R. K., MEDAL, R., SHOREY, W. D., HANSELMAN, R. C., PARROTT, J. C., & TAYLOR, C. B. (1957). Selective Inductive Heating of Lymph Nodes. *Annals of Surgery*, *146*(4), 596–606. https://doi.org/10.1097/00000658-195710000-00007

Gray, J. R., Frith, C. H., & Parker, J. D. (2000). In vivo enhancement of chemotherapy with static electric or magnetic fields. *Bioelectromagnetics*, *21*(8), 575–583. https://doi.org/10.1002/1521-186X(200012)21:8<575::AID-BEM3>3.0.CO;2-F

Guo, Z., Saw, P. E., & Jon, S. (2024). Non-Invasive Physical Stimulation to Modulate the Tumor Microenvironment: Unveiling a New Frontier in Cancer Therapy. *BIO Integration*, *5*(1). https://doi.org/10.15212/bioi-2024-0012

Gurhan, H., Bruzon, R., Kandala, S., Greenebaum, B., & Barnes, F. (2021). Effects Induced by a Weak Static Magnetic Field of Different Intensities on HT-1080 Fibrosarcoma Cells. *Bioelectromagnetics*, *42*(3), 212–223. https://doi.org/10.1002/bem.22332

Hajipour Verdom, B., Abdolmaleki, P., & Behmanesh, M. (2018). The Static Magnetic Field Remotely Boosts the Efficiency of Doxorubicin through Modulating ROS Behaviors. *Scientific Reports*, *8*(1), 990. https://doi.org/10.1038/s41598-018-19247-8

Han, Q., Chen, R., Wang, F., Chen, S., Sun, X., Guan, X., Yang, Y., Peng, B., Pan, X., Li, J., Yi, W., Li, P., Zhang, H., Feng, D., Chen, A., Li, X., Li, S., & Yin, Z. (2018). Pre-exposure to 50 Hz-electromagnetic fields enhanced the antiproliferative efficacy of 5-fluorouracil in breast cancer MCF-7 cells. *PLOS ONE*, *13*(4), e0192888. https://doi.org/10.1371/journal.pone.0192888

Hao, Q., Wenfang, C., Xia, A., Qiang, W., Ying, L., Kun, Z., & Runguang, S. (2011). Effects of a moderate-intensity static magnetic field and adriamycin on K562 cells. *Bioelectromagnetics*, *32*(3), 191–199. https://doi.org/10.1002/bem.20625

Herring, N. P., Panda, A. B., AbouZeid, K., Almahoudi, S. H., Olson, C. R., Patel, A., & El-Shall, M. S. (2013). Microwave Synthesis of Metal Oxide Nanoparticles. In *Metal Oxide Nanomaterials for Chemical Sensors* (pp. 245–284). Springer New York. https://doi.org/10.1007/978-1-4614-5395-6_8

Hildebrandt, B. (2002). The cellular and molecular basis of hyperthermia. *Critical Reviews in Oncology/Hematology*, *43*(1), 33–56. https://doi.org/10.1016/S1040-8428(01)00179-2

Hunt, R. W., Zavalin, A., Bhatnagar, A., Chinnasamy, S., & Das, K. C. (2009). Electromagnetic Biostimulation of Living Cultures for Biotechnology, Biofuel and Bioenergy Applications. *International Journal of Molecular Sciences*, *10*(10), 4515–4558. https://doi.org/10.3390/ijms10104515

Israel, M., Zaryabova, V., & Ivanova, M. (2013). Electromagnetic field occupational exposure: Non-thermal vs. thermal effects. *Electromagnetic Biology and Medicine*, *32*(2), 145–154. https://doi.org/10.3109/15368378.2013.776349

Jing, D., Shen, G., Cai, J., Li, F., Huang, J., Wang, Y., Xu, Q., Tang, C., & Luo, E. (2010). Effects of 180 mT static magnetic fields on diabetic wound healing in rats. *Bioelectromagnetics*, *31*(8), 640–648. https://doi.org/10.1002/bem.20592

Jordan, A., Scholz, R., Wust, P., Schirra, H., Thomas Schiestel, Schmidt, H., & Felix, R. (1999). Endocytosis of dextran and silan-coated magnetite nanoparticles and the effect of intracellular hyperthermia on human mammary carcinoma cells in vitro. *Journal of Magnetism and Magnetic Materials*, *194*(1–3), 185–196. https://doi.org/10.1016/S0304-8853(98)00558-7

Kamalipooya, S., Abdolmaleki, P., Salemi, Z., Javani Jouni, F., Zafari, J., & Soleimani, H. (2017). Simultaneous application of cisplatin and static magnetic field enhances oxidative stress in HeLa cell line. *In Vitro Cellular & Developmental Biology - Animal*, *53*(9), 783–790. https://doi.org/10.1007/s11626-017-0148-z

Khan, M. W., Juutilainen, J., Auvinen, A., Naarala, J., Pukkala, E., & Roivainen, P. (2021). A cohort study on adult hematological malignancies and brain tumors in relation to magnetic fields from indoor transformer stations. *International Journal of Hygiene and Environmental Health*, *233*, 113712. https://doi.org/10.1016/j.ijheh.2021.113712

Kim, T., Cho, E., Chae, Y., Kim, M., Oh, A., Jin, J., Lee, E., Baik, H., Haam, S., Suh, J., Huh, Y., & Lee, K. (2011). Urchin-Shaped Manganese Oxide Nanoparticles as pH-Responsive Activatable T 1 Contrast Agents for Magnetic Resonance Imaging. *Angewandte Chemie International Edition*, *50*(45), 10589–10593. https://doi.org/10.1002/anie.201103108

Kiss, B., Gyires, K., Kellermayer, M., & László, J. F. (2013). Lateral gradients significantly enhance static magnetic field-induced inhibition of pain responses in mice—a double blind experimental study. *Bioelectromagnetics*, *34*(5), 385–396. https://doi.org/10.1002/bem.21781

Ko, J.-K., Choi, K.-H., Pan, Z., Lin, P., Weisleder, N., Kim, C.-W., & Ma, J. (2007). The tail-anchoring domain of Bfl1 and HCCS1 targets mitochondrial membrane permeability to induce apoptosis. *Journal of Cell Science*, *120*(16), 2912–2923. https://doi.org/10.1242/jcs.006197

Koh, E. K., Ryu, B.-K., Jeong, D.-Y., Bang, I.-S., Nam, M. H., & Chae, K.-S. (2008). A 60-Hz sinusoidal magnetic field induces apoptosis of prostate cancer cells through reactive oxygen species. *International Journal of Radiation Biology*, *84*(11), 945–955. https://doi.org/10.1080/09553000802460206

Kolosnjaj-Tabi, J., Wilhelm, C., Clément, O., & Gazeau, F. (2013). Cell labeling with magnetic nanoparticles: Opportunity for magnetic cell imaging and cell manipulation. *Journal of Nanobiotechnology*, *11*(S1), S7. https://doi.org/10.1186/1477-3155-11-S1-S7

Kossatz, S., Ludwig, R., Dähring, H., Ettelt, V., Rimkus, G., Marciello, M., Salas, G., Patel, V., Teran, F. J., & Hilger, I. (2014). High Therapeutic Efficiency of Magnetic Hyperthermia in Xenograft Models Achieved with Moderate Temperature Dosages in the Tumor Area. *Pharmaceutical Research*, *31*(12), 3274–3288. https://doi.org/10.1007/s11095-014-1417-0

Kumar, C. S. S. R., & Mohammad, F. (2011). Magnetic nanomaterials for hyperthermia-based therapy and controlled drug delivery. *Advanced Drug Delivery Reviews*, *63*(9), 789–808. https://doi.org/10.1016/j.addr.2011.03.008

LeBrun, A., & Zhu*, L. (2018). Magnetic Nanoparticle Hyperthermia in Cancer Treatment: History, Mechanism, Imaging-Assisted Protocol Design, and Challenges. In *Theory and Applications of Heat Transfer in Humans* (pp. 631–667). Wiley. https://doi.org/10.1002/9781119127420.ch29

Liu, F., Laurent, S., Fattahi, H., Elst, L. Vander, & Muller, R. N. (2011). Superparamagnetic Nanosystems Based on Iron Oxide Nanoparticles for Biomedical Imaging. *Nanomedicine*, *6*(3), 519–528. https://doi.org/10.2217/nnm.11.16

Liu, X., Zhang, Y., Wang, Y., Zhu, W., Li, G., Ma, X., Zhang, Y., Chen, S., Tiwari, S., Shi, K., Zhang, S., Fan, H. M., Zhao, Y. X., & Liang, X.-J. (2020). Comprehensive understanding of magnetic hyperthermia for improving antitumor therapeutic efficacy. *Theranostics*, *10*(8), 3793–3815. https://doi.org/10.7150/thno.40805

Liu, Y., Tang, Q., Tao, Q., Dong, H., Shi, Z., & Zhou, L. (2024a). Low-frequency magnetic field therapy for glioblastoma: Current advances, mechanisms, challenges and future perspectives. *Journal of Advanced Research*. https://doi.org/10.1016/j.jare.2024.03.024

Liu, Y., Tang, Q., Tao, Q., Dong, H., Shi, Z., & Zhou, L. (2024b). Low-frequency magnetic field therapy for glioblastoma: Current advances, mechanisms, challenges and future perspectives. *Journal of Advanced Research*. https://doi.org/10.1016/j.jare.2024.03.024

Liu, Z.-L., Chen, H.-H., Zheng, L.-L., Sun, L.-P., & Shi, L. (2023). Angiogenic signaling pathways and anti-angiogenic therapy for cancer. *Signal Transduction and Targeted Therapy*, *8*(1), 198. https://doi.org/10.1038/s41392-023-01460-1

Maffei, M. E. (2022a). Magnetic Fields and Cancer: Epidemiology, Cellular Biology, and Theranostics. *International Journal of Molecular Sciences*, *23*(3), 1339. https://doi.org/10.3390/ijms23031339

Maffei, M. E. (2022b). Magnetic Fields and Cancer: Epidemiology, Cellular Biology, and Theranostics. *International Journal of Molecular Sciences*, *23*(3), 1339. https://doi.org/10.3390/ijms23031339

Martinelli, C., Pucci, C., & Ciofani, G. (2019). Nanostructured carriers as innovative tools for cancer diagnosis and therapy. *APL Bioengineering*, *3*(1). https://doi.org/10.1063/1.5079943

Miyakoshi, J. (2005). Effects of static magnetic fields at the cellular level. *Progress in Biophysics and Molecular Biology*, *87*(2–3), 213–223. https://doi.org/10.1016/j.pbiomolbio.2004.08.008

Mohammad, R. M., Muqbil, I., Lowe, L., Yedjou, C., Hsu, H.-Y., Lin, L.-T., Siegelin, M. D., Fimognari, C., Kumar, N. B., Dou, Q. P., Yang, H., Samadi, A. K., Russo, G. L., Spagnuolo, C., Ray, S. K., Chakrabarti, M., Morre, J. D., Coley, H. M., Honoki, K., … Azmi, A. S. (2015). Broad targeting of resistance to apoptosis in cancer. *Seminars in Cancer Biology*, *35*, S78–S103. https://doi.org/10.1016/j.semcancer.2015.03.001

Mokhtari, R. B., Kumar, S., Islam, S. S., Yazdanpanah, M., Adeli, K., Cutz, E., & Yeger, H. (2013). Combination of carbonic anhydrase inhibitor, acetazolamide, and sulforaphane, reduces the viability and growth of bronchial carcinoid cell lines. *BMC Cancer*, *13*(1), 378. https://doi.org/10.1186/1471-2407-13-378

Nie, Y., Chen, Y., Mou, Y., Weng, L., Xu, Z., Du, Y., Wang, W., Hou, Y., & Wang, T. (2013). Low Frequency Magnetic Fields Enhance Antitumor Immune Response against Mouse H22 Hepatocellular Carcinoma. *PLoS ONE*, *8*(11), e72411. https://doi.org/10.1371/journal.pone.0072411

Nie, Y., Du, L., Mou, Y., Xu, Z., Weng, L., Du, Y., Zhu, Y., Hou, Y., & Wang, T. (2013). Effect of low frequency magnetic fields on melanoma: tumor inhibition and immune modulation. *BMC Cancer*, *13*(1), 582. https://doi.org/10.1186/1471-2407-13-582

Otto, T., & Sicinski, P. (2017). Cell cycle proteins as promising targets in cancer therapy. *Nature Reviews Cancer*, *17*(2), 93–115. https://doi.org/10.1038/nrc.2016.138

Pan, J., Hu, P., Guo, Y., Hao, J., Ni, D., Xu, Y., Bao, Q., Yao, H., Wei, C., Wu, Q., & Shi, J. (2020). Combined Magnetic Hyperthermia and Immune Therapy for Primary and Metastatic Tumor Treatments. *ACS Nano*, *14*(1), 1033–1044. https://doi.org/10.1021/acsnano.9b08550

Pantelis, P., Theocharous, G., Veroutis, D., Vagena, I.-A., Polyzou, A., Thanos, D.-F., Kyrodimos, E., Kotsinas, A., Evangelou, K., Lagopati, N., Gorgoulis, V. G., & Kotopoulos, N. (2024). Pulsed Electromagnetic Fields (PEMFs) Trigger Cell Death and Senescence in Cancer Cells. *International Journal of Molecular Sciences*, *25*(5), 2473. https://doi.org/10.3390/ijms25052473

Partridge, A. H., Burstein, H. J., & Winer, E. P. (2001). Side Effects of Chemotherapy and Combined Chemohormonal Therapy in Women With Early-Stage Breast Cancer. *JNCI Monographs*, *2001*(30), 135–142. https://doi.org/10.1093/oxfordjournals.jncimonographs.a003451

Pasi, F., Fassina, L., Mognaschi, M. E., Lupo, G., Corbella, F., Nano, R., & Capelli, E. (2016). Pulsed Electromagnetic Field with Temozolomide Can Elicit an Epigenetic Pro-apoptotic Effect on Glioblastoma T98G Cells. *Anticancer Research*, *36*(11), 5821–5826. https://doi.org/10.21873/anticanres.11166

Peiravi, M., Eslami, H., Ansari, M., & Zare-Zardini, H. (2022). Magnetic hyperthermia: Potentials and limitations. *Journal of the Indian Chemical Society*, *99*(1), 100269. https://doi.org/10.1016/j.jics.2021.100269

Portt, L., Norman, G., Clapp, C., Greenwood, M., & Greenwood, M. T. (2011). Anti-apoptosis and cell survival: A review. *Biochimica et Biophysica Acta (BBA) - Molecular Cell Research*, *1813*(1), 238–259. https://doi.org/10.1016/j.bbamcr.2010.10.010

Prša, M. A., & Kasaš-Lažetić, K. K. (2018). Electromagnetic fields and their impacts. *IOP Conference Series: Materials Science and Engineering*, *294*, 012001. https://doi.org/10.1088/1757-899X/294/1/012001

Rajan, A., & Sahu, N. K. (2020). Review on magnetic nanoparticle-mediated hyperthermia for cancer therapy. *Journal of Nanoparticle Research*, *22*(11), 319. https://doi.org/10.1007/s11051-020-05045-9

Schuster, N. M., & Rapoport, A. M. (2016). New strategies for the treatment and prevention of primary headache disorders. *Nature Reviews Neurology*, *12*(11), 635–650. https://doi.org/10.1038/nrneurol.2016.143

Shang, W., Chen, G., Li, Y., Zhuo, Y., Wang, Y., Fang, Z., Yu, Y., & Ren, H. (2019). Static Magnetic Field Accelerates Diabetic Wound Healing by Facilitating Resolution of Inflammation. *Journal of Diabetes Research*, *2019*, 1–11. https://doi.org/10.1155/2019/5641271

Shin, H.-G., Lee, J., Yun, Y. H., Yoo, S. H., Jang, J., Oh, S.-H., Nam, Y., Jung, S., Kim, S., Fukunaga, M., Kim, W., Choi, H. J., & Lee, J. (2021). χ-separation: Magnetic susceptibility source separation toward iron and myelin mapping in the brain. *NeuroImage*, *240*, 118371. https://doi.org/10.1016/j.neuroimage.2021.118371

Shubayev, V. I., Pisanic, T. R., & Jin, S. (2009). Magnetic nanoparticles for theragnostics. *Advanced Drug Delivery Reviews*, *61*(6), 467–477. https://doi.org/10.1016/j.addr.2009.03.007

Solak, K., Mavi, A., & Yılmaz, B. (2021). Disulfiram-loaded functionalized magnetic nanoparticles combined with copper and sodium nitroprusside in breast cancer cells. *Materials Science and Engineering: C*, *119*, 111452. https://doi.org/10.1016/j.msec.2020.111452

Song, C., Yu, B., Wang, J., Ji, X., Zhang, L., Tian, X., Yu, X., Feng, C., Wang, X., & Zhang, X. (2021). Moderate Static Magnet Fields Suppress Ovarian Cancer Metastasis via ROS-Mediated Oxidative Stress. *Oxidative Medicine and Cellular Longevity*, *2021*(1). https://doi.org/10.1155/2021/7103345

Strauch, B., Patel, M. K., Navarro, J. A., Berdichevsky, M., Yu, H.-L., & Pilla, A. A. (2007). Pulsed Magnetic Fields Accelerate Cutaneous Wound Healing in Rats. *Plastic and Reconstructive Surgery*, *120*(2), 425–430. https://doi.org/10.1097/01.prs.0000267700.15452.d0

Strelczyk, D., Eichhorn, M. E., Luedemann, S., Brix, G., Dellian, M., Berghaus, A., & Strieth, S. (2009). Static magnetic fields impair angiogenesis and growth of solid tumors in vivo. *Cancer Biology & Therapy*, *8*(18), 1756–1762. https://doi.org/10.4161/cbt.8.18.9294

Sun, R.-G., Chen, W.-F., Qi, H., Zhang, K., Bu, T., Liu, Y., & Wang, S.-R. (2012). Biologic effects of SMF and paclitaxel on K562 human leukemia cells. *General Physiology and Biophysics*, *31*(01), 1–10. https://doi.org/10.4149/gpb_2012_002

Suszyński, K., Marcol, W., Szajkowski, S., Pietrucha-Dutczak, M., Cieślar, G., Sieroń, A., & Lewin-Kowalik, J. (2014). Variable spatial magnetic field influences peripheral nerves regeneration in rats. *Electromagnetic Biology and Medicine*, *33*(3), 198–205. https://doi.org/10.3109/15368378.2013.801351

Szwed, M., & Marczak, A. (2024). Application of Nanoparticles for Magnetic Hyperthermia for Cancer Treatment—The Current State of Knowledge. *Cancers*, *16*(6), 1156. https://doi.org/10.3390/cancers16061156

Tao, Q., Zhang, L., Han, X., Chen, H., Ji, X., & Zhang, X. (2019). Magnetic Susceptibility Difference-Induced Nucleus Positioning in Gradient Ultrahigh Magnetic Field. *Biophysical Journal*. https://doi.org/10.1016/j.bpj.2019.12.020

Tian, X., Lv, Y., Fan, Y., Wang, Z., Yu, B., Song, C., Lu, Q., Xi, C., Pi, L., & Zhang, X. (2021). Safety evaluation of mice exposed to 7.0–33.0 T high-static magnetic fields. *Journal of Magnetic Resonance Imaging*, *53*(6), 1872–1884. https://doi.org/10.1002/jmri.27496

Tofani, S. (2003). Static and ELF magnetic fields enhance the in vivo anti-tumor efficacy of cis-platin against lewis lung carcinoma, but not of cyclophosphamide against B16 melanotic melanoma. *Pharmacological Research*. https://doi.org/10.1016/S1043-6618(03)00062-8

Tofani, S., Barone, D., Peano, S., Ossola, P., Ronchetto, F., & Cintorino, M. (2002). Anticancer activity by magnetic fields: inhibition of metastatic spread and growth in a breast cancer model. *IEEE Transactions on Plasma Science*, *30*(4), 1552–1557. https://doi.org/10.1109/TPS.2002.804209

Tracey A. Martin, Lin Ye, Andrew J. Sanders, Jane Lane, and W. G. J. (n.d.). Cancer Invasion and Metastasis: Molecular and Cellular Perspective. *Madame Curie Bioscience Database [Internet]*.

Van Huizen, A. V., Morton, J. M., Kinsey, L. J., Von Kannon, D. G., Saad, M. A., Birkholz, T. R., Czajka, J. M., Cyrus, J., Barnes, F. S., & Beane, W. S. (2019a). Weak magnetic fields alter stem cell–mediated growth. *Science Advances*, *5*(1). https://doi.org/10.1126/sciadv.aau7201

Van Huizen, A. V., Morton, J. M., Kinsey, L. J., Von Kannon, D. G., Saad, M. A., Birkholz, T. R., Czajka, J. M., Cyrus, J., Barnes, F. S., & Beane, W. S. (2019b). Weak magnetic fields alter stem cell–mediated growth. *Science Advances*, *5*(1). https://doi.org/10.1126/sciadv.aau7201

Wang, S., Zheng, M., Lou, C., Chen, S., Guo, H., Gao, Y., Lv, H., Yuan, X., Zhang, X., & Shang, P. (2022). Evaluating the biological safety on mice at 16 T static magnetic field with 700 MHz radio-frequency electromagnetic field. *Ecotoxicology and Environmental Safety*, *230*, 113125. https://doi.org/10.1016/j.ecoenv.2021.113125

Williams, C. D., Markov, M. S., Hardman, W. E., & Cameron, I. L. (2001). Therapeutic electromagnetic field effects on angiogenesis and tumor growth. *Anticancer Research*, *21*(6A), 3887–3891.

Wyszkowska, J., Jędrzejewski, T., Piotrowski, J., Wojciechowska, A., Stankiewicz, M., & Kozak, W. (2018). Evaluation of the influence of in vivo exposure to extremely low-frequency magnetic fields on the plasma levels of pro-inflammatory cytokines in rats. *International Journal of Radiation Biology*, *94*(10), 909–917. https://doi.org/10.1080/09553002.2018.1503428

Xu, A., Wang, Q., Lv, X., & Lin, T. (2021a). Progressive Study on the Non-thermal Effects of Magnetic Field Therapy in Oncology. *Frontiers in Oncology*, *11*. https://doi.org/10.3389/fonc.2021.638146

Xu, A., Wang, Q., Lv, X., & Lin, T. (2021b). Progressive Study on the Non-thermal Effects of Magnetic Field Therapy in Oncology. *Frontiers in Oncology*, *11*. https://doi.org/10.3389/fonc.2021.638146

Xu, J., Jarocha, L. E., Zollitsch, T., Konowalczyk, M., Henbest, K. B., Richert, S., Golesworthy, M. J., Schmidt, J., Déjean, V., Sowood, D. J. C., Bassetto, M., Luo, J., Walton, J. R., Fleming, J., Wei, Y., Pitcher, T. L., Moise, G., Herrmann, M., Yin, H., … Hore, P. J. (2021). Magnetic sensitivity of cryptochrome 4 from a migratory songbird. *Nature*, *594*(7864), 535–540. https://doi.org/10.1038/s41586-021-03618-9

Xu, Y., Wang, Y., Yao, A., Xu, Z., Dou, H., Shen, S., Hou, Y., & Wang, T. (2017). Low Frequency Magnetic Fields Induce Autophagy-associated Cell Death in Lung Cancer through miR-486-mediated Inhibition of Akt/mTOR Signaling Pathway. *Scientific Reports*, *7*(1), 11776. https://doi.org/10.1038/s41598-017-10407-w

Yap, T. A., Omlin, A., & de Bono, J. S. (2013). Development of Therapeutic Combinations Targeting Major Cancer Signaling Pathways. *Journal of Clinical Oncology*, *31*(12), 1592–1605. https://doi.org/10.1200/JCO.2011.37.6418

Yu, Y., Cao, L., Yang, L., Kang, R., Lotze, M., & Tang, D. (2012). microRNA 30A promotes autophagy in response to cancer therapy. *Autophagy*, *8*(5), 853–855. https://doi.org/10.4161/auto.20053

Yuan, L., Wang, C., Zhu, K., Li, H., Gu, W., Zhou, D., Lai, J., Zhou, D., Lv, Y., Tofani, S., & Chen, X. (2018). The antitumor effect of static and extremely low frequency magnetic fields against nephroblastoma and neuroblastoma. *Bioelectromagnetics*, *39*(5), 375–385. https://doi.org/10.1002/bem.22124

Zablotskii, V., Polyakova, T., & Dejneka, A. (2018). Cells in the Non-Uniform Magnetic World: How Cells Respond to High-Gradient Magnetic Fields. *BioEssays*, *40*(8). https://doi.org/10.1002/bies.201800017

Zadeh-Haghighi, H., & Simon, C. (2022). Magnetic field effects in biology from the perspective of the radical pair mechanism. *Journal of The Royal Society Interface*, *19*(193). https://doi.org/10.1098/rsif.2022.0325

Zafari, J., Rastegar-Pouyani, N., Javani Jouni, F., Najjar, N., Azarshin, S. Z., Jafarzadeh, E., Abdolmaleki, P., & Hoseini Shirazi, F. (2024). Static magnetic field reduces cisplatin resistance via increasing apoptosis pathways and genotoxicity in cancer cell lines. *Scientific Reports*, *14*(1), 5792. https://doi.org/10.1038/s41598-024-56605-1

Zhang, G., Liu, X., Liu, Y., Zhang, S., Yu, T., Chai, X., He, J., Yin, D., & Zhang, C. (2023a). The effect of magnetic fields on tumor occurrence and progression: Recent advances. *Progress in Biophysics and Molecular Biology*, *179*, 38–50. https://doi.org/10.1016/j.pbiomolbio.2023.04.001

Zhang, G., Liu, X., Liu, Y., Zhang, S., Yu, T., Chai, X., He, J., Yin, D., & Zhang, C. (2023b). The effect of magnetic fields on tumor occurrence and progression: Recent advances. *Progress in Biophysics and Molecular Biology*, *179*, 38–50. https://doi.org/10.1016/j.pbiomolbio.2023.04.001

Zhang, L., Ji, X., Yang, X., & Zhang, X. (2017). Cell type- and density-dependent effect of 1 T static magnetic field on cell proliferation. *Oncotarget*, *8*(8), 13126–13141. https://doi.org/10.18632/oncotarget.14480

Zhang, M., Li, X., Bai, L., Uchida, K., Bai, W., Wu, B., Xu, W., Zhu, H., & Huang, H. (2013). Effects of low frequency electromagnetic field on proliferation of human epidermal stem cells: An in vitro study. *Bioelectromagnetics*, *34*(1), 74–80. https://doi.org/10.1002/bem.21747

Zhao, J., Li, Y., Deng, K., Yun, P., & Gong, T. (2017). Therapeutic Effects of Static Magnetic Field on Wound Healing in Diabetic Rats. *Journal of Diabetes Research*, *2017*, 1–5. https://doi.org/10.1155/2017/6305370

Zhu, Y., Wang, S., Long, H., Zhu, J., Jian, F., Ye, N., & Lai, W. (2017). Effect of static magnetic field on pain level and expression of P2X3 receptors in the trigeminal ganglion in mice following experimental tooth movement. *Bioelectromagnetics*, *38*(1), 22–30. https://doi.org/10.1002/bem.22009